

SO(N) gauge theories in 2+1 dimensions: glueball spectra and confinement

Richard Lau and Michael Teper

Rudolf Peierls Centre for Theoretical Physics, University of Oxford,
1 Keble Road, Oxford OX1 3NP, UK

Abstract

We calculate the spectrum of light glueballs and the string tension in a number of $SO(N)$ lattice gauge theories in 2+1 dimensions, with N in the range $3 \leq N \leq 16$. After extrapolating to the continuum limit and then to $N = \infty$ we compare to the spectrum and string tension of the $SU(N \rightarrow \infty)$ gauge theory and find that the most reliably and precisely calculated physical quantities are consistent in that limit. We also compare the glueball spectra of those pairs of $SO(N)$ and $SU(N')$ theories that possess the same Lie algebra, i.e. $SO(3)$ and $SU(2)$, $SO(4)$ and $SU(2) \times SU(2)$, $SO(6)$ and $SU(4)$, and find that for the very lightest glueballs the spectra are consistent within each such pair, as are the string tensions and the couplings. Where there are apparent discrepancies they are typically for heavier glueballs, where the systematic errors are much harder to control. We calculate the $SO(N)$ string tensions with a particular focus on the confining properties of $SO(2N + 1)$ theories which, unlike $SO(2N)$ theories, possess a trivial centre. We find that for both the light glueballs and for the string tension $SO(2N)$ and $SO(2N + 1)$ gauge theories appear to form a single smooth sequence.

E-mail: r.lau1@physics.ox.ac.uk, m.teper1@physics.ox.ac.uk

Contents

1	Introduction	2
2	Relations between $SU(N)$ and $SO(N)$	4
2.1	large N	4
2.2	Lie algebra equivalences	5
2.2.1	$SU(2)$ and $SO(3)$	5
2.2.2	$SU(4)$ and $SO(6)$	6
2.2.3	$SU(2)\times SU(2)$ and $SO(4)$	7
2.3	predicting $SO(N)$ from $SU(N)$	8
3	Preliminaries	8
3.1	calculating on the lattice	8
3.2	calculating energies	9
3.2.1	glueball masses	9
3.2.2	string tensions	11
3.3	continuum limit	12
3.4	large N limit	12
3.5	bulk transition	13
3.6	systematic errors	14
3.6.1	wrong quantum numbers	14
3.6.2	missing states	14
3.6.3	identifying energy plateaux	15
3.6.4	finite volume corrections	19
3.6.5	multi-glueball states	21
3.6.6	reliability grades	21
4	Confinement	22
4.1	$SO(2N)$ and confinement	23
4.2	$SO(2N+1)$ and confinement	25
5	String tensions	30
5.1	lattice results	30
5.2	continuum limit and N -dependence	31
5.3	Lie algebra equivalences	32
6	Glueball spectrum	33
6.1	$SO(N)$ glueball masses	33
6.2	large N : odd and even N	34
6.3	Lie algebra equivalences: mass gap and couplings	36
6.4	Lie algebra equivalences: mass ratios	38
6.4.1	$SO(3)$ and $SU(2)$	38
6.4.2	$SO(4)$ and $SU(2)$	39

6.4.3	$SO(6)$ and $SU(4)$	40
7	Other results	41
7.1	large- N scaling	41
7.2	spinorial states in the spectrum	42
7.3	strong coupling	43
8	Conclusions	44

1 Introduction

While the continuum physics of $SU(N)$ gauge theories has been extensively studied via lattice calculations in both 2+1 and 3+1 dimensions, much less is known about $SO(N)$ gauge theories. The fact that $SO(N)$ theories are different from $SU(N)$ and yet are ‘near neighbours’, suggests that studying these theories is worthwhile.

$SU(N)$ and $SO(N)$ gauge theories are ‘near neighbours’ in at least two ways. Firstly, the large N limits of these theories are known to coincide [1] at the diagrammatic level (up to a factor of 2 in g^2). Moreover the orbifold equivalence [2] between $SO(2N)$ and $SU(N)$ gauge theories implies that they have the same physics in the common sector of states when $N \rightarrow \infty$ [3]. So it would be interesting to confirm these expectations with a non-perturbative lattice calculation of, for example, their common (positive charge conjugation) mass spectra, and also to investigate how $SO(2N + 1)$ gauge theories fit in with this. Secondly, certain low N pairs of theories possess the same Lie algebras: $SU(2)$ and $SO(3)$; $SU(2) \times SU(2)$ and $SO(4)$; $SU(4)$ and $SO(6)$. Again it would be interesting to know if the spectra are the same or if the differences in the global properties of the groups, to which large fields may be sensitive, influence the spectrum. We recall, for example, that the centre of $SU(N)$ is Z_N while the centre of $SO(2N)$ is only Z_2 and that of $SO(2N + 1)$ is trivial. In models of confinement based on dual disorder loops (centre vortices) [4], one might expect the differing centres to lead, for example, to differing string tensions. In the case of $SO(2N + 1)$ theories, which have a trivial centre, do we in fact have linear confinement? And what of the deconfining transition and its critical exponents? If the spectra of the pairs of unitary and orthogonal theories that share a common Lie algebra are in fact identical (as naively expected) how does this constrain their N -dependence, both in $SU(N)$ and $SO(N)$ gauge theories?

These and other interesting questions about $SO(N)$ gauge theories can be addressed by lattice calculations in both 2 + 1 and 3 + 1 dimensions. The $D = 3 + 1$ case is clearly of more direct physical interest, but standard lattice calculations encounter an obstacle in the existence of a first-order strong to weak coupling phase transition that, for small N , occurs at a small value of the lattice spacing [5]. This means that a lattice on the weak coupling side will need to be very large in lattice units if it is to have an adequately large physical volume. While this obstacle should be surmountable, it has led us to give priority to calculations in $D = 2 + 1$ where the analogous transition is more manageable and where the interesting field theoretic questions can also be addressed with, moreover, greater precision.

In this paper our aim is to calculate the masses of the lightest glueball states of $D = 2 + 1$ $SO(N)$ gauge theories for various values of N with sufficient accuracy to be able to extrapolate the lattice results to the continuum limit. We choose the range of values of N , $N \in [3, 16]$, to be large enough to allow a plausible extrapolation to the $N = \infty$ limit where we can compare to existing results for $SU(N)$ theories. En route we will compare the various pairs of theories with the same Lie algebras, and we will comment on what this might imply for the N -dependence of the physics. We will also calculate string tensions, both in $SO(2N)$ theories where confinement can be linked to their non-trivial Z_2 centre and, more interestingly, in $SO(2N + 1)$ gauge theories, where the centre is trivial. We will address the question of whether $SO(2N + 1)$ and $SO(2N)$ gauge theories form two separate sequences that only converge (if at all) at $N = \infty$ or if the two sets do in fact form a single sequence.

To achieve a truly convincing comparison between $SO(N)$ and $SU(N)$ gauge theories we would need to obtain accurate calculations of at least a few states in each spin-parity (J^P) sector of $SO(N)$, just as one already has in $SU(N)$ [6]. However it turns out that we are not able to achieve that ideal in the present work, primarily because our lattice glueball operators have poorer overlaps onto the glueball states than in the case of $SU(N)$, particularly so for small values of N . Nonetheless we are able to calculate the lightest $J^P = 0^+, 2^\pm$ glueball masses with the necessary precision, as well as the string tension (at least for $N > 3$). More massive states are subject to increasing systematic errors as the mass increases. To indicate the seriousness of these systematic errors in our Tables of masses (where the errors shown are purely statistical) we provide a ‘reliability’ grade ranging from α , indicating no significant systematic error, to ϕ , the opposite extreme. These are discussed in detail in Section 3.6.6, and should be taken into account in all the comparisons we show.

In the next section we begin by recalling the large N behaviour of $SO(N)$ and $SU(N)$ gauge theories and we outline our expectations for the relationship between those $SO(N)$ and $SU(N')$ theories that share a common Lie algebra. We only briefly mention how this might constrain the N -dependence of the glueball spectra of $SO(N)$ and $SU(N)$ theories since this question is discussed in detail in a recent letter [7] that makes use of some preliminary results of the present paper. In Section 3 we describe how the lattice calculations are performed and we discuss what we believe to be the principal sources of systematic error. We present in Section 4 our evidence for linear confinement in $SO(2N)$ and, more interestingly, in $SO(2N + 1)$. We follow that with detailed calculations of the string tension in Section 5 and, in Section 6, of the glueball spectrum. Then in Section 7 we touch upon three further issues: we look at how well our results confirm the usual expectations of how one takes the large- N limit; we compare mass ratios in strong and weak coupling; and we demonstrate that the spectrum of $SO(4)$ gauge theories appears to know about the spinorial excitations even though there are no explicit spinorial fields present. Finally our concluding section summarises and discusses the results of this paper.

Another interesting physics question which we have addressed elsewhere in some detail is the deconfining transition [8] and, as remarked above, in [7] we showed how the fact that certain $SO(N)$ theories have the same Lie algebras as certain $SU(N')$ theories, may impose strong constraints upon the N -dependence of both $SO(N)$ and $SU(N)$ gauge theories. In addition the question of whether the Z_N centre symmetry, or at least its manifestation in

k -strings, is recovered in some sense as one approaches $N = \infty$ will be addressed elsewhere. Finally we remark that our initial exploratory calculations comparing $SO(N)$ and $SU(N)$ gauge theories were presented some time ago in [5], and some of the results of the present paper have appeared in [9].

2 Relations between $SU(N)$ and $SO(N)$

2.1 large N

In $SU(N)$ gauge theories all-order diagrammatic arguments [10], supported by lattice calculations [11, 6], indicate that mass ratios equal their $N = \infty$ values up to $O(1/N^2)$ corrections:

$$\frac{M_i}{M_j} \stackrel{N \rightarrow \infty}{\cong} \tilde{r}_{ij} + \frac{\tilde{c}_{1,ij}}{N^2} + \frac{\tilde{c}_{2,ij}}{N^4} + \dots \quad : \quad SU(N) \quad (1)$$

where \tilde{r}_{ij} is the value of the mass ratio in the $SU(\infty)$ theory. In $SO(N)$ gauge theories a similar diagrammatic analysis [1] suggests that

$$\frac{M_i}{M_j} \stackrel{N \rightarrow \infty}{\cong} r_{ij} + \frac{c_{1,ij}}{N} + \frac{c_{2,ij}}{N^2} + \dots \quad : \quad SO(N) \quad (2)$$

Moreover the leading planar diagrams are the same in both cases [1], so we might expect an identical $N = \infty$ spectrum, i.e.

$$\tilde{r}_{ij} = r_{ij} \quad (3)$$

in the common $C = +$ sector of the two theories. One of the purposes of our calculations in this paper is to test this expectation. We also recall that a planar $N = \infty$ limit requires that we hold $g^2 N$ fixed as $N \rightarrow \infty$, and to obtain the same limit in $SO(N)$ and $SU(N)$ we need to match the couplings as [1]

$$g^2|_{SO(N)} \stackrel{N \rightarrow \infty}{\cong} 2 \times g^2|_{SU(N)} \quad (4)$$

or, equivalently, we need to match $SO(2N)$ and $SU(N)$ theories at the same coupling. That this holds beyond perturbation theory is something we will test in this paper. Finally we remark that there exists a large- N orbifold equivalence between $SO(2N)$ and $SU(N)$ gauge theories [2] which has been shown [3] to imply that at $N = \infty$ the theories have the same physics, in their common sector of states.

We recall that g^2 has dimensions of mass in $D = 2+1$ and so we can compare dimensionless ratios $M_i/g^2 N$ in the different theories, which we will do later on in this paper. In addition, one of the masses can be the square root of the confining string tension σ .

An important aside is that although $SO(2N)$ and $SU(N)$ gauge theories have identical planar limits, the former has just a Z_2 centre while the latter's centre is Z_N , and the centre of $SO(2N + 1)$ is trivial. This raises interesting questions about the confining properties of these theories, especially for odd N .

2.2 Lie algebra equivalences

Where an $SO(N)$ and $SU(N')$ gauge group share the same Lie algebra the naive expectation is that corresponding physical quantities should be equal. For colour singlet quantities such as $C = +$ ‘glueball’ masses, what the ‘corresponding physical quantities’ are is obvious. For flux tubes and string tensions this is less obvious, because these carry flux in a certain representation of the group, and one needs to establish the ‘corresponding’ representations. One needs to be equally careful with couplings, since these can be defined in various ways. In this section we briefly summarise what the correspondences are for the three such pairs of groups.

Testing these expectations is necessary because, for example, $SU(2)$ and $SO(3)$ have different topology, and so large field fluctuations will not be identical. This may affect the glueball spectrum and/or the string tension. (It will certainly do so at strong coupling.) One of the main purposes of our calculations is to test the validity of these naive expectations.

2.2.1 $SU(2)$ and $SO(3)$

As is well known, $SO(3)$ is locally equivalent to $SU(2)$ in the adjoint representation. Since the fundamental of $SO(3)$ is a $\underline{3}$ and this is just the $J = 1$ (adjoint) representation of $SU(2)$, fundamental $SO(3)$ flux tubes will correspond to $SU(2)$ flux tubes carrying adjoint flux. These adjoint flux tubes are expected to be unstable (they can be broken by gluon pairs from the vacuum) and can decay to the vacuum and, once they are long and massive enough, into glueballs. This instability is consistent with the fact that $SO(3)$ does not possess a non-trivial center which would prevent the mixing of a winding flux tube operator with the contractible operators that project onto glueball states. Thus the σ extracted in $SO(3)$ corresponds to the adjoint string tension in $SU(2)$. This is not straightforward to test since there are no really precise calculations of the $SU(2)$ adjoint string tension. Existing calculations of the latter [6, 12] do however support the approximate validity of Casimir scaling [13], which asserts that the ratio of string tensions corresponding to flux tubes carrying flux in representations R and R' is given by

$$\frac{\sigma_R}{\sigma_{R'}} = \frac{C_2(R)}{C_2(R')} \quad (5)$$

where $C_2(R)$ is the quadratic Casimir of R . In our case this predicts

$$\frac{\sigma_{adj}}{\sigma_f} = \frac{8}{3} \quad ; \quad SU(2). \quad (6)$$

In practice we shall use the values obtained in [6, 12] rather than this very rough estimate, since those calculations use the same methods as used in this paper.

To compare $SU(2)$ and $SO(3)$ couplings it is useful to recall the study of mixed fundamental-adjoint $SU(2)$ actions, where the fundamental and adjoint lattice actions have $1/g_f^2$ and $1/g_a^2$ factors respectively [14]. Using the standard plaquette action (for notation see Section 3.1)

we can write this mixed lattice action, for $SU(N)$, as

$$S = \beta_f \sum_p \left\{ 1 - \frac{1}{N_f} \text{ReTr}_f U_p \right\} + \beta_a \sum_p \left\{ 1 - \frac{1}{N_a} \text{Tr}_a U_p \right\} \quad (7)$$

where U_p is the ordered product of link matrices around the boundary of the plaquette p . Here the first term is in the fundamental and the second is in the adjoint, with f, a denoting fundamental and adjoint respectively. For $SU(N)$, we have $N_f = N$, $N_a = N^2 - 1$, $\beta_f = 2N_f/ag_f^2 = 2N/ag_f^2$ and $\beta_a = 2N_a/ag_a^2 = 2(N^2 - 1)/ag_a^2$. Using $\text{Tr}_a U = |\text{Tr}_f U|^2 - 1$ we expand the group elements in terms of Lie algebra potentials, and obtain the standard continuum action with a prefactor of $1/g^2$ if we choose

$$\frac{1}{g^2} = \frac{1}{g_f^2} + \frac{2N}{g_a^2}. \quad (8)$$

So if we use actions that are entirely adjoint or entirely fundamental, then we will get the same physics if we use

$$g_a^2 = 2Ng_f^2 \stackrel{SU2}{=} 4g_f^2 \quad (9)$$

and this is one of the relations we will wish to test via the $SO(3)$ lattice calculations in this paper.

2.2.2 $SU(4)$ and $SO(6)$

Since $SU(4)$ and $SO(6)$ also have the same Lie algebra, we might expect that their $C = +$ glueball spectra will be identical. For the string tensions, we need to know what the fundamental of $SO(6)$ corresponds to in $SU(4)$. Now we recall that in $SU(4)$

$$\underline{4} \otimes \underline{4} = \underline{6} \oplus \underline{10} \quad (10)$$

where the $\underline{6}$ corresponds to the $k = 2$ antisymmetric representation (which indeed is $C = +$ for $SU(4)$) and this will map to the fundamental $\underline{6}$ of $SO(6)$. Thus in testing the equivalence of $SU(4)$ and $SO(6)$ we should compare the $SO(6)$ fundamental string tension to the $k = 2A$ string tension in $SU(4)$ which, in terms of the fundamental $SU(4)$ string tension, has the value [6] (see also [15])

$$\frac{\sigma_{2A}}{\sigma_f} = 1.357 \pm 0.003 \quad ; \quad SU(4). \quad (11)$$

This implies that when we calculate glueball masses in units of the string tension, the relevant comparison to make is

$$\left. \frac{M_G}{\sqrt{\sigma}} \right|_{so6} \stackrel{?}{=} \left. \frac{M_G}{\sqrt{\sigma_{2A}}} \right|_{su4} \quad (12)$$

To determine the relationship between the $SU(4)$ and $SO(6)$ couplings we use the same argument as for $SU(2)$ and $SO(3)$. Working with the $SO(6)$ action should be equivalent to

working in $SU(4)$ with the fields in the $k = 2A$ representation. So one can think of using a mixed $SU(N)$ lattice plaquette action

$$S = \beta_f \sum_p \left\{ 1 - \frac{1}{N_f} \text{ReTr}_f U_p \right\} + \beta_{2A} \sum_p \left\{ 1 - \frac{1}{N_{2A}} \text{Tr}_{2A} U_p \right\} \quad (13)$$

where

$$\beta_f = 2N_f/g_f^2 \quad ; \quad \beta_{2A} = 2N_{2A}/g_{2A}^2 \quad (14)$$

analogous to the mixed fundamental-adjoint action in eqn(7). For $SU(4)$, the sizes of the representations are $N_f = 4$, $N_{2A} = 6$. Using

$$\text{Tr}_{2A} U_p = \frac{1}{2} \{ (\text{Tr}_f U_p)^2 - \text{Tr}_f U_p^2 \} \quad (15)$$

and performing a weak coupling expansion we find that

$$g^2|_{so6} = g_{2A}^2|_{su4} = 2g_f^2|_{su4} \quad (16)$$

It is interesting to compare this to the leading-order large- N expectation that we should match fundamental couplings of $SO(2N)$ and $SU(N)$ theories, i.e. $g^2|_{so6} = g^2|_{su3}$ in the present case. For $SU(N)$ theories the leading order expectation is that we keep the 't Hooft coupling constant, i.e. $4g^2|_{su4} = 3g^2|_{su3}$. All this leads to the expectation

$$g^2|_{so6} \stackrel{\text{large } N}{=} g^2|_{su3} \stackrel{\text{large } N}{=} \frac{4}{3} g^2|_{su4} \quad (17)$$

which is quite different from eqn(16). That is to say, the leading large- N result is certainly a poor approximation when applied to g^2 at small values of N .

2.2.3 $SU(2) \times SU(2)$ and $SO(4)$

The Lie algebra equivalence of $SO(4)$ and $SU(2) \times SU(2)$ suggests that the glueball spectra of these two gauge theories might be the same. Now, the glueball spectrum of $SU(2) \times SU(2)$ will consist of two sets of glueballs that do not interact with each other, each being identical to that of $SU(2)$. There will be multi-glueball states consisting of some glueballs from one $SU(2)$ and some from the other, so the spectrum of $SU(2) \times SU(2)$ is not identical to that of $SU(2)$. (Especially in a finite volume.) However the single particle spectrum should be the same, and that is what we are primarily interested in calculating in this paper.

Along the same lines, we would naively expect that the fundamental $SO(4)$ flux tube contains fundamental flux of each of the two $SU(2)$ groups, and since these two fluxes do not interact, we should have

$$\sigma|_{so4} = 2 \sigma|_{su2} . \quad (18)$$

We will test this relation below.

As for the couplings, one would expect the $SU(2)$ and $SO(4)$ couplings to be the same, except for the fact that the $SU(2)$ group elements are 4×4 matrices. To compensate for the extra trace factors, we expect the actual relationship between the couplings to be

$$g^2|_{so4} = 2 g_f^2|_{su2} \quad (19)$$

2.3 predicting $SO(N)$ from $SU(N)$

Let us assume we know the glueball spectrum of $SU(N)$ theories. What does that tell us about the spectrum of $SO(N)$ gauge theories? If we assume that (i) the single particle spectra of both $SO(3)$ and $SO(4)$ are the same as that of $SU(2)$, (ii) the spectrum of $SO(6)$ is the same as that of $SU(4)$, (iii) the spectra of $SO(\infty)$ and $SU(\infty)$ are the same, then this will strongly constrain the spectrum of $SO(N)$ gauge theories for all N . In particular for any mass ratio where the expansion in eqn(2) needs only terms up to $O(1/N^3)$ to accurately describe the N -dependence for $N \geq 3$, these constraints means that the N -dependence is completely determined by the values in $SU(N)$.

More generally the $SO(N)$ and $SU(N)$ mass ratios are mutually constrained through eqn(2) and eqn(1) by such Lie algebra and large- N equivalences. Obviously these constraints become stronger the fewer the terms needed in eqns(1,2) to describe the mass ratio for $SO(N \geq 3)$ and $SU(N \geq 2)$. What makes these observations relevant is that in practice, as we shall see below, one only needs one or two corrections to describe the N -dependence of ratios of a number of the lightest masses in $SO(N)$ gauge theories. And this is also the case in $SU(N)$ [6]. This interesting relation between $SO(N)$ and $SU(N)$ gauge theories is explored in detail in [7] and we refer the reader to that paper.

3 Preliminaries

3.1 calculating on the lattice

Our lattice field variables are $SO(N)$ matrices, U_l , residing on the links l of the $L_s^2 L_t$ or $L_x L_y L_t$ lattice whose spacing is a and upon which we impose periodic boundary conditions. The Euclidean path integral is $Z = \int \mathcal{D}U \exp\{-S[U]\}$ where $\mathcal{D}U$ is the Haar measure. We use the standard plaquette action,

$$S = \beta \sum_p \left\{ 1 - \frac{1}{N} \text{Tr} U_p \right\} \quad ; \quad \beta = \frac{2N}{ag^2} \quad (20)$$

where U_p is the ordered product of link matrices around the plaquette p . As a convenient shorthand, we shall use $u_p \equiv \frac{1}{N} \text{Tr} U_p$. We have written $\beta = 2N/ag^2$, but strictly speaking ag^2 is just one possible definition of the dimensionless coupling on the length scale a , so if we were to be punctilious we would write $\beta = 2N/ag_p^2$ with $ag_p^2 = ag^2 + ca^2g^4 + \dots \rightarrow ag^2$ as $a \rightarrow 0$.

We update the fields using a natural extension to $SO(N)$ [5, 9] of the standard $SU(N)$ Cabibbo-Marinari algorithm. Suppose we generate N_z field configurations, $\{U_l\}^{I=1, \dots, N_z}$, with the measure $\mathcal{D}U \exp\{-S[U]\}$. Then we can estimate the expectation value of some functional Φ of the fields (this may be a correlation function) by the simple average,

$$\langle \Phi[U] \rangle = \frac{1}{Z} \int \mathcal{D}U \Phi[U] \exp\{-S[U]\} = \frac{1}{N_z} \sum_{I=1}^{N_z} \Phi[U^I] + O(1/\sqrt{N_z}), \quad (21)$$

where the last term denotes the statistical error. In our calculations we only use heat bath updates, although it would be desirable to include over-relaxation so as to accelerate the exploration of the theory's phase space.

3.2 calculating energies

Our $SO(N)$ calculations closely parallel those in $SU(N)$, so we will be brief here and refer the reader to other papers [11, 6] for details. It is of course important to be aware when these calculations become less reliable, and this will be addressed in Section 3.6.

3.2.1 glueball masses

In two spatial dimensions the rotation group is Abelian and spins are $J = 0, \pm 1, \pm 2, \dots$ (ignoring more exotic possibilities such as anyons). Parity, P , does not commute with rotations, $J \xrightarrow{P} -J$, so particle ('glueball') states can be labelled by parity $P = \pm$ and $|J|$. (Charge conjugation is necessarily positive for $SO(N)$.) For $J \neq 0$ the above implies that continuum $P = \pm$ states in an infinite volume are necessarily degenerate although this is not necessarily true for even J at finite lattice spacing and/or in a finite volume [11, 16]. Thus a useful check that our volume is large enough and that our lattice is fine enough, is provided by comparing the $J^P = 2^+$ and 2^- masses.

Ground state masses M are calculated from the asymptotic time dependence of correlators, i.e.

$$\langle \phi^\dagger(t)\phi(0) \rangle = \sum_n |\langle vac | \phi^\dagger | n \rangle|^2 e^{-E_n t} \xrightarrow{t \rightarrow \infty} e^{-Mt} \quad (22)$$

where M is the mass of the lightest state with the quantum numbers of the operator ϕ . The operator ϕ will be the product of $SO(N)$ link matrices around some closed path, with the trace then taken. We will use zero momentum operators so that there is no momentum integral on the right side of eqn(22). To calculate the excited states E_n in eqn(22), one calculates (cross)correlators of several operators and uses these as a basis for a systematic variational calculation in e^{-Ht_1} where H is the Hamiltonian (corresponding to our lattice transfer matrix) and t_1 is some convenient distance. (Typically we choose $t_1 = a$.) To have good overlaps onto the desired states, so that one can evaluate masses at values of t where the signal has not yet disappeared into the statistical noise, one uses blocked and smeared operators. (For more details see e.g. [11, 6].)

An obvious remark. On a lattice $t = an_t$ and what we know is the number of lattice spacings n_t . So fitting an exponential as in eqn(22) to some correlation function, will give us the value of $Mt = Man_t$. That is to say, what we obtain is a value for aM , the mass in lattice units.

Another remark: in reality the $t \rightarrow \infty$ limit is not accessible in a numerical calculation. This is trivially so because our lattice has a finite extent in time, but more importantly because the statistical errors on pure glue correlators are (usually) roughly constant in t so the error to signal ratio grows roughly exponentially in t . In practice what one does is to find the lowest value $t = t_0$ such that the correlator $C(t) = \langle \phi^\dagger(t)\phi(0) \rangle$ can be fitted with a single exponential

$\propto \exp(-Mt)$ for $t \geq t_0$, and one takes M as the estimate of the true mass. This procedure works well if aM is small enough that many values of $C(t = an_t \geq t_0)$ have small errors. Otherwise the fact of a ‘good’ fit may not be very significant. This will be a problem when the mass aM is not small, but also when the overlap of the glueball wave-functional onto our operator basis is not close to unity. The latter turns out, unfortunately, to be the case in our $SO(N)$ calculations at small N , in contrast to $SU(N)$. The accompanying systematic errors are discussed in more detail in Section 3.6.3

We are on a square lattice so we have exact rotational invariance only under rotations of $\pi/2$. So for each operator ϕ_0 we can construct the rotated operators, $\phi_{\pi/2}$, ϕ_π , $\phi_{3\pi/2}$ and we can use these to construct a spin J operator

$$\phi_J(t) = \sum_{n=0}^3 \phi_{n\pi/2}(t) \exp\{iJn\pi/2\}. \quad (23)$$

Since this sum is invariant under $J \rightarrow J + 4$, such an operator will in fact project onto the tower of spins $J + 4n$ with n any integer. For simplicity we will refer to the states as having a spin equal to the minimum of these spins. (Often, but not always, the lightest glueball in such a tower does indeed possess the minimal spin.) If we decide to use parity eigenstates, then we start with the operator $\phi_0^{P=\pm} = (1 \pm P)\phi_0$, construct its rotations $\phi_{n\pi/2}^{P=\pm}$, and sum these up as in eqn(23) to obtain $\phi_J^{P=\pm}(t)$. Note that in this sum the parity inverse of the rotated operator ϕ_θ is a rotation by $-\theta$ of $P\phi_0$, i.e. the $P = \pm$ operators have definite $|J|$ but not definite J . For notational simplicity we shall, nonetheless, label our operators by the symbol J . Thus using $J = 0, 1, 2$ and $P = \pm$ operators we can obtain states of all spins and parities, $J^P = 0^\pm, 1^\pm, 2^\pm, \dots$

We now briefly describe one of the two sets of operators that we use in our glueball calculations. We take products of $SO(N)$ matrices around closed curves \mathcal{C} . The simplest such curves are the 1×1 plaquette, and the 1×2 , 1×3 , \dots rectangles. The square plaquette is invariant under $\pi/2$ rotations and so will only project on to $J = 0$ states while the rectangles are invariant under π rotations and so will only project on to $J = 0$ and $J = 2$ states. These curves are also invariant under parity and so will only project on to $P = +$ states. Hence, we need to consider more complicated curves to project on to $J = 1$ and $P = -$ states. To do this, we consider curves constructed from squares and rectangles that have no rotational or reflection symmetry. We show four such curves in Figure 1. We use twelve such curves to build, by rotations and reflections, a basis for each J^P state of twelve operators as described above. We also use two rectangle-based operators for 0^+ and 2^+ states and the plaquette for the 0^+ state. This means that we have a basis of fifteen elementary operators for the 0^+ state and a basis of fourteen elementary operators for the 2^+ state. We then add operators based on the same curves but with the links replaced by ‘blocked links’. We recall [11] that these blocked link matrices join pairs of sites that are 1, 2, 4, 8, \dots lattice spacings apart: 2^{n_B-1} spacings apart at blocking level n_B . We typically include all blocking levels such that the blocked link fits into the lattice e.g. up to blocking level 6 (length=32) on a 44^2 spatial lattice. So, for example, in this case the total number of operators is $6 \times 15 = 80$ for the 0^+ and the variational analysis will produce for us 80 supposed (approximate) eigenstates. It is

not implausible that this basis is large enough that we have a good enough overlap onto the lightest few states in each J^P channel, without missing any. As an explicit check of this we will later compare spectra obtained with this basis and the somewhat different (and larger) basis that is being used in similar $SU(N)$ calculations [6]. We remark that this alternative basis is the one used in our $SO(3)$, $SO(5)$ and $SO(6)$ spectrum calculations.

3.2.2 string tensions

To calculate the string tension σ we calculate the ground state energy $E(l)$ of a flux tube that winds around a periodic spatial torus of length l . If the length $l = aL_s$ of the torus is large then $E(l) \simeq \sigma l$ where σ is the string tension. At finite l there are corrections to this and we assume that for our range of l these are accurately incorporated in the simple ‘Nambu-Goto’ expression

$$E(l) = \sigma l \left\{ 1 - \frac{\pi}{3\sigma l^2} \right\}^{1/2} \quad (24)$$

which is what we shall use to extract σ from $E(l)$. This expression incorporates all the known universal corrections to the flux tube energy, when one expands $E(l)$ in powers of $1/l^2\sigma$ [17]. (See also [18].) It has also been shown to arise as a good approximation at small l from the near-integrability of the world-sheet action [19]. Moreover it has been checked numerically with some precision in $SU(N)$ for flux tubes carrying both fundamental and higher representation fluxes. (See e.g. [12, 20] and references therein.) We shall provide some checks for $SO(N)$ in Section 4.

The flux tube energy can be calculated just like a glueball mass, except that instead of taking products of our matrices around contractible loops, we do so about the non-contractible loops that wind once around the torus. The simplest such operator is the Polyakov loop l_p , i.e. the trace of the product of link matrices along a minimal length curve that closes around the spatial torus,

$$l_p(n_t) = \sum_{n_y} \text{Tr} \left\{ \prod_{n_x=1}^{L_x} U_x(n_x, n_y, n_t) \right\}, \quad (25)$$

where we have taken the product of the link matrices in the x -direction around the x -torus of length $l = aL_x$, with $(x, y, t) = (an_x, an_y, an_t)$, and we sum over n_y to produce an operator with zero transverse momentum, $p_\perp = p_y = 0$. We also use blocked/smeared versions of this. Most of our calculations of the string tension use this set of operators. However some calculations, in particular most of the $SO(3)$, $SO(5)$ and $SO(6)$ ones, use a much larger basis of operators, which incorporates a variety of non-minimal winding curves. Such a large basis is essential for obtaining excited flux tube states, but makes little difference to the ground state calculations that are of interest in this paper.

For even N , the theory has a Z_2 symmetry that ensures that $\langle l_p \rangle = 0$ as long as the symmetry is not spontaneously broken, and indeed that $\langle l_p \phi_G \rangle \equiv 0$ where ϕ_G is any contractible loop (such as one uses for glueball operators). That is to say we have a stable flux tube state that winds around the torus. (Of course, linear confinement only arises if the flux does not spread out arbitrarily far, which is an additional dynamical question.) For N odd we have

no Z_2 symmetry to invoke and whether such theories are linearly confining is an interesting question that we shall address later on in this paper.

3.3 continuum limit

Given a value of β in eqn(20) we can calculate some masses (or energies) am_i and the string tension, $a^2\sigma$, in lattice units, as described above. However what we want is the spectrum in some physical units in the continuum limit $\beta \rightarrow \infty$. We can take ratios of masses so that the lattice units cancel $am(a)/a\mu(a) = m(a)/\mu(a)$, but this ratio will still depend on the discretisation a . However the fact that the theory becomes free at short distances, since g^2 has dimensions of $[m]$ so that the dimensionless expansion parameter for physics on the length scale l will be $g^2 l \xrightarrow{l \rightarrow 0} 0$, allows us to control the expansion of the lattice action in terms of continuum fields as $a \rightarrow 0$. For our plaquette action it is known that the leading correction is $O(a^2)$, i.e.

$$\frac{am_i(a)}{am_j(a)} = \frac{m_i(a)}{m_j(a)} = \frac{m_i(0)}{m_j(0)} + c_{ijk}a^2m_k^2(a) + O(a^4). \quad (26)$$

One can use any (sensible) mass m_k to set the scale of the corrections; different choices, as well as the a -dependence of m_k , will merely reshuffle the higher order terms. It clearly makes sense to use for m_k , and indeed for m_j , the most accurately calculated mass. For $SU(N)$ this is usually the string tension, i.e. we use eqn(26) with $am_j = am_k = a\sqrt{\sigma}$ and determine the ratio $m_i/\sqrt{\sigma}$ in the continuum limit for each m_i . For $SO(N)$ the lightest scalar glueball is equally accurate and one can use that to set the scale just as well.

Since the coupling g^2 has dimensions of mass, we can perform an alternative continuum extrapolation for individual masses as follows:

$$\frac{\beta}{2N}am_i(a) = \frac{m_i}{g^2} + \frac{c_i}{\beta} + \dots \quad (27)$$

where we have used $\beta = 2N/ag^2$. Note that here the leading correction is $O(a)$ rather than $O(a^2)$. This has to be so because different couplings are related by $ag_p^2 = ag_q^2 + c(ag_q^2)^2 + \dots$. In fact we shall often make use of this freedom to replace β in eqn(27) by the ‘mean-field improved’ coupling $\beta_I = \beta\langle TrU_p \rangle/N$ [21]. While the approach to the continuum in eqn(27) is slower than in eqn(26), the error on βam_i is smaller than that on $m_i/\sqrt{\sigma}$ because there is no error on the value of β . We shall use both forms of extrapolation in this paper.

3.4 large N limit

Once we have continuum limits of mass ratios for various $SO(N)$ groups we can extrapolate these to $N = \infty$ just as for $SU(N)$ except that the leading correction is expected to be $O(1/N)$ [1]:

$$\left. \frac{m_i}{\mu} \right|_N = \left. \frac{m_i}{\mu} \right|_\infty + \frac{c}{N} + \frac{c'}{N^2} + \dots \quad (28)$$

Here μ may be a glueball mass, e.g. the mass gap, or the string tension $\sqrt{\sigma}$, or the coupling g^2 . In this last case, large N counting tells us that we should use the 't Hooft coupling g^2N :

$$\left. \frac{m_i}{g^2N} \right|_N = \left. \frac{m_i}{g^2N} \right|_\infty + \frac{c}{N} + \frac{c'}{N^2} + \dots \quad (29)$$

In performing the extrapolations it makes sense to choose an energy scale μ which does not possess unusually large $O(1/N)$ corrections. In particular we will need to be cautious about using the string tension σ , since the Lie algebra equivalences tell us that the $SO(N)$ fundamental string tensions at low N map onto higher representation string tensions in $SU(N)$. We also need to be cautious about using g^2N since we have seen in Section 2.2 that the matching of g^2 between $SO(N)$ and $SU(N)$ at small N deviates strongly from the leading large- N expectations.

3.5 bulk transition

Lattice gauge theories generally possess a ('bulk') transition between the strong and weak coupling regions, where the natural expansion parameters are $\beta \propto 1/ag^2$ and $1/\beta \propto ag^2$ respectively. Since the extrapolation to the continuum limit should, á priori, be made from values of masses calculated within the weak coupling region, it is important to locate any such bulk transition, whether it be a cross-over or a genuine phase transition. It is clearly desirable that this transition should occur at a value of β where the value of a on the weak coupling side is not very small, otherwise prohibitively large lattices may be needed to ensure that the volume is adequately large, in physical units, when in the weak coupling confining phase. The location of the transition will depend on the lattice action used and all our remarks here are for the simple plaquette action.

For $D=3+1$ $SU(N)$ gauge theories it is known that the transition is first order for $N \geq 5$ and is a cross-over for smaller N [11]. In $D=2+1$ $SU(N)$ gauge theories it appears [22] to be quite similar to the Gross-Witten transition in $D=1+1$ [23] i.e. a gentle cross-over for all $N < \infty$ developing into a third-order transition at $N = \infty$. It's location in $D = 3 + 1$ is such that on the weak coupling side we can readily go to $a \sim 1/5T_c$ where T_c is the deconfining temperature (taking advantage of the metastable region when the transition is first order). In $D = 2 + 1$, we can go to even larger a , $a \sim 1/1.6T_c$. These lattice spacings are large enough that, for $SU(N)$, the bulk transition presents no significant obstacle to continuum extrapolations.

For $SO(N)$ lattice gauge theories the situation is different. In $D = 3 + 1$ one finds that the transition is again first order, but now for all $N \geq 3$ [5]. Moreover at low N the value of a on the weak coupling side is very small and can pose an obstacle to accessing the continuum limit [5]. (Indeed, in the case of $SO(3)$ this has been known for a long time; for a recent discussion see [24].) Fortunately in $D = 2 + 1$, the case of relevance here, the corresponding problems are much less severe. There is a transition [5, 9] whose signature is a finite region of β in which the mass gap decreases towards zero as we increase β towards some β_b . The approximate values of β_b are listed in Table 1, where we also give the value of the lightest scalar glueball obtained on the weak coupling side of the transition. One can use this, as

discussed in Section 3.6.4, to provide a rough lower bound on the spatial volume needed to avoid large finite volume effects on the lightest scalar and tensor glueball states. This bound is also given in Table 1. We see that quite a large lattice is needed, especially for $SO(3)$, but since we are in $D = 2 + 1$ this problem is readily surmountable.

The fact that at low N , e.g. for $SO(3)$, the bulk transition occurs at a small value of a , prompts the question of how precisely ‘strong-coupling’ manifests itself below the bulk transition. We shall address this in Section 7.3.

The bulk transition in $D = 2 + 1$ $SO(N)$ gauge theories does not possess the usual features of a second-order phase transition despite the (nearly) vanishing mass gap. In particular it has a peculiar volume dependence. Its unusual characteristics presumably flow from the fact that the $SO(N)$ group is not simply connected. This makes it an interesting transition which merits a more detailed investigation.

3.6 systematic errors

Our aim in this paper is to calculate the string tension and the lighter part of the glueball spectrum. Such a calculation is affected by a number of ‘systematic’ errors that cannot be easily quantified. In this Section we briefly discuss what we believe to be the most important of these, how they may affect our results, and how we try to minimise them.

3.6.1 wrong quantum numbers

Our square spatial lattice is invariant under a subgroup of the full rotation group. Thus our rotationally invariant operator will project onto states not only with continuum spin $J = 0$ but also with $|J| = 4, 8, \dots$. Similarly the ‘ $|J| = 2$ ’ operator will project onto $|J| = 2, 6, \dots$ and ‘ $|J| = 1$ ’ projects onto $|J| = 1, 3, \dots$. To the extent that we only calculate the lowest one or two masses in each representation it is plausible that labelling the states by the lowest continuum J that can contribute will often turn out to be correct. However there are known counter examples in the closely related case of $SU(N)$ gauge theories. In particular there is very good evidence that the ground state ‘ 0^- ’ state is in fact 4^- [16, 25] and also that the lightest ‘ $J = 1$ ’ state is in fact $J = 3$ [16, 25]. In principle one could imagine using parity doubling to distinguish $J = 4$ states from $J = 0$ states (more discriminatory in $D = 3 + 1$ because of the varying multiplet structure) but the anticipated 4^+ mass is in a region of the ‘ $J^P = 0^+$ ’ spectrum which is already quite dense and identifying near-degeneracies, given the usual statistical errors, would pose a formidable numerical challenge. We shall therefore make no attempt here to distinguish spins that differ by a multiple of 4, and will simply label states by the lowest contributing J . Anyone who uses our spectrum to confront a model calculation needs to be aware of this potential mislabelling.

3.6.2 missing states

Our variational calculation purports to give the spectrum of a number of states starting with the ground state. How well it does this will of course depend on how well the basis of operators

encodes the desired states. The blocking/smearing was designed to produce operators with a good projection onto the lightest states, which we expect to have minimal structure, but we do not know enough about excited glueball wavefunctionals to be confident that we do well for such states. Since in practice we have trouble identifying a state (within errors) unless its overlap (normalised and squared) onto our basis is well above 0.5, it is quite possible that our calculated spectrum has some missing intermediate states.

While one way to check for this possibility is to redo the calculations using ever larger operator bases, another way is to compare the spectrum with what one obtains using a completely different basis of operators. Since we have two independently produced bases, one used for calculating the spectra for $N = 3, 5, 6$ (labelled A) and the other for $N = 4, 7, 8, 12, 16$ (labelled B) we have been able to perform such a comparison in a few cases. A typical example is provided in Table 2 where we compare the spectra obtained in $SO(4)$ at $\beta = 51$ using the two different bases A and B. (The lattice volumes are not identical, but are similar enough that this mismatch can be ignored.) We include here all the states of the spectrum that we will be considering later on in this paper. We see that in most cases the energies of corresponding states agree within 2σ . (We use the same symbol for the standard deviation and the string tension; which is meant should be clear from the context.) Only for the 2^\pm and the 0^{+**} are the differences more than 2σ , although still within 3σ . We conclude that within the (sometimes quite large) errors this provides no evidence that there are missing states in the part of the spectrum shown.

This result is not in fact an accident. If we go to higher excited states then we do find that some states with one operator basis do not appear when using the other basis, i.e we have evidence of missing states. Our choice of where to cut off the spectrum in our study was, in fact, partly determined by this comparison.

Finally we should mention that the statistics of the ‘Ops A’ calculation in Table 2 is much higher than that of our other calculations, including the ‘Ops B’ calculation listed in Table 2, This means that the statistical errors on the correlators $C(t)$ are smaller and hence one can extract more reliably the range $t \geq t_0$ from which one determines the mass. This typically leads to a larger estimate of t_0 and, given the positivity of the correlator, to a lower value for the mass. This is presumably the reason that the ‘Ops A’ masses in Table 2 are all slightly below those of the ‘Ops B’ calculation.

3.6.3 identifying energy plateaux

For any given set of quantum numbers our variational calculation produces a set of $p = 0$ operators Ψ_i ; $i = 0, 1, ..$ that are approximate energy eigenoperators (ordered in energy). While the eigenvalues give us a rough first estimate of the energies, to obtain our final best estimate we take the correlators $\langle \Psi_i^\dagger(t)\Psi_i(0) \rangle$ and look for the single exponential decays at larger t , as in eqn(22), so obtaining the corresponding energy E_i . This is the crucial step in obtaining glueball masses and it is important to be aware that some of the resulting mass estimates will be less reliable than others.

Consider first extracting the ground state energy E_0 in some J^P channel. We can define

an effective energy $E_{eff}(t)$ by

$$\frac{\langle \Psi_0^\dagger(t) \Psi_0(0) \rangle}{\langle \Psi_0^\dagger(t-a) \Psi_0(0) \rangle} = e^{-aE_{eff}(t)}. \quad (30)$$

(We shall sometimes use $M_{eff}(t)$ in place of $E_{eff}(t)$.) From eqn(22) we know that $E_{eff}(t \rightarrow \infty) = E_0$. However we have finite statistical errors on E so we cannot access the $t \rightarrow \infty$ limit and instead we search for a t_0 such that $E_{eff}(t) = \text{constant}$ for $t \geq t_0$, within the errors, and this constant then provides our estimate of E_0 . The range $t \geq t_0$ is where we have an ‘effective energy (or mass) plateau’ and identifying such a plateau is a crucial step in estimating E_0 . The major obstacle here is that for typical glueball calculations the statistical error on the correlator is roughly constant in t while its average value is decreasing exponentially in t , at least as fast as $\propto \exp\{-E_0 t\}$. Thus when the ground state energy aE_0 is large, there will be very few values of $E_{eff}(t)$ with small errors and it may be that the apparent plateau is not statistically significant. So heavier ground states are generally less reliable than lighter ones and with our statistics one has to be cautious once $aE > 1$ (roughly speaking). The obvious danger is that one estimates E_0 using a value of $E_{eff}(t)$ at a value of t that is too small. Since $E_{eff}(t)$ decreases monotonically with t (because of the reflection positivity of our plaquette action) this means that we overestimate the true energy, E_0 . For light states this error will usually be insignificant but, as we shall shortly see, for our heaviest states this may well not be the case. (As we have already noted above, when discussing the comparison between the two $SO(4)$ calculations in Table 2.)

For an excited state Ψ_i we can also define an effective energy $E_{eff}(t)$ using eqn(30) with $\Psi_0 \rightarrow \Psi_i$, and there is a similar caveat for heavy states. However now, even if we can identify the start of a plateau in $E_{eff}(t)$, it is possible that Ψ_i may have a small overlap onto one of the lighter states, so that at sufficiently large t $E_{eff}(t)$ will drop away from the plateau to a smaller value. Thus our criterion is that there should be an ‘effective’ energy plateau $E_{eff}(t) = \text{constant} : t_0 \leq t \leq t_0 + \Delta t$ over some finite range Δt that is large enough for the plateau to be convincing. An additional physical reason for such a behaviour could be that the excited glueball is heavy enough to be unstable. If its decay width is small, so that it is a narrow resonance, it should show a temporary effective energy plateau within errors. As N increases it will become more stable and will extrapolate to a completely stable glueball at $N = \infty$. So it is certainly part of the spectrum that we wish to identify. However a temporary plateau clearly makes that identification more ambiguous.

It is clearly important to assess the importance of the above comments for the mass calculations in this paper. To do this we begin by showing in Figs 2,3 the effective masses we obtain in $SO(12)$ at $\beta = 250$. (Note that in all such plots in this paper we stop plotting the effective energies once the error exceeds about 10% of the value, so as not to confuse the plot with large error bars that usually carry little information.) This β corresponds to the smallest value of the lattice spacing, and therefore provides an important contribution to our continuum extrapolation. Moreover $N = 12$ is one of our largest values of N , so it also plays an important role in the extrapolation to $N = \infty$. It is clear from the plot in Fig. 2 that we can identify the plateaux for the lightest two 0^+ states very accurately, and for at least 2 of

the other 3 states reasonably well. The lightest 2^\pm plateaux in Fig. 3 are well defined, and the excited 2^\pm identification is plausible although not entirely compelling. However the 0^- and 1^\pm plateaux in Fig. 3 are clearly somewhat optimistic. The lesson is that while our 0^+ and 2^\pm estimates should be reliable, at least at these larger values of N , the 0^- and 1^\pm estimates should be treated with caution. All this is characteristic of our mass calculations at larger N when we are on lattices that are close to the continuum limit. Of course a significant role is also played by the masses at smaller β since they help to determine the coefficient of the $O(a^2)$ lattice spacing corrections in our continuum extrapolations. Here the uncertainties are naturally larger. As an example we show in Figs 4, 5 effective mass plots at $\beta = 155$, which corresponds to our second coarsest lattice spacing. Clearly the systematic errors associated with identifying the effective mass ‘plateaux’ are much larger on this lattice. While the ground state 0^+ is unambiguous, and the first excited 0^+ is plausible, the higher excitation plateaux are much less well defined. Identifying the 2^\pm ground states requires some optimism, although this can be argued for on the plausible basis that if the gaps $aM_{eff}(a) - aM_{eff}(2a)$ and $aM_{eff}(2a) - aM_{eff}(3a)$ are small and rapidly decreasing, and the statistical errors are small enough for this statement to be meaningful, then one would expect the effective mass plateau to have a value that is close to $aM_{eff}(3a)$. For the excited 2^\pm states and the ground state 0^- and 1^\pm identifying a plateau from our plots is clearly guesswork. One can make some progress, by noting that with our basis of iteratively blocked operators, the overlap of our best variational operator onto the corresponding excited state should be (very roughly) independent of β . So where we can estimate such an overlap reliably at large β , we can assume roughly the same value at coarser $a(\beta)$ and so estimate at what value of $t = an_t$ we should see an effective mass plateau. In this way we can sometimes estimate effective masses at smaller β even if the statistical errors do not allow a direct identification of the plateau. Such an indirect estimate possesses systematic errors that are presumably not large but are hard to quantify.

We now turn to smaller values of N and, in particular, to $SO(3)$. The reason for doing so is that our comparisons between $SO(N)$ and $SU(N')$ involve small values of N and, as we shall now see, the overlaps turn out to be poorer at small N . We begin by showing in Fig. 6 the effective mass plots for, once again, the lightest five 0^+ states, this time in $SO(3)$. The calculation is at a very small value of a , so we are effectively in the continuum limit here. Comparing to Fig. 2 it is clear that the overlaps of our operators onto the corresponding states are considerably worse in $SO(3)$ than in $SO(12)$, so that the plateaux are pushed out to larger t . While the mass identification for the lightest 3 states looks reliable, it clearly becomes shaky for the higher 2 states. For comparison we also show the corresponding $SU(2)$ effective masses, taken from [6] at a similar small value of a (in units of the mass gap). It is clear that the $SU(2)$ calculation is far more accurate, basically because of the far better overlaps. In Fig. 7 we provide a similar plot for the lightest two 2^- states, and the lightest 0^- and 1^- states. Here only the lightest 2^- mass can be extracted reliably, with some hint of a temporary plateau for the excited 2^- . For the 0^- and 1^- we do the best that we can, which is to use the values at larger t where the energy values overlap within their very large errors. We remark, that the $SO(3)$ overlaps appear to be the worst, with a rapid improvement as N increases.

Given that $SO(3)$ and $SU(2)$ share the same Lie algebra, one might wonder why the overlaps in the former should be so much worse than in the latter. However we should recall that the fundamental of $SO(3)$ corresponds to the adjoint of $SU(2)$, so one should really compare with the overlaps in $SU(2)$ when one uses glueball operators that are in the adjoint representation rather than in the fundamental. This we do in Fig. 8 where we show the effective masses of the lightest three 0^+ glueball states, and the lightest 2^+ , on a $96^2 64$ lattice at $\beta = 23.5$ in $SU(2)$. We also show the effective masses using the same basis of operator loops, but taken (as one would usually do) in the fundamental representation. (For this comparison the operator basis is smaller than that used in Figs. 6, 7.) We see that the adjoint operators have an overlap that gets worse for the 0^+ excited states, and are already much worse for the 2^+ ground state. Comparing the $SU(2)$ adjoint correlators in Fig. 8 against the fundamental $SO(3)$ correlators in Figs. 6, 7, we see that in fact $SO(3)$ and $SU(2)$ do have similar overlaps when we compare corresponding operators. (Aside: in $SU(2)$ we block our links in the fundamental and only take the adjoint at the very end: ideally we should transform our elementary link variables to the adjoint first and then block.)

One plausible argument why adjoint loops in $SU(2)$ might produce poor eigenoperators is as follows. Consider the example of a 2^+ operator. We suppose that a single loop ϕ_0 minus its $\pi/2$ rotation, $\phi_{\pi/2}$ provides our best $|J| = 2$ adjoint eigenoperator, $\phi_a^{J=2} = \text{Tr}_a \phi_0 - \text{Tr}_a \phi_{\pi/2}$, where we indicate that the trace is taken in the adjoint. Using the relation between adjoint and fundamental traces, $\text{Tr}_a l = |\text{Tr}_f l|^2 - 1$, we see that

$$\phi_a^{J=2} = (\text{Tr}_f \phi_0 - \text{Tr}_f \phi_{\pi/2}) \times (\text{Tr}_f \phi_0 + \text{Tr}_f \phi_{\pi/2}) \quad (31)$$

i.e. $\phi_a^{J=2}$ is actually a composite operator that is a product of scalar and tensor operators taken in the fundamental. In a correlator this will project onto states that simultaneously contain scalars and tensors. The lightest scalar state is the vacuum so at large t we will still see the lightest tensor mass, but it is plausible (given that the best fundamental operator has a very good projection) that the overlap of the scalar operator onto scalar glueballs will worsen the overlap onto the lightest tensor. While this argument becomes more elaborate for linear combinations of loops, the basic idea is that $SU(2)$ adjoint operators are composite in terms of the underlying fundamental operators, and that this naturally suggests a poorer overlap if we use the kind of operator basis that works well for the fundamental. A slight variation of this argument can be made to apply to $SO(4)$ if one treats it as $SU(2) \times SU(2)$, but clearly loses applicability as one increases N .

We finish with an important practical observation. As remarked already, the reflection positivity of the action ensures that in an expansion such as eqn(22), the coefficients of the exponentials are indeed non-negative. This means that $E_{eff}(t)$ decreases monotonically with increasing t . That is to say, as we approach the effective energy plateau by increasing t we necessarily do so from above. Thus the characteristic feature of the error that occurs in misidentifying the plateau (something that readily occurs when the overlaps are mediocre) is that the estimate of the energy is larger than the true value. This should be borne in mind when, later on in this paper, we compare masses in various $SO(N)$ and $SU(N')$ theories.

3.6.4 finite volume corrections

As we reduce the spatial volume, l^2 , we eventually encounter a transition at $l \sim l_c = 1/T_c$ where T_c is the deconfining temperature. This is a cross-over at finite N , becoming a phase transition at $N = \infty$. It is related to the phase transition that occurs on a space-time volume $l_x l_y l_t$ when $l_y, l_t \rightarrow \infty$ and $l_x = 1/T_c$, which is, of course, just the deconfining transition with an interchange of spatial and temporal labels. To avoid the dramatic finite volume effects associated with this transition we shall always choose volumes $l \gg l_c$ for our glueball calculations. Note that this finite volume effect is one that survives the $N \rightarrow \infty$ limit.

Once the spatial volume is sufficiently large, the leading finite volume correction to the mass of a glueball G arises from the virtual emission by G of the lightest glueball, g , which then propagates around a spatial torus before being reabsorbed by G . This contribution is $\delta m_G \propto \alpha_{gGG} \exp\{-cml\}$ where m is the mass gap, l is the size of the torus, $c = O(1)$, and α_{gGG} is the triple-glueball coupling squared [26]. Since $ml_c \sim 4$ for both $SO(N)$ [8] and $SU(N)$ [27] theories, this correction is negligibly small if we choose, as we do, to use $l \gg l_c$. In addition, large N counting tells us that $\alpha_{gGG} \rightarrow 0$ as $N \rightarrow \infty$. So this correction vanishes as $N \rightarrow \infty$ for any $l > l_c$.

In practice, in a theory that is linearly confining the important finite volume corrections have to do with the finite volume eigenstates of the Hamiltonian that correspond to flux tubes winding around a spatial torus. In $SO(2N)$ gauge theories the Z_2 center symmetry ensures that a single winding flux loop operator has zero overlap onto a contractible glueball operator, just as in $SU(N)$. However a pair of winding flux loops can have a non-zero overlap and will contribute to glueball correlators. These ‘torelon’ states will have (after subtracting any vacuum expectation value) an energy that is, roughly, twice that of a single flux loop

$$E_T(l) \simeq 2E(l) \simeq 2\sigma l. \quad (32)$$

Here we have neglected the interaction energy between the two flux loops (the first equality) and also finite l string corrections (the second equality). Their interaction means that there may be a whole tower of such resonant torelon states. By adding or subtracting the torelons around the orthogonal spatial tori we obtain torelons with $J^p = 0^+$ and $J^p = 2^+$ respectively. The mixing between these orthogonal torelons means that the $0^+, 2^+$ torelon energies will be (slightly) different from the value of $E_T(l)$ in eqn(32). Now, as l is reduced, $E_T(l)$ decreases and the torelon may become the 0^+ or 2^+ ground state, and even before that may appear as one of the low-lying excited glueball states. As an example consider the 2^+ glueball ground state. For larger N this satisfies, as we shall see, $m_{2^+} \sim 7\sqrt{\sigma}$. The torelon will have a similar energy if we reduce l to $2\sigma l \simeq 7\sqrt{\sigma}$. This corresponds to $l \sim 3.5l_c$ using the fact that one finds $\sqrt{\sigma}/T_c = l_c\sqrt{\sigma} \sim 1$ at large N [8, 27]. This type of estimate allows us to control this type of finite volume correction. For $SO(2N+1)$ there is no centre symmetry and there may be a torelon composed of a single winding flux loop. However as we shall see below such theories are ‘almost’ confining and the overlap of such torelons onto glueball operators appears to be negligible, except possibly for $SO(3)$. So the situation is in practice just as for $SO(2N)$. Finally we note that the mixing between the two flux loops and the local glueball will vanish as $N \rightarrow \infty$ since it involves the matrix element of a single trace operator with a double trace

operator. and so these finite volume corrections should become unimportant at larger N .

In the above paragraph we discussed torelon contributions to the 0^+ and 2^+ . There will also be contributions with other quantum numbers, but these will require at least one of the flux tubes to be in an excited state. These are much heavier [12, 20] and so we assume they will not affect our calculations in this paper. An important remark is that since the 2^+ and 2^- glueball spectra are identical in the continuum limit in an infinite volume, and since the low-lying 2^- spectrum is unaffected by torelons, a comparison between the two spectra at a finite but small lattice spacing provides a good tool for identifying those 2^+ states which are affected by torelons. For the 0^+ spectrum we unfortunately have no analogous procedure.

There is a subtlety to this that is important for low values of N . In addition to torelons composed of pairs of flux tubes in the fundamental representation, there may be torelons composed of pairs of flux tubes in the spinorial representation. As N increases the dimension of the spinorial representation becomes large and so, presumably, will the associated string tension, so any such torelons will be very massive and irrelevant. At low N however they may be light enough to dominate. So, in $SO(3)$ the spinorial is just the fundamental of $SU(2)$ and the corresponding torelon should therefore be about 2.5 times lighter than the fundamental torelon of $SO(3)$ which corresponds to the adjoint of $SU(2)$. In $SO(6)$ the spinorial representation is the fundamental of $SU(4)$ and so the corresponding torelon energy will be about $3/4$ that of the fundamental. So for $N \leq 6$ this needs to be taken into account in coming to a conservative estimate of what is a ‘large enough’ spatial volume for a glueball calculation.

While one can make theoretical estimates of finite volume effects, as we have done above, additional numerical finite volume studies are essential to make sure we have not missed something. So in Table 3 we show the low-lying glueball spectrum as a function of spatial volume in $SO(8)$. The value $\beta = 84.0$ chosen for this study is representative of the values used in our later calculations. (See Table 25.) We note that strong finite volume corrections appear only for $l < 24$ and that they appear most strongly in the 0^+ and 2^+ channels as one would expect from our above discussion. In units of the string tension this suggests that volumes with $l\sqrt{\sigma} \geq 3.2$ are ‘large enough’ for the purposes of this paper, at least for $N \geq 8$, much as predicted by our preceding theoretical discussion. So the volumes we use for $N \geq 8$, as listed in Tables 25,26,27, are chosen to satisfy this constraint.

For smaller N we incorporate into our choice of volumes, listed in Tables 20–24, not only the constraint $l\sqrt{\sigma} \geq 3.2$ but also the more demanding one based on rough estimates of the spinorial torelon energies. As an explicit check we show in Table 4 a comparison between the spectra obtained on two different volumes for each of $SO(3)$, $SO(4)$ and $SO(6)$. In each case one of the two volumes is the standard volume we use in our later calculations. In the cases of $SO(3)$ and $SO(6)$ the corresponding masses on the two volumes are well within 2σ , as they are for nearly all the $SO(4)$ masses. In the latter case, only the 0^{+*} values are more than 3σ apart. (Note that the respective labelling of the 0^{+***} and 0^{+****} states for $l = 34$ in $SO(4)$ is determined by the effective masses at $t = a$, but the actual mass estimates indicate a reversed ordering, which agree much better with the $l = 44$ values.)

We take the above arguments and explicit checks as reasonably good evidence that the volumes we use, as shown in Table 5, are large enough to avoid significant finite volume

corrections.

3.6.5 multi-glueball states

We are primarily interested in the mass spectrum of glueballs, i.e. stable particles, or resonances that are narrow enough to be unambiguous. At large N resonance widths are expected to vanish so that our $N = \infty$ spectrum, as calculated by correlators of single trace operators, will indeed consist of some tower of stable particles. This is what we hope to obtain via our large- N extrapolations. However at finite N our single trace ‘glueball’ operators will have a non-zero overlap onto multi-glueball states that are naturally represented by multi-trace operators. So for example we may have in the $p = 0$ 0^+ channel states composed of two scalar glueballs with equal and opposite momenta. Similarly for the 2^+ channel (except that now the momenta must be non-zero). In the $p = 0$ $J = 1$ sector the two glueballs cannot be the same (otherwise the state will be null) so these states will be heavier. Since these multiglueball states are heavy and since they should in any case disappear from the single-trace spectrum as N increases, we shall ignore here the possibility that some of our heavier states might not be single glueballs but might be, say, pairs of glueballs. At smaller N this assumption might not be correct, but an explicit calculation to check this, by putting a large basis of multi-glueball operators in our variational basis would take us beyond the scope of this paper.

A particular caveat attaches to states in $SO(4)$. If the continuum spectrum is indeed the same as that of $SU(2) \times SU(2)$ then there will be states with one glueball from each of the $SU(2)$ groups with a possible shift in mass due to lattice spacing corrections. There is no obvious reason for the projection of such states onto our operator basis to be any less than that of single glueball states, and such extra states can both confuse a simple minded extrapolation of states to $N = \infty$, and complicate the comparison between the glueball spectra of $SO(4)$ and $SU(2)$.

3.6.6 reliability grades

The errors that we will provide on the mass estimates in our Tables will be purely statistical since only these can be easily quantified. However, as will be apparent from the above discussion, we expect the systematic errors to be substantial in many cases. Clearly it would be useful to provide the reader with some guidance as to how reliable we believe our individual mass estimates are. To do so we have assigned a grade ranging from α to ϕ to each of our mass estimates, which we shall now define.

Our finite volume checks confirm our expectation that at larger N we do not have significant finite volume corrections. At smaller N we avoid torelon corrections by making the volume large enough that two (spinorial) flux tubes are heavier than our heaviest 0^+ excitation. Multi-glueball states should only be visible, if at all, at small N , and it is only the 4'th 0^+ excitation that is heavy enough to be possibly affected. Similarly for two glueball states in $SO(4)$. There may be mis-identifications of the spin, but these do not impinge on the quoted masses.

So the main systematic error arises in trying to identify the ‘effective mass plateau’ as described in Section 3.6.3, and this is what our grades are designed to reflect. We denote by

α mass estimates for which we believe any such error is insignificant and much smaller than the quoted statistical error. Thus we grade the lightest 3 0^+ states in Fig. 2 as α , as well as the lightest 2^\pm states in Fig. 3. Also the ground state 0^+ on the coarser lattice in Fig. 4. The grade β indicates a systematic error that is possibly significant, but probably smaller than the statistical error. Thus the 4'th excited 0^+ state in Fig. 2, the excited 2^\pm states in Fig. 3, as well as the first excited 0^+ state in Fig. 4. With the grade γ we indicate a systematic error that may be significant although the pattern of effective masses suggests it will not be much larger than the statistical error. Thus the 3rd excited 0^+ in Fig. 2, the 0^- in Fig. 3, the second excited 0^+ in Fig. 4 and the lightest 2^\pm in Fig. 5. With grades δ and ϕ we indicate mass estimates where we largely lose control of the systematic error, but assume we can extract a mass from the furthest point at which the statistical errors allow a mass to be extracted. This is likely to provide some kind of estimate as long as the overlap is not anomalously small. (Where what is anomalous is determined by the overlaps of the lighter states whose overlaps can be estimated.) States that we label δ are the 1^\pm in Fig. 3, and states we label ϕ are the excited 2^\pm , the 0^- and the 1^\pm in Fig. 5.

To avoid cluttering up the Tables of masses we do not show the individual grades but instead provide an overall grade for the continuum limit of each state. This grade takes all the grades at the various lattice spacings into account, but with a weighting to the grades at the smaller three lattice spacings. Note however that this overall grade does not attempt to reflect any systematic error in making the continuum (or large N) extrapolations. The quality of these fits is indicated separately.

Finally we remark that our calculations of flux loop masses, from which we extract the string tensions, are all α except for $SO(3)$, which is discussed in much more detail in Section 4.2, and sometimes for the very coarsest value of a , particularly in the case of $SO(4)$ and $SO(5)$.

4 Confinement

We begin with our calculation of the string tension in $SO(N)$ gauge theories. This is the energy per unit length of the confining flux tube carrying flux in the fundamental representation. Of course this assumes that the theories are linearly confining, just like $SU(N)$ gauge theories, and this needs to be established. The question is particularly delicate for $SO(2N+1)$ since these groups have a trivial centre and in $SU(N)$ theories the deconfined and confined phases are the ones in which the Z_N centre symmetry is or is not spontaneously broken. We sketch the usual simple argument. Consider (the trace of) an operator $\phi_t(x, y)$ which consists of the trace of a product of link matrices on a path that winds on a timelike loop once around the timelike t -torus of length l_t . This is just a Polyakov loop and is the operator associated with the world line of a static fundamental source located at the point (x, y) . Now suppose we change the field on the lattice by multiplying all the link matrices emanating in the t -direction from lattice sites at a fixed value of t , say $t = t_0$, by a non-trivial element of the centre, $z \in Z_N$. Clearly $\phi_t \rightarrow z\phi_t$. But this new field has exactly the same weight in the path integral as the original field since the Haar measure is invariant, $\mathcal{D}(U_l) = \mathcal{D}(zU_l)$, and so is the

action because it is composed of contractible closed loops that acquire a factor of z^\dagger for each factor of z . That is to say, this transformation is a symmetry of the theory. So if we assume the vacuum is unchanged under the symmetry transformation (i.e. that the symmetry is not spontaneously broken) we immediately deduce that $\langle\phi_t\rangle = z\langle\phi_t\rangle = 0$ and hence that

$$\langle\phi_t^\dagger(x, 0)\phi_t(0, 0)\rangle \xrightarrow{x\rightarrow\infty} |\langle\phi_t\rangle|^2 = 0. \quad (33)$$

Since this correlator is just $\propto \exp\{-E(x)l_t\}$ where $E(x)$ is the (free) energy of a pair of conjugate fundamental sources a distance x apart, this tells us that $E(x) \rightarrow \infty$ as $x \rightarrow \infty$, i.e. the theory is confining. (Of course, whether it is *linearly* confining is another matter.) In this way the non-trivial centre symmetry leads to confinement when it is not spontaneously broken. One can carry this kind of argument further. When we calculate the string tension we use lattices of size $l_x l_y l_t$, we make l_y, l_t large and we then calculate the energy of a flux tube winding around the x -torus from correlators of operators $\phi_x(y, t)$ defined on paths that wind around the x -torus. If we apply the same centre symmetry transformation as above, but with $t \rightarrow x$, then $\phi_x \rightarrow z\phi_x$. On the other hand an operator $\phi_o(x, y, t)$ defined on a closed contractible spatial loop is unchanged. Hence

$$\langle\phi_x(y, t)\phi_o(x, y, 0)\rangle = z\langle\phi_x(y, t)\phi_o(x, y, 0)\rangle = 0. \quad (34)$$

Since operators of the form ϕ_o provide a basis for glueballs and for the vacuum, this tells us that when the centre symmetry (around the x torus) is not broken, the winding flux tubes cannot break into glueballs and/or the vacuum. Thus we see that in the familiar context of pure $SU(N)$ gauge theories the fate of the centre symmetry is tied to that of confinement. Of course things are less simple in the even more familiar case of QCD, where the quarks break the centre symmetry and break flux tubes, but nonetheless the theory possesses quasi-stable flux tubes and is confining. The fact that $SO(2N + 1)$ gauge theories have a trivial centre makes us ask in what sense they might be confining and this is something we will address at some length in this section, after first remarking on the more straightforward case of $SO(2N)$ gauge theories.

4.1 $SO(2N)$ and confinement

$SO(2N)$ gauge theories have a Z_2 centre symmetry that ensures confinement, as long as the symmetry is not spontaneously broken: as described above, the expectation value of a Polyakov loop is zero so (at least naively) the free energy of an isolated fundamental charge is infinite. Of course what we are really interested in is something more: linear confinement. To demonstrate this we need to show that the energy of the ground state that couples to the Polyakov loop of length l grows linearly with l , up to $O(1/l)$ corrections, i.e. that it is a flux ‘tube’. To do this we take the correlator of a Polyakov loop type of operator that winds once around the x -torus of an $l_x \times l_y \times l_t$ lattice, where l_y and l_t are sufficiently large that finite volume corrections are negligible, and we calculate the energy of the ground state energy $E(l)$ as a function of $l = l_x$ to see if it grows (roughly) linearly with l .

We provide two examples of such calculations, one in $SO(6)$ at $\beta = 46.0$ and one in $SO(8)$ at $\beta = 86.0$. These β values correspond to small enough values of a that the $O(a^2)$ lattice corrections should be very small. The lattices that we use and the values of $E(l)$ that we extract are listed in Table 6. We plot these values in Fig. 9. It is clear that at larger l the energy, $E(l)$, grows roughly linearly with l in both cases. This is an approximate statement because there are $O(1/l)$ corrections to the linear dependence. However for a string-like flux tube it is known that up to $O(1/l^5)$ the corrections to $E(l)$ are universal [17] and coincide with what one gets by expanding the Nambu-Goto formula

$$E(l) = \sigma l \left(1 - \frac{\pi}{3\sigma l^2}\right)^{1/2} \quad (35)$$

in powers of $1/\sigma l^2$. We therefore fit our calculated values of $E(l)$ to the expression in eqn(35). We find that for $SO(8)$ we obtain a good fit to all our values of l , with a resulting string tension

$$a^2\sigma = 0.017065(57) \quad l \in [12, 40], \quad \chi^2/n_{dof} = 0.82 \quad : SO(8), \quad (36)$$

where n_{dof} is the number of degrees of freedom in the fit. It is interesting to note that in order to get a good fit down to a flux tube as short as $l = 12a$ one really needs the higher order universal string corrections encoded in eqn(35): one cannot get a good fit with just the leading $O(1/l)$ Luscher correction [28]. In the more accurate case of $SO(6)$ we again have a very good fit

$$a^2\sigma = 0.016014(27) \quad l \in [18, 42], \quad \chi^2/n_{dof} = 0.89 \quad : SO(6). \quad (37)$$

We note that in this case a fit with just an $O(1/l)$ Luscher correction is perfectly adequate, essentially because the range of $l\sqrt{\sigma}$ does not include values as small as in the case of $SO(8)$. All this provides convincing evidence that $SO(2N)$ gauge theories are indeed linearly confining, as one might expect.

Of course these results are only as robust as our identification of the effective energy plateaux, from which we obtain our values of $E(l)$. We display the effective energies in Fig. 10 and Fig. 11. It should be clear we do indeed have unambiguous plateaux for all our values of l .

The fact that the centre of $SO(2N)$ is Z_2 in contrast to the Z_N centre of $SU(N)$, does create some differences in the confining properties of the two sets of theories. In $SU(N)$ we have stable flux tubes in higher representations. Consider a source that transforms as z^k under a global gauge transformation $z \in Z_N$. If $k \leq N/2$ the flux tube carrying the flux from that source will be stable since the gluons in the vacuum that might screen the source in fact transform trivially under z . So the Z_N symmetry implies that we have $N/2$ k -strings, with $k = 1$ corresponding to the fundamental. In $SO(N)$ our Z_2 centre only leads to a stable $k = 1$ string. This raises an interesting question of how the $SO(2N)$ gauge theories recover the Z_N physics as $N \rightarrow \infty$, given the common planar limit. This is a subtle question because even in $SU(N)$ the k strings, which one might think of as bound states of k fundamental strings, become unbound at $N = \infty$. We do not pursue this issue further in this paper, but hope to address it in detail elsewhere.

4.2 $SO(2N+1)$ and confinement

The question of confinement in $SO(2N + 1)$ gauge theories is more delicate, since here the centre is trivial and we cannot argue on symmetry grounds that there is a phase in which the expectation value of the Polyakov loop will vanish. Moreover we expect that at small values of N the flux tubes may be unstable.

In particular consider $SO(3)$. Here the fundamental flux tube corresponds to the $SU(2)$ adjoint flux tube which can be broken by pairs of gluons from the vacuum, and hence can decay into glueballs, just as the QCD flux tube is broken by quark-antiquark pairs from the vacuum, and can decay into mesons. In addition estimates of the $SU(2)$ adjoint string tension suggest $\sigma_{adj}^{SU2} > 2\sigma_f^{SU2}$ [12]. So in $SU(2)$ an adjoint flux tube is energetically capable of decay into a fundamental flux tube and its conjugate and will acquire an additional decay width due to this process. One naively expects that $\sigma_f^{SO3} = \sigma_{adj}^{SU2}$ and that the $SO(3)$ fundamental flux tube should have a decay width that is identical to the decay width of the adjoint flux tube in $SU(2)$. (Recall that the fundamental of $SU(2)$ corresponds to the spinorial of $SO(3)$.) Of course if this decay width is very small, as is the case in QCD , then it should still be possible to identify numerically an approximate linear growth of the flux tube energy with its length. And in any case since $SU(2)$ is exactly confining in the sense that colour is confined, irrespective of the adjoint flux tube instability, one can presumably think of the $SO(3)$ theory as also being exactly confining even if, just like QCD, it does not provide us with an asymptotic area law for Wilson loops in the fundamental representation.

More generally, we recall that the above relationship between $SO(3)$ and $SU(2)$, with $SU(2)$ being the largest simply connected group that has the same Lie algebra as $SO(3)$, is a special case of the same relationship between $SO(N)$ and $Spin(N)$ ¹. And $Spin(N)$, the double cover of $SO(N)$, has a nontrivial centre that is Z_2 , Z_4 or $Z_2 \times Z_2$ depending on the value of N . Thus for $Spin(N)$ we have the usual link between the centre symmetry and confinement and if that confinement is ‘linear’ there will be absolutely stable flux tubes in that theory, corresponding to spinorial flux tubes in $SO(N)$. If this is so then this suggests that $SO(2N + 1)$ theories should be thought of as confining, just like $SO(3)$, even if the fundamental flux tube is not perfectly stable. The deconfinement transition for $Spin(5)$ and $Spin(6)$ has been investigated in [29].

In $SO(3)$ the fact that the flux tube can break is obvious since the fundamental of $SO(3)$ is also the representation of the gluons in the theory so that it can be broken by gluon pairs from the vacuum. For larger odd values of N this is no longer the case and it is less clear to us what might be the mechanism for any instability of the fundamental flux tube. For example, as N increases the spinorial flux tubes should have a rapidly increasing string tension and hence energy (using the quadratic Casimir as a guide) and will become irrelevant. It is therefore interesting to investigate what happens to linear confinement in $SO(2N + 1)$ gauge theories. Our investigation here does not attempt to be definitive, something that in any case is beyond the capability of a numerical calculation, but we will at least try to establish whether it makes sense to calculate a confining string tension for such theories.

We begin with $SO(5)$. We perform a calculation of $E(l)$ on lattices at $\beta = 27.5$. As

¹We thank Michele Pepe for emphasising to us the relevance of this in the present context

we shall shortly see, this corresponds to a string tension $a^2\sigma \simeq 0.02$, so the $O(a^2)$ lattice corrections to continuum confining physics should be negligible. We list the ground state flux tube energies in Table 7. In Fig. 12 we display these energies as a function of l . It is clear that $E(l)$ does indeed rise (roughly) linearly at larger l . In fact we find that we get an acceptable fit to all l using the Nambu-Goto formula in eqn(35)

$$a^2\sigma = 0.019185(35) \quad l \in [14, 42], \quad \chi^2/n_{dof} = 1.70 \quad : SO(5). \quad (38)$$

(and a very good fit, with $a^2\sigma = 0.019208(36)$, if we exclude the smallest value of l). Moreover there is no difference to these results whether we use correlators of vacuum subtracted operators or not. Thus it certainly looks as if $SO(5)$ is linearly confining. Of course this conclusion is only reliable if our extraction of $E(l)$ is reliable. So in Fig. 13 we display the effective energies, as defined in eqn(30), from whose ‘plateaux’ we extract the values of $E(l)$. We show separately the values obtained from the correlators of operators with and without the vacuum expectation value subtracted. As one can see, any difference is much smaller than the statistical errors. That is to say, any overlap of the ground state flux tube onto the vacuum is invisible within our errors. Indeed the ‘plateaux’ appear to be just as well-defined as they are for $SO(6)$ or $SO(8)$, and we see no indication that any of these flux tubes is unstable.

The calculations above demonstrate that the ground state of the flux tube in $SO(5)$ has at most a very small overlap onto the vacuum. So it is interesting to ask if we have any good evidence that it is in fact non-zero. Another interesting question is whether the vacuum has a non-zero overlap onto our whole basis of winding operators. To address the first of these questions we take at each l the ground state winding operator $\phi_{gs}(l)$ that arises from our variational procedure and calculate its vacuum expectation value, $\langle\phi_{gs}\rangle$. To answer the second question we take the orthonormal set of operators $\{\phi_i\}$ that are produced by our variational calculation, and which therefore span our space of winding operators, and construct the total projection onto that space by $\sum_i |\langle\phi_i\rangle|^2$. The values of both these measures are listed in Table 8. For each l we show the values as obtained with two bases of operators, characterised by the largest blocking level bl_{max} .

Of course our best variational operator $\phi_{gs}(l)$ does not have a 100% overlap onto the real ground state, $|gs\rangle$, because our basis is finite. We show estimates of the overlap $O_{gs}^2 = |\langle vac|\phi_{gs}|gs\rangle|^2$ in the Table, and $1 - O_{gs}^2$ is then the size of the overlap onto the non-ground-state contributions to the correlator of ϕ_{gs} . So it is only if we find that

$$|\langle\phi_{gs}\rangle|^2 > 1 - O_{gs}^2 \quad (39)$$

that we can claim that the vacuum overlap cannot be just onto the small excited state component of ϕ_{gs} , but must be, at least in part, onto the ground state as well. Turning back to Table 8 we see that most of the overlaps onto ϕ_{gs} are consistent with zero and those that appear not to be are very small and much too small to satisfy the bound in eqn(39), despite the fact that O_{gs}^2 is very close to unity. That is to say, we have no evidence in these calculations that the true ground state wave-functional has a non-zero overlap onto the vacuum.

On the other hand we see from Table 8 that $\sum_i |\langle\phi_i\rangle|^2$, the vacuum overlap onto our whole basis of winding operators, is non-zero. In fact this non-zero overlap arises entirely (within

errors) from the most highly blocked operators, which extend in the transverse directions right around the lattice torus, and further. It might appear that the values of the overlaps for the lower value of bl_{max} are also non-zero compared to the errors, even if they are very small. This is true, but it is consistent with being the result of the fact that we are summing here positive definite quantities, so the fluctuations will appear to give non-zero results. We find that we get comparable results in our $SO(6)$ calculation, which supports this interpretation. We also show the effective energy at $t = a$ for each basis. The fact that the pairs of values are equal within errors indicates that the smaller basis already contains all of the ground state that one finds with the larger basis. So we conclude that while there certainly is a non-zero vacuum overlap onto our winding operators, this overlap arises entirely, within our errors, from the operators that are so highly smeared that they wrap right around the transverse directions and, moreover, these operators do not contribute to the wave-functional of the ground state of the $SO(5)$ flux tube.

We now turn to the more delicate case of $SO(3)$ where we expect that the ground state flux tube will be unstable because it can be broken by the gluons in the vacuum. We perform at $\beta = 9.0$ a similar calculation to the one described above for $SO(5)$. Here the lattice spacing is much smaller (in units of the mass gap) than in our $SO(5)$ example, so we expect lattice corrections to be even smaller. In $SO(3)$ the vacuum overlap onto our operator basis turns out, as expected, to be much larger than in the case of $SO(5)$, so we choose to calculate $E(l)$ separately for correlators with and without an explicit vacuum subtraction. In the latter case the ground state of our variational procedure may be the vacuum and in that case we take the first excited state to be the flux tube ground state. This we need to do for $l = 34, 38, 62$. (Recall that our ‘ground state’ operator is defined to be the one that maximises $E_{eff}(t = a)$ and if the overlap of the vacuum onto the basis is small, then its $E_{eff}(t = a)$ will be large, even though $E_{eff}(t)$ will drop to zero at larger t .) In addition, for our smallest value of l the vacuum mixes into both the ground state and the first excited state so in that case we drop the operators at the highest blocking level (which have most of the vacuum projection) and use the remaining basis for the calculation. Obviously the vacuum subtracted correlators do not need to be tweaked in this way. The resulting ground state flux tube energies are listed in Table 7 and displayed in Fig. 14. We show what one obtains with and without vacuum subtraction and one sees that there is no appreciable difference. In both cases the approximate linear growth with l at larger l is evident. The behaviour at smaller l appears to be more complicated. Our expectation that the flux tube should be unstable, makes it useful to display the effective energies, which we do in Fig. 15 for the vacuum unsubtracted case. We see that the determination of an effective energy plateau is much harder than in the case of $SO(5)$ or $SO(6)$. The main culprit is not the instability, if any, of the flux tube, but rather a mediocre overlap of our operator basis onto the ground state. This means that at the larger values of l our correlator disappears into the noise before we can be confident that we have identified a plateau. Nonetheless the plateau identification appears plausible for $l \leq 46$ and perhaps also for $l = 52$, but one cannot put it more strongly than that. For $l = 62, 82$ the choices are clearly speculative and are essentially motivated by assuming that the plateau will start at roughly the same value of $t = an_t$ as at the lower values of l where it is more clearly identifiable.

In fact the mediocre overlaps in $SO(3)$ should not come as a surprise since we have already seen in Figs 6,7 that the same is true for glueballs. Moreover we can see the same behaviour in $SU(2)$ when we perform calculations with flux tubes in the adjoint representation. We show in Fig. 16 a comparison of the effective energies of ground state flux tubes in the fundamental and adjoint representations in $SU(2)$ at $\beta = 16$, which corresponds to a value of the lattice spacing similar to the one we have in $SO(3)$ at $\beta = 9$. For the purposes of comparison we have renormalised the adjoint $E_{eff}(t)$ values at each value of l to asymptote to the same value as the fundamental effective energies at that l . We see from Fig. 16 that the adjoint overlaps are much worse than the fundamental ones, which means that the plateau in the effective energies is reached much more slowly and is much harder to identify, just as in $SO(3)$.

A further issue arises when one looks at the excited states of the flux tube. One finds that several of these have effective energies that decrease at larger t , possibly to values comparable to or below that of our ‘ground state’. To understand this behaviour (which we do not see in $SO(5)$ or with any other value of N) it is again useful to consider the adjoint flux tube in $SU(2)$ where one sees a very similar behaviour [12]. In the latter case there is a ready interpretation: we are seeing states composed of a pair of winding fundamental flux tubes with various equal and opposite transverse momenta. (And possibly glueballs as well.) We can carry this interpretation over to $SO(3)$, with the fundamental flux tubes of $SU(2)$ becoming spinorial flux tubes. Although this is reasonable and provides a resolution of the puzzle of the numerous low-lying states, we also need to assume that it is our (variational) ground state, rather than one of the excited states, that is the ground state of the flux tube. The argument is that the states composed of two spinorial flux tubes will have a suppressed coupling to our fundamental operators, which is why they have larger values of $E_{eff}(t = a)$ and appear as excited states in the variational calculation. This is essentially a large- N argument and is only partially convincing here, since the value $N = 3$ is not large.

All this suggests that in $SO(3)$ we do indeed have some kind of partially stable ground state flux tube, although the mediocre quality of the effective energy ‘plateaux’, does leave room for substantial instability. To proceed further we need to be more quantitative, so we calculate the same overlaps that we calculated for $SO(5)$. We list the results in Table 9. The vacuum overlap onto our whole winding basis is clearly larger than in $SO(5)$ but, just as in the latter case, most of the overlap is onto operators at the very largest blocking level. In most cases if we discard these highly smeared operators, the remaining basis has an overlap onto the ground state that is very nearly the same, as we infer from the values of $E_{eff}(t = a)$ listed in Table 9, and this slightly reduced basis has essentially no overlap on to the vacuum. If we just look at $|\langle\phi_{gs}\rangle|^2$ we see that it is remarkably small, even when we keep the largest blocking level. Although it is usually non-zero, the overlap of ϕ_{gs} on to excited states, as measured by $1 - O_{gs}^2$ is always very much larger so we cannot infer that the true ground state flux tube wave-functional has a non-zero overlap onto the vacuum. This conclusion is of course almost inevitable given the mediocre overlap of the ground state onto our operator basis in $SO(3)$, and so one should not read too much significance into it.

We have remarked that the vacuum overlap typically finds its way into states that our variational criterion labels as highly excited. As an example of this we show in Fig. 17 some

correlation functions obtained on a $100^2 80$ lattice at $\beta = 11.0$ in $SO(3)$, with the quantum numbers of the ground state of the flux tube. We show those of our 4 lightest states (including the ground state) none of which exhibit any significant instability, together with corresponding exponential fits. We then show the 8'th excited state, which is the first one to exhibit a significant vacuum expectation value. We also show the 10'th which shows the maximum vacuum expectation value. The accompanying exponential lines are the fits to the 8'th and 10'th excited states that one obtains if one explicitly subtracts the vacuum expectation value from the operators.

We have seen above that the signals for confinement in $SO(5)$ are much more convincing than for $SO(3)$. This prompts the question; what happens as we increase N further, with N odd? To address this question we have calculated the properties of flux loops of length $l = 36$ for $N = 3, 5, 7, 9, 11$. We choose values of β such that the lattice spacing is comparable (in physical units) between these different gauge groups. We perform the same analysis of vacuum overlaps as we did above for $SO(3)$ and $SO(5)$, and we display our results in Table 10. It is striking that even though the overlap squared of our variational ground state operator onto the true ground state is at least 99.5% at larger N , any vacuum expectation of that operator is so tiny that it provides no evidence for the instability of the true ground state. We also see that even when our basis includes operators that wrap around the boundaries, with $bl_{max} = 6$, the total projection of the vacuum onto the basis decreases very rapidly with increasing N , apparently much faster than a low inverse power of N . We also see that for $N \geq 5$ the $bl_{max} = 6$ basis does not have (within small errors) any more projection onto the ground state than the smaller $bl_{max} = 5$ basis. And for $N \geq 5$ the vacuum expectation value of our variationally selected ground state operator in this latter basis is consistent with being exactly zero within the very small errors.

In summary, the message from these calculations is that for odd $N \geq 5$ we have a (ground state) flux tube that is stable within our very small errors so that, for all practical purposes, we have linear confinement with a well-defined string tension. For $SO(3)$ our errors are much larger, although here too we can identify a flux tube, albeit one that may not be very stable. We note from Tables 8, 9 that if we restrict ourselves to operators up to a given maximum blocking level, the vacuum overlaps decrease quite rapidly as l increases, leaving open the interesting if speculative scenario that the flux tubes might become exactly confining in the large l limit.

It would of course be useful to go beyond this focus on vacuum overlaps, and calculate overlaps onto glueballs as well. (This would require enlarging our basis so as to include cross-correlations with glueball operators and although straightforward would represent a quite different calculation and would take us outside the scope of the present paper.) It is, after all, well-known that in practice it is very difficult to obtain statistically significant evidence for string breaking in QCD without explicitly including in the basis of flux tube operators the typical meson pairs into which the flux tube breaks. While we cannot compare our results to most of those calculations, which involve flux tubes ending at sources, there do exist calculations using blocked Polyakov loop operators similar to ours. An example is [30] where the calculations are performed with moderately heavy quarks on $L_s = 16$ lattices. As we see from Fig.1 of [30] the vacuum expectation values of the blocked Polyakov loops

are, while small, very visible even for the lower blocking levels where the smearing does not extend around the whole lattice. In comparison our vacuum expectation values are very much smaller, except possibly for $SO(3)$. That is to say, the indications are that any string breaking in $SO(N \geq 5)$ theories is much weaker than in QCD .

5 String tensions

5.1 lattice results

We list in Tables 11-18 the result of our calculations of the ground state flux tube energy for various values of β and for our various $SO(N)$ groups. The length l of the flux tube is equal to the size, L_s , of the spatial direction which our winding operator encircles.

For most values of N we use the same lattices for our glueball and for our string tension calculations. However for $SO(3)$, $SO(4)$ and $SO(6)$ we use smaller spatial volumes for the string tension calculations than for the glueball ones. One reason is that we need to use larger physical volumes for glueballs at the smallest values of N in order to minimise the systematic errors discussed in Section 3.6.4. In addition, the string tensions σ turn out to be larger at small N when expressed in units of the mass gap, so for the ground state flux tube energy not to become so large that its determination becomes susceptible to the systematic errors discussed in Section 3.6.3, we need to choose values of l that are small enough for the correlator not to have disappeared into the statistical noise before the desired effective energy plateau can be identified. This is particularly important for $SO(3)$ and $SO(4)$ because the overlap of the ground state onto our operator basis is quite mediocre for these two small values of N , which means that the energy plateaux will only appear at larger t . For these reasons we perform our $SO(3)$ and $SO(4)$ string tension calculations on separate series of smaller lattices. For $SO(3)$ we choose a lattice size that corresponds to $l = 46$ at $\beta = 9.0$. As we see from our finite volume study in Fig. 14 this value of l is large enough to be well fit by the Nambu-Goto expression in eqn(35). That is to say, we can extract a string tension using that formula for this value of l . Our glueball calculations, on the other hand, are performed on spatial lattice sizes that corresponds to $l = 82$ at $\beta = 9.0$, and, as should be apparent from Fig. 15, extracting a flux tube energy on such a large lattice would be beset with potential systematic errors. Similar comments apply to our $SO(4)$ calculations.

Given our caveats about the low N calculations, it is useful to display the effective energies from which we estimate the ‘plateau’ energies listed in Table 11 and Table 12. This we do in Fig. 18 and Fig. 19. It appears plausible that these plateaux have been correctly identified for at least the four smallest lattice spacings, and these are the ones that will dominate our continuum extrapolations. When we move to $SO(5)$ we find that the overlaps have become much better, as we can see from the effective energies plotted in Fig. 20. Here the spatial volumes used are still quite large, and therefore so are the flux tube energies, but since the overlaps are now very good, the identification of an energy plateau is convincing. (Except for the coarsest $a(\beta)$, which is largely irrelevant for the continuum limit.) For $SO(6)$ the calculations on our smaller volumes are at least as convincing. For $N \geq 7$ we use smaller

volumes for the glueballs and since the overlaps are now very good (as we can infer from Fig. 11 and Fig. 10) the energy estimates become quite unambiguous.

Our finite l studies for various N make us confident that the Nambu-Goto expression in eqn(35) encodes all the finite- l corrections that are significant, at our value of l , given our errors. As remarked earlier, this is to be expected since we know that all correction terms to σl up to $O(1/l^5)$ are universal [17, 19] for any effective string action describing flux tubes and these terms are precisely what one obtains when expanding the Nambu-Goto expression in powers of $1/\sigma l^2$. Of course when the flux tube is not stable it is not clear that it should be described by an effective string action, and here our numerical tests in $SO(3)$ and $SO(5)$ are useful. We therefore use the Nambu-Goto formula to extract the string tension values, $a^2\sigma$, from the flux tube masses, am_p , and we list these in Tables 11-18.

5.2 continuum limit and N -dependence

What we ultimately want of course is not so much lattice values of σ , but the continuum limit in some physical units. Since g^2 has dimensions of mass in $D = 2 + 1$, we can use that to set our units, i.e. we calculate the continuum limit of the dimensionless ratio $\sqrt{\sigma}/g^2N$. To do so we could use the standard lattice coupling defined through $\beta = 2N/ag^2$, but we instead choose to use the mean-field improved coupling [21], g_I^2 , defined by $\beta_I = \beta\langle u_p \rangle = 2N/ag_I^2$, with $\langle u_p \rangle = \langle \text{Tr}U_p \rangle/N$ the average plaquette. (In the case of $SU(N)$ gauge theories this is found to provide a slightly more rapid approach to the continuum limit.) Using this we extrapolate to the continuum limit using

$$\frac{\beta_I}{2N^2}a\sqrt{\sigma} \equiv \left. \frac{\sqrt{\sigma}}{g_I^2N} \right|_{\beta_I} \stackrel{\beta_I \rightarrow \infty}{=} \left. \frac{\sqrt{\sigma}}{g^2N} \right|_{\infty} + \frac{c}{\beta_I} + O\left(\frac{1}{\beta_I^2}\right) \quad (40)$$

We show our resulting continuum extrapolations in Fig. 21 where we plot the values of $\sqrt{\sigma}/g_I^2N$ against ag_I^2N . In general we obtain good fits with just the linear $O(1/\beta_I)$ correction in eqn(40). We list the resulting continuum values of $\sqrt{\sigma}/g^2N$ in Table 19.

We now plot these values against $1/N$ in Fig. 22. We expect the $N \rightarrow \infty$ limit to be some finite non-zero number and we expect the finite- N corrections to begin at $O(1/N)$. We find that a single $O(1/N)$ correction will not do for all $N \geq 3$, and that one needs at least a further $O(1/N^2)$ term to obtain a barely acceptable fit. Without $SO(3)$ we obtain a better fit, and can even get by with a single correction term. In summary, one obtains

$$\frac{\sqrt{\sigma}}{g^2N} = \begin{cases} 0.09821(57) - \frac{0.142(6)}{N} - \frac{0.048(31)}{N^2} & N \geq 4 \quad \frac{\chi^2}{n_{dof}} \simeq 1.67 \\ 0.09897(25) - \frac{0.1542(19)}{N} & N \geq 4 \quad \frac{\chi^2}{n_{dof}} \simeq 1.76 \\ 0.09749(43) - \frac{0.129(6)}{N} - \frac{0.100(17)}{N^2} & N \geq 3 \quad \frac{\chi^2}{n_{dof}} \simeq 2.32 \end{cases} \quad (41)$$

Given the fact that the $SO(3)$ string may have a significant decay width, it seems safer to discount the last of these fits. The two fits for $N \geq 4$ almost overlap within errors and one can regard the difference as providing a measure of the systematic error in the choice of large- N extrapolation. Given that the much more accurate $SU(N)$ extrapolation (see below) requires

the inclusion of an $O(1/N^4)$ correction, we are inclined to take the higher order fit to the $SO(N \geq 4)$ string tension as being the most realistic.

Given that we expect $SU(N)$ and $SO(N)$ to have a common planar limit, it is interesting to compare our $SO(N)$ results to those obtained in $SU(N)$. We therefore list in Table 19 some $SU(N)$ values of $\sqrt{\sigma}/2g^2N$ taken from [6]. The extra factor of 2 encodes the fact that in identifying the planar limits of $SO(N)$ and $SU(N)$ one equates g^2N in the former with $2g^2N$ in the latter [1]. We plot these $SU(N)$ values in Fig. 22. Since the leading large- N correction in $SU(N)$ is $O(1/N^2)$, the points near $N = \infty$ will fall on a quadratic curve. To get a good fit one needs to include a subleading correction, giving for our best fit

$$\frac{\sqrt{\sigma}}{2g^2N} = 0.09818(6) - \frac{0.0543(16)}{N^2} - \frac{0.0143(58)}{N^4} \quad N \geq 2 \quad \frac{\chi^2}{n_{dof}} \simeq 1.25 : \quad SU(N) \quad (42)$$

which we plot in Fig. 22. We observe that the large N limits of $SO(N)$ and $SU(N)$ do indeed coincide (within errors) despite the very different values at finite N .

Another interesting question is whether the values of the string tension in $SO(2N)$ and $SO(2N+1)$ gauge theories form a single ‘continuous’ sequence or two separate sequences that only coincide at $N = \infty$. The fact that we can perform a single smooth extrapolation to $N = \infty$ using all our values of $\sqrt{\sigma}/2g^2N$ confirms, within small errors, that there is in fact a single sequence as we see in Fig. 23 where we plot the difference between our calculated values of $\sqrt{\sigma}/g^2N$ and the fit in eqn(41), normalised by the former. It appears that the fact that $SO(2N+1)$ gauge theories have only a trivial centre does not affect the value of the confining string tension.

5.3 Lie algebra equivalences

As we remarked earlier, it is interesting to see whether pairs of $SO(N)$, $SU(N')$ gauge theories that share the same Lie algebra lead to the same physics. Here we look at $\sqrt{\sigma}/g^2N$, taking advantage of the fact that in $D = 2 + 1$, g^2 has dimensions of mass.

There are two subtleties: firstly the fundamental string tension in the $SO(N)$ gauge theory will correspond to a higher representation string tension in the $SU(N')$ theory. Secondly the relation between the g^2 will also be non-trivial. There is also a caveat. As discussed in Section 3.3, the continuum extrapolation of $\sqrt{\sigma}/g^2$ begins with a correction at $O(1/\beta) \sim O(a)$ rather than at $O(a^2)$ which means that the systematic error is larger than where we consider ratios of physical energies, and may well be significantly larger than our quoted statistical error.

We begin by comparing the adjoint string tension in $SU(2)$ with the fundamental string tension in $SO(3)$. This is the case where we encounter the largest uncertainties since in both cases the overlaps of our operators are mediocre and this affects how reliable is the identification of the plateaux in the effective energies. In $SU(2)$ the relevant coupling is the adjoint coupling, g_a^2 , which is related to the fundamental coupling g_f^2 in eqn(9). So taking the $SO(3)$ and $SU(2)$ values of $\sqrt{\sigma_f}/g_f^2N$ from Table 19, using $\sqrt{\sigma_f}/g_f^2|_{so3} = \sqrt{\sigma_{adj}}/g_a^2|_{su2}$, and

imposing $g_a^2|_{su2} = 4g_f^2|_{su2}$ from eqn(9), we obtain the prediction for $SU(2)$

$$\frac{\sqrt{\sigma_f}}{g^2}\Big|_{so3} = 0.1281(20) \implies \frac{\sigma_{adj}}{\sigma_f}\Big|_{su2} = 2.34(8). \quad (43)$$

This can be compared to the value one obtains directly in $SU(2)$, $\sigma_{adj}/\sigma_f|_{su2} = 2.24(3)$. (See Table B2 of [6].) We see that the two values are in reasonable agreement given the statistical errors – perhaps surprisingly so given the systematic errors discussed above.

We turn now to $SO(4)$ and $SU(2) \times SU(2)$. Taking the $SO(4)$ value of $\sqrt{\sigma_f}/g_f^2$ from Table 19, and imposing the relations eqns(18,19) we obtain a predicted value for $SU(2)$

$$\frac{\sqrt{\sigma_f}}{g^2}\Big|_{so4} = 0.2408(22) \implies \frac{\sqrt{\sigma_f}}{g^2}\Big|_{su2} = 0.3405(31) \quad (44)$$

which is to be compared to the directly calculated $SU(2)$ value of $\simeq 0.3349(3)$ shown in Table 19. The two values are numerically very close, and while there is a ~ 1.8 standard deviation discrepancy, this includes only the statistical errors and given our earlier comments about the possible systematic errors, one need not regard this tension as being significant.

Finally we compare $SO(6)$ with $SU(4)$. As discussed in Section 2.2.2 the fundamental $SO(6)$ string tension corresponds to the $k = 2a$ $SU(4)$ string tension and the $SO(6)$ coupling is related to the $SU(4)$ coupling as in eqn(16). Using the latter, together with the $SO(6)$ value in Table 19, we obtain a prediction

$$\frac{\sqrt{\sigma_f}}{g^2}\Big|_{so6} = 0.4403(9) \implies \frac{\sqrt{\sigma_{k=2a}}}{g^2}\Big|_{su4} = 0.8806(18) \quad (45)$$

which is entirely consistent with the directly calculated $SU(4)$ value $\sqrt{\sigma_{k=2a}}/g^2 = 0.8833(11)$. (See tables B1,B2 in [6].)

We conclude that within our quite small uncertainties, there does indeed appear to be consistency between the values of $\sqrt{\sigma}/g^2$ within pairs of $SO(N)$ and $SU(N')$ theories that share a common Lie algebra.

6 Glueball spectrum

Most of our calculations in this paper concern the glueball spectrum. The glueballs we focus upon are the ground state glueballs with $J^P = 0^\pm, 2^\pm, 1^\pm$, the first four 0^+ excited states and the first 2^\pm excited states. We have chosen the lattice sizes with a view to avoiding significant finite volume corrections to these states, as discussed in Section 3.6.4.

6.1 $SO(N)$ glueball masses

We list in Tables 20-27 our results for a number of the lightest glueballs in $SO(N)$ gauge theories for $N = 3, 4, 5, 6, 7, 8, 12, 16$. This range of N is designed to allow us to make plausible

large- N extrapolations and also to compare the N dependence of $SO(2N)$ and $SO(2N + 1)$ gauge theories.

We shall mostly extrapolate ratios of physical masses to the continuum limit since the corrections will be $O(a^2)$ and will therefore converge much faster to $a = 0$ than if we were to express our masses in units of g^2N , where the correction is $O(a)$. Since for most values of N the string tension is the most accurately calculated physical quantity (with a caveat for $SO(3)$) we shall usually extrapolate the values of $aM_G/a\sqrt{\sigma}$, for our various glueballs G .

We use a variant of eqn(26) to extrapolate to the continuum limit

$$\frac{aM_G(a)}{a\sqrt{\sigma(a)}} = \frac{M_G(a)}{\sqrt{\sigma(a)}} = \frac{M_G(0)}{\sqrt{\sigma(0)}} + ca^2\sigma(a) \quad (46)$$

suppressing obvious indices. We truncate to just the leading correction since that usually suffices in practice. The fits are to all the values listed in Tables 20-27 except in a few cases where the value at the largest a is excluded from the fit. The resulting continuum limits, and the corresponding values of χ^2/n_{dof} for the extrapolations, are listed in Tables 28, 29. Most values of χ^2/n_{dof} are modest, but a few are large. However given that typically $n_{dof} = 4$ this is not fatal. We illustrate all this in Fig. 24 for the lightest 0^+ and 2^+ glueballs in $SO(3)$, $SO(6)$ and $SO(12)$.

We observe that our results are reassuringly consistent with the parity doubling expected in $D = 2 + 1$, i.e. 2^+ is degenerate with 2^- (also 2^{+*} with 2^{-*}) and 1^+ with 1^- . A striking contrast is provided by the $J = 0$ sector where no parity doubling is expected or observed.

It will also be useful for our analysis below to calculate the mass gap in units of the 't Hooft coupling g^2N . To calculate the continuum value of M_{0^+}/g^2N we perform an extrapolation

$$\frac{\beta_I}{2N^2}aM_{0^+} \equiv \left. \frac{M_{0^+}}{g_I^2N} \right|_{\beta_I} \stackrel{\beta_I \rightarrow \infty}{=} \left. \frac{M_{0^+}}{g^2N} \right|_{\infty} + \frac{c}{\beta_I} \quad (47)$$

using the mean-field improved lattice coupling $\beta_I = \beta\langle u_p \rangle$ that we introduced and used in Section 5.2. (We use the values of aM_{0^+} in Tables 20-27 and the plaquette values in Tables 11-18.) It turns out that we can obtain reasonable fits to all our lattice data using just the leading $O(1/\beta_I)$ correction, and the results of these fits are listed in Table 30.

6.2 large N: odd and even N

We now perform an extrapolation of our continuum results to $N = \infty$ where we can compare to the known $SU(N \rightarrow \infty)$ values [6]. We note that the large- N expansion can be performed at a non-zero lattice spacing [31] so we could in principle perform the comparison between $SO(N \rightarrow \infty)$ and $SU(N \rightarrow \infty)$ at a fixed a . There are however some extra complications (and hence errors) in fixing a across these theories, and we do not choose to make use of this possibility here.

We have already discussed the N -dependence of the string tension (expressed in units of the 't Hooft coupling) in Section 5.2. We saw that the large- N limit of $\sqrt{\sigma}/g^2N$ is, within errors, the same as that of $SU(N)$, up to a predicted factor of two. We also saw that to

have a reasonable fit we had to add an $O(1/N^2)$ correction to the leading $O(1/N)$ correction. One can treat the mass gap M_{0+}/g^2N in the same way. Using the continuum values listed in Table 30 we find that

$$\frac{M_{0+}}{g^2N} = 0.4017(14) - \frac{0.802(7)}{N} \quad N \geq 3, \quad \chi^2/n_{dof} = 0.81 \quad (48)$$

provides a good fit to all our values of N . It is surprising that in this case the leading correction suffices, given the relatively large coefficient of the correction term. No doubt our substantial statistical errors obscure the need for the inclusion of a further $\propto 1/N^2$ correction term. If we nonetheless perform a fit with such an extra term we obtain

$$\frac{M_{0+}}{g^2N} = 0.4079(35) - \frac{0.871(36)}{N} + \frac{0.165(82)}{N^2} \quad N \geq 3, \quad \chi^2/n_{dof} = 0.36, \quad (49)$$

which provides us with a measure of the systematic error associated with truncating the large- N expansion in eqn(48). The corresponding $SU(N \rightarrow \infty)$ value, as given in Table B1 of [6], is $M_{0+}/2g^2N = 0.4051(6)$, which is in reasonable agreement with the above $SO(N)$ values. Note that we include the factor of 2 in the matching of the couplings as prescribed by the large- N diagrammatic analysis [1].

Repeating the exercise in units of the string tension, we obtain

$$\frac{M_{0+}}{\sqrt{\sigma}} = 4.179(16) - \frac{3.17(11)}{N} \quad N \geq 3, \quad \chi^2/n_{dof} \simeq 1.30. \quad (50)$$

From Table B10 of [6] we obtain the value $M_{0+}/\sqrt{\sigma} \simeq 4.116(6)$ for $SU(\infty)$. This is very close to our above $SO(\infty)$ value. Although the difference is at the slightly uncomfortable level of $\sim 3.7\sigma$, the error is statistical, so we can regard the values as reasonably compatible. For example, if we perform an extrapolation to $N = \infty$ with an extra $\propto 1/N^2$ correction term, and if we exclude the $SO(3)$ value (which relies on a significantly unstable string tension) we obtain $M_{0+}/\sqrt{\sigma} = 4.106(39)$ with a much better fit, $\chi^2/n_{dof} \simeq 0.58$. This is entirely consistent with the $SU(\infty)$ value. Given the substantial coefficient of the $\propto 1/N$ correction term in eqn(50) it is very likely that a significant $\propto 1/N^2$ is present even if our relatively large statistical errors do not force us to include it in the extrapolation.

We now repeat such extrapolations for various other states and present the results in Table 31. In many cases a reasonable leading order fit in $1/N$ is acceptable but, once again, given that the coefficient of the $O(1/N)$ term is usually substantial, one should worry that the only reason we can get by with a leading order fit for some of the more massive states is that the errors are so large. So we present in all cases the results of fits with just a leading correction and, separately, with an added non-leading correction. In each case we indicate the range of N fitted as well as the χ^2 per degree of freedom. (This information allows the reader to estimate the p -value in each case.) We see that in many cases the $N = \infty$ values differ between the two fits by more than the statistical errors. We may, again, regard the difference between the two fits as providing an estimate of the systematic error associated with the large- N extrapolation. One also sees that in all cases the lower-order fit has a larger extrapolated value than the higher order fit and has smaller statistical errors.

We also display, in the same Table, the results for $SU(N \rightarrow \infty)$ taken from Tables B10-B12 in [6]. We see reasonable consistency between the $SO(\infty)$ and $SU(\infty)$ mass ratios in almost all cases, especially if one uses the higher order fits, although in most cases the errors are substantial and this obviously reduces the significance one can read into the agreement. The only comparison that works badly is the one for the first excited 0^+ . Here the discrepancy is a worrying ~ 7.4 standard deviations if one uses the leading order fit, and is only reduced to ~ 4.7 standard deviations if one takes the error from the higher order extrapolation. The first excited 2^- comparison is also quite poor, but here we grade the reliability of the mass estimate as quite poor, and this is supported by the apparent gap between the mass of the 2^{-*} and that of the 2^{+*} with which it should be degenerate.

As we remarked above, the variation with N of the typical glueball mass when expressed in units of the string tension is quite large compared to what one sees in $SU(N)$ gauge theories. As an example we show in Fig. 25 the values of $M/\sqrt{\sigma}$ for the lightest two 0^+ glueballs, in both $SO(N)$ and $SU(N)$. One can ask whether one can get a weaker N -dependence by using different units in which to express the mass. As an example we show in Fig. 26 the dependence one obtains using the 't Hooft coupling, g^2N , the string tension, $\sqrt{\sigma}$, and the mass gap, M_{0^+} for the lightest 2^+ glueball. We see that the weakest N -dependence occurs when using the mass gap as the scale, and this is in fact typical. This motivates extrapolating the ratio M_G/M_{0^+} to $N = \infty$, and we show in Table 32 what one obtains in that case. Here we only show what one obtains with just a leading $O(1/N)$ correction, $M_G/M_{0^+} = c_0 + c_1/N$, and we see that c_1/c_0 , the normalised coefficient of the correction, is invariably very small. We find reasonable agreement between the $SO(N \rightarrow \infty)$ and $SU(N \rightarrow \infty)$ values, except for the 0^{+*} and the 2^{-*} , although now the 0^{+*} difference is $\sim 4\sigma$.

We have obtained acceptable fits without distinguishing between odd and even values of N . This already indicates that these values are compatible with lying on a single smooth interpolating curve. Our most accurate mass is the mass gap, and we show in Fig. 27 how the odd and even values differ from our interpolation in eqn(50). As we can see, just as for the string tension, there is no indication that the odd and even values of N differ in some systematic fashion.

6.3 Lie algebra equivalences: mass gap and couplings

In Section 5.3 we compared the ratio $\sqrt{\sigma}/g^2$ within the three pairs of $SO(N)$ and $SU(N')$ gauge theories that share a common Lie algebra. We assumed the relationship between the couplings and the matching between flux tube representations given in Section 2 and found that the resulting values of the string tension were consistent between all three pairs of gauge theories. We turn now to the mass gap, the lightest scalar glueball. We will first calculate the ratios $M_{0^+}/\sqrt{\sigma}$ in $SO(3)$, $SO(4)$ and $SO(6)$ and compare them to the values that one obtains in $SU(2)$, $SU(2)$ and $SU(4)$ respectively. Since we have seen that the string tensions are in agreement, this will provide us with a test of whether the mass gap agrees or not. We shall see that they do in fact agree, and we then move on to a comparison of the values of M_{0^+}/g^2 which will provide us with a test of the relationship between the couplings.

We begin with $SO(6)$ and $SU(4)$. From the $SO(6)$ value of $M_{0^+}/\sqrt{\sigma}$ listed in Table 28 we

obtain the predicted value in $SU(4)$ as follows:

$$\frac{M_{0+}}{\sqrt{\sigma_f}} \Big|_{so6} = 3.656(13) = \frac{M_{0+}}{\sqrt{\sigma_{2A}}} \Big|_{su4} \Rightarrow \frac{M_{0+}}{\sqrt{\sigma_f}} \Big|_{su4} = 4.259(16), \quad (51)$$

where in the last step we use $\sqrt{\sigma_{2A}}/\sqrt{\sigma_f}|_{su4} = 1.1649(11)$ [6]. This is entirely consistent with the value $M_{0+}\sqrt{\sigma_f} = 4.242(9)$ that one obtains by direct calculation in $SU(4)$ [6].

Similarly we obtain a prediction for $SU(2)$ from our calculation in $SO(4)$:

$$\frac{M_{0+}}{\sqrt{\sigma_f}} \Big|_{so4} = 3.343(23) \Rightarrow \frac{M_{0+}}{\sqrt{\sigma_f}} \Big|_{su2} = 4.728(33), \quad (52)$$

where we use $\sigma_f|_{so4} = 2 \sigma_f|_{su2}$. This is to be compared to the value $M_{0+}\sqrt{\sigma_f} = 4.737(6)$ that one obtains by direct calculation in $SU(2)$ [6].

Finally we obtain another prediction for $SU(2)$, this time from our calculation in $SO(3)$:

$$\frac{M_{0+}}{\sqrt{\sigma_f}} \Big|_{so3} = 3.132(34) = \frac{M_{0+}}{\sqrt{\sigma_{adj}}} \Big|_{su2} \Rightarrow \frac{M_{0+}}{\sqrt{\sigma_f}} \Big|_{su2} = 4.689(60), \quad (53)$$

where in the last step we use $\sigma_{adj}/\sigma_f|_{su2} = 2.24(3)$. (See Table B2 of [6].) Again this is consistent with the value $M_{0+}\sqrt{\sigma_f} = 4.737(6)$ that one obtains by direct calculation in $SU(2)$ [6].

Having established that the mass gap is the same (within errors) in the above pairs of theories, we can now ask whether the values we obtain for M_{0+}/g^2 predict the expected relations between the couplings.

We begin with $SO(3)$ and $SU(2)$. From Table 30 we obtain $M_{0+}/g^2|_{so3} = 0.4071(42)0.4080(41)$ whereas for $SU(2)$ one finds $M_{0+}/g^2|_{su2} = 1.5860(22)$. (See Table B1 of [6].) Assuming the mass gap is identical in $SU(2)$ and $SO(3)$, we obtain a relationship between the couplings

$$\frac{g_{f,so3}^2}{g_{f,su2}^2} = \frac{g_{a,su2}^2}{g_{f,su2}^2} = 3.896(41) \quad (54)$$

which should be compared to the expected value of 4 in eqn(9). The agreement is reasonably good.

We repeat the comparison for $SO(4)$ and $SU(2)$. Using the value in Table 30 we obtain $M_{0+}/g^2|_{so4} = 0.8032(72)$. Then, assuming the mass gap is identical in $SU(2) \times SU(2)$ and $SO(4)$, we obtain a relationship between the couplings

$$\frac{g_{f,so4}^2}{g_{f,su2}^2} = 1.975(18) \quad (55)$$

which agrees reasonably well with the expected value of 2 given in eqn(19).

Finally we repeat the exercise for $SO(6)$ and $SU(4)$. Again using the values in Table 30 we obtain $M_{0+}/g^2|_{so6} = 1.6074(84)$. Averaging the large and medium lattice values for $SU(4)$

in Table B1 of [6], we find $M_{0+}/g^2|_{su4} = 3.2212(68)$. We thus obtain a relationship between the couplings

$$\frac{g_{f,so6}^2}{g_{f,su4}^2} = 2.004(11) \quad (56)$$

which agrees well with the expected value of 2 derived in eqn(16).

The above results appear to show, within small errors, that the ratios of the mass gap, string tension and couplings are not influenced by the differing global properties of these pairs of groups.

As an aside, we remark that it can be interesting to perform such comparisons not only in the continuum limit but also at finite lattice spacing, because we expect the global properties of the group to make some difference at larger a (smaller β), since the field fluctuations will be larger there. We limit our comparison to comparing the values of $M_{0+}/\sqrt{\sigma_f}$ in $SO(6)$ with those of $M_{0+}/\sqrt{\sigma_{k=2A}}$ in $SU(4)$. We find these ratios to be independent of β in both cases, and equal to each other, within errors. Since our coarsest $a(\beta)$ in $SO(6)$ is close to the strong-to-weak coupling bulk transition, this suggests that the lattice physics is insensitive to the global properties of the group as soon as we are on the weak coupling side of the bulk transition.

6.4 Lie algebra equivalences: mass ratios

As discussed above, it is interesting to ask whether the single particle mass spectra of the pairs of $SO(N)$ and $SU(N')$ theories that share the same Lie algebra are in fact the same. We have just seen that this appears to be the case for the mass gap. So if the differing global properties of the groups are unimportant we would expect the value of M_G/M_{0+} to be the same for the $SO(3)$, $SO(4)$ and $SU(2)$ gauge theories and, separately, for the $SO(6)$ and $SU(4)$ gauge theories. To address this question we list in Table 33 the continuum ratio of the mass of each of our glueballs M_G to that of the lightest scalar glueball M_{0+} , for the groups $SO(3)$, $SO(4)$ and $SO(6)$, together with the corresponding mass ratios for $SU(2)$ and $SU(4)$ as obtained from [6].

6.4.1 $SO(3)$ and $SU(2)$

We begin by comparing $SO(3)$ with $SU(2)$. The lightest and hence best determined mass ratios are those of the 0^{+*} and of the 2^\pm glueballs and these we see from Table 33 are consistent between $SO(3)$ and $SU(2)$. The only other state graded as reliable, i.e. α or β , is the 0^{+**} which is also quite consistent, albeit within its large errors. The remaining masses do appear to differ, but mostly at no more than the $\sim 2\sigma$ level. Since we know that the overlaps of the glueballs onto our operators are much poorer in $SO(3)$ than in $SU(2)$, one possibility is that the effective energy plateaux are not being accurately identified in $SO(3)$ for these heavier states. This is indeed indicated by our reliability grading in Table 33. And the fact that where there are significant differences, it is the the $SO(3)$ masses in Table 33 that are in every case heavier than the corresponding $SU(2)$ ones is consistent with this interpretation.

Since the resolution of our correlators and the associated effective masses is greatest when the lattice spacing is smallest, and since in any case it is this calculation that is closest to the continuum limit, it is useful to look at the effective masses of our $SO(3)$ calculation at $\beta = 11$ and compare it to an $SU(2)$ calculation at a similar lattice spacing (in units of the mass gap). This we have already done in Figs 6 and 7. From Fig. 6 we see that while the overlap of the lightest scalar on our basis is almost as good for $SO(3)$ as for $SU(2)$, the $SO(3)$ overlaps rapidly worsen for the heavier scalars. Nonetheless it seems clear from the figure that the ratios $M_{0^{+*}}/M_{0^+}$, $M_{0^{+**}}/M_{0^+}$ are quite consistent between $SO(3)$ and $SU(2)$. It is also clear from Fig. 6 that we cannot be confident that there is any real mismatch between $SO(3)$ and $SU(2)$ for the ratios $M_{0^{+***}}/M_{0^+}$ and $M_{0^{+****}}/M_{0^+}$. Similar comments apply to the ratios M_{0^-}/M_{0^+} and M_{1^-}/M_{0^+} shown in Fig. 7. Only the $SO(3)$ $M_{2^{-*}}/M_{0^+}$ appears to show a sign of a plateau around $t = 4a, 5a$ that is quite different from the $SU(2)$ one, but even in that case the effective masses at large t show some indication of convergence. We also show the effective masses for the $M_{2^{+*}}/M_{0^+}$, which should be degenerate with $M_{2^{-*}}/M_{0^+}$ (in the large volume continuum limit), but here we do not see much sign of this plateau, suggesting that it may well be a fluctuation in the case of the 2^{-*} . So, in summary, what this brief analysis of our ‘best’ $SO(3)$ calculation shows is that for all but the lightest states the systematic errors that arise in our identification of the effective mass plateau are quite possibly large compared to the quoted statistical error, something which our grading of the states is intended to capture. The culprit is the poor overlap onto our basis in $SO(N)$ gauge theories when N is small, the effect of which is greater at larger value of $a(\beta)$, and this can of course affect the reliability of the continuum extrapolation.

6.4.2 $SO(4)$ and $SU(2)$

We now turn to a comparison of the $SO(4)$ and $SU(2)$ spectra in Table 33. Here the mass ratios that match within, say, a relatively innocuous $\sim 2\sigma$ are the $M_{0^{+*}}/M_{0^+}$ and the $M_{2^{\pm}}/M_{0^+}$. Since these are precisely the states that our grading judges to be reasonably reliable, this is reassuring. However the mismatch in the other cases is typically much larger than for $SO(3)$ which is, at first sight, surprising since the $SO(4)$ overlaps, while not very good, are significantly better than those in $SO(3)$ – which should imply a more reliable identification of the effective energy plateaux. However we also note, comparing Table 21 to Table 20, that the $SO(3)$ calculation is at much smaller lattice spacings than the $SO(4)$ calculation, when expressed in units of the mass gap. (We recall that the $SO(3)$ choice of lattice spacings was forced upon us by the the awkward location of the ‘bulk’ transition.) Since locating the energy plateau is less reliable at larger $a(\beta)$, this will serve to counteract the effect of better overlaps. This is well exemplified in Fig. 18 and Fig. 19 where we plotted the effective energies for the flux tube energy in our $SO(3)$ and $SO(4)$ calculations respectively. For a given $a(\beta)$, i.e. a given $aE_{eff}(t_0)$, the $SO(4)$ plateau is indeed better identified, but the calculations at the smallest values of a are indeed better for $SO(3)$ than $SO(4)$. This effect is even more marked for the glueball masses, since the $SO(3)$ string tension is larger than the $SO(4)$ one, and in comparing Fig. 18 and Fig. 19 we are effectively comparing values of $a(\beta)$ expressed in units of the string tension.

Given these uncertainties, it is interesting to compare the $SO(4)$ and $SU(2)$ mass calculations for a specific and similar lattice spacing. For this we return to Table 2 where we list $SU(2)$ masses taken from [6] in a calculation with a mass gap similar to the $SO(4)$ one in the table. The listed $SU(2)$ masses have been rescaled by the ratio of $SU(2)$ and $SO(4)$ mass gaps, so the apparent exact agreement for the mass gap is not significant. In addition to the ‘Ops B’ calculation, which is used in our continuum extrapolations, we list masses obtained with much higher statistics and with an operator basis that is the same as used in the $SU(2)$ calculation. The higher statistics should allow a somewhat better identification of the energy plateaux and so the ‘Ops A’ calculation should better represent the true $SO(4)$ spectrum at this value of $a(\beta)$. Comparing the ‘Ops A’ masses to the $SU(2)$ ones we see much less disagreement than for the continuum extrapolations listed in Table 33. The only discrepancy (slightly) greater than $\sim 3\sigma$ is for the 2^{-*} . This comparison suggests that the difference between the continuum extrapolations in Table 33 of $SO(4)$ and $SU(2)$ may indeed be driven, at least in large part, by a poor identification of the effective energy plateaux, particularly at the larger lattice spacings.

Finally, one needs to recall that the Lie algebra of $SO(4)$ is identical to that of $SU(2) \times SU(2)$ and not to that of $SU(2)$. Thus we would expect the spectrum of $SO(4)$ to contain states composed of two non-interacting glueballs, one from each of the $SU(2)$ colour groups. Of course $SU(2)$ also contains two glueball states, but their contribution is likely to be somewhat suppressed by the usual ‘large- N ’ suppression of single-trace/double-trace matrix elements. Thus we might expect the spectrum of $SO(4)$ to possess extra states, compared to $SU(2)$, once we are looking at masses $\geq 2m_{0+}$. (Up to some shift due to interactions induced by lattice spacing corrections.) We note that almost all the states in Table 33 where we have disagreement do indeed lie above this bound.

6.4.3 $SO(6)$ and $SU(4)$

For $SO(6)$ the overlaps are reasonably good and the calculation extends to a smaller value of $a(\beta)$ than for $SO(4)$ (in units of the mass gap). Hence the ambiguities in identifying an effective energy plateau should, in principle, be much less. And indeed the level of agreement between the $SO(6)$ and $SU(4)$ mass ratios listed in Table 33 is much better than that between $SO(4)$ and $SU(2)$. In fact the only states for which the discrepancy is greater than $\sim 2\sigma$ are the 0^{+**} and the 0^{+***} . These are states which, by our grading, should not be regarded as being very reliable.

The likelihood is that there is in fact a problem with our identification of the effective energy plateaux for these heavier states, and that this will be worse at the larger lattice spacings, where we have a coarser resolution of the correlators. The resulting systematic errors could then be magnified by the extrapolations involved in taking the continuum limit. This suggests that it might be useful to perform a comparison of the mass spectra at our smallest values of $a(\beta)$, rather than taking a continuum limit. We now do this, plotting the effective energies obtained from various glueball correlators in $SO(6)$ on a $62^2 70$ lattice at $\beta = 60.0$ and in $SU(4)$ on a $70^2 80$ lattice at $\beta = 86.0$ [6] which correspond to our smallest values of $a(\beta)$ in each case. We normalise the effective masses to our estimate of the mass gap in each case.

We can now directly compare the effective mass plots. This we do for the lightest five 0^+ states in Fig. 28 and for the lightest two 2^+ states, and the lightest 0^- and 1^+ in Fig. 29. (The lightest $J = 1, 2$ negative parity states are essentially the same as their positive parity partners.) What we observe in Fig. 29 is that in all the cases shown, it is entirely plausible that the $SO(6)$ effective energies are approaching the corresponding $SU(4)$ energies at large t . It is of course not possible to be confident in all cases that they actually do so, given what are clearly poorer overlaps in $SO(6)$ than in $SU(4)$. In Fig. 28 we see that the 0^{+*} masses are certainly consistent between $SO(6)$ and $SU(4)$, as are the 0^{+***} masses. (The agreement of the 0^+ ground state masses is of course enforced by our choice of normalisation.) However there is a substantial mismatch in the case of the 0^{+**} and of the 0^{+****} which shows no sign of disappearing as t increases.

So while we can conclude from our comparison at the smallest value of $a(\beta)$ that most of the masses we calculate in $SO(6)$ are consistent with their $SU(4)$ counterparts, there is an issue with the second and third excitations in the 0^+ sector. Here the effective masses do appear to display reasonably convincing plateaux, but these are different from the corresponding $SU(4)$ plateaux. One possibility is that due to quite different overlaps what we identify as the 0^{+*} is in fact the 0^{+***} and vice-versa, so that the $SO(6)$ state we label as the 0^{+*} should in fact be compared to the $SU(4)$ 0^{+***} . As we can see from Fig. 28, these states do in fact agree. One then has to speculate that what we label as the $SO(6)$ 0^{+***} will at large enough t become consistent with the $SU(4)$ 0^{+*} . The effective masses in Fig. 28 of the former state do show some hint that they decrease at larger t , but this is no more than a speculation with the calculations as they stand. So whether these mismatches are due to a sensitivity to the difference in the global properties of the $SO(6)$ and $SU(4)$ groups, or there are some significant systematic errors that we have not taken into account, is a question that needs to be addressed.

7 Other results

7.1 large- N scaling

We have assumed throughout that the large- N limit requires keeping g^2N fixed and that the leading correction is $O(1/N)$, following the all-orders analysis of diagrams [1] The fact that, as we have seen, such fits work well provides good evidence for their non-perturbative validity. Here we will try to be a little more quantitative.

We begin with the obvious comment that keeping g^2N fixed is necessary if one wants to obtain an $SO(\infty)$ theory that is perturbative (and asymptotically free) at short distances. If the correct limit was to keep g^2N^γ constant with $\gamma < 1$ then at any distance, however short, the theory would not be perturbative; and if $\gamma > 1$ then the theory would be free on all scales. In neither case could one regard that as a ‘smooth’ large- N limit. So we begin by assuming this scaling of the coupling and determine the power of the leading correction for the mass

gap in units of the 't Hooft coupling:

$$\frac{M_{0+}}{g^2 N} \Big|_{SO(N \rightarrow \infty)} = c_0 + \frac{c_1}{N^\alpha}, \quad SO(N \geq 3). \quad (57)$$

We find that $\alpha = 0.94 \pm 0.08$. So if the power of the correction is an integer, then this confirms that it must be $O(1/N)$.

It is worthwhile to see if our results also demand that $g^2 N$ should be kept constant. We can fit

$$\frac{M_{0+}}{g^2 N^\gamma} \Big|_{SO(N \rightarrow \infty)} = c_0 + \frac{c_1}{N}, \quad SO(N \geq 3). \quad (58)$$

and doing so we find a tight constraint $\gamma = 1.015 \pm 0.017$, just as expected.

7.2 spinorial states in the spectrum

In contrast to $SU(N)$, not all representations of $SO(N)$ can be obtained from products of the fundamental. In particular operators that project onto a single winding flux tube containing spinorial flux cannot be constructed using products of fundamental $SO(N)$ fields and so one might be tempted to assume that they do not appear in the spectrum of the $SO(N)$ Hamiltonian (or transfer matrix). On the other hand we would expect that a state consisting of a winding spinorial flux tube together with its conjugate (widely separated) would appear in the finite volume spectrum of the $SO(N)$ theory, because the net winding flux is a singlet, and so it will have a non-zero projection onto the contractible loops used for the glueball spectrum. (Such a state is often called a ‘torelon’.) This may appear mildly surprising and in this subsection we shall provide evidence that this is indeed the case.

We consider $SO(4)$ where, as we have seen in Sections 2.2.3 and 5.3 the string tension is twice that of $SU(2)$, i.e. $\sigma_f^{so4} = 2\sigma_f^{su2}$ when expressed in units of, say, the lightest scalar glueball mass. Torelon states composed of a winding flux tube and its conjugate will have an energy $E_T(l) \sim 2\sigma l + O(1/l)$, neglecting their interaction. On a symmetric $l \times l$ spatial volume we can consider $J^P = 0^+, 2^+$ states obtained by adding or subtracting the torelons winding around the x and y spatial tori. Once l is small enough that the torelon mass is smaller than the large l glueball mass, the torelon will become the lightest glueball with that J and from then on we will find that the glueball mass decreases with decreasing l roughly like $2\sigma l$. In $SU(2)$ this will occur with $\sigma = \sigma_f^{su2}$ and so for $2\sigma_f^{su2} l \leq M_G(l = \infty)$ we expect the glueball mass to decrease (roughly) linearly with l , as indeed one observes. In the case of $SO(4)$ one would naively expect the decrease to set in when $2\sigma_f^{so4} l \leq M_G(l = \infty)$, i.e. at a much smaller value of l than in $SU(2)$. (We need two winding flux tubes since a single one transforms non-trivially under the Z_2 centre symmetry, and this is why we consider $SO(4)$ rather than $SO(3)$.) If however the glueball mass in $SO(4)$ is the same as in $SU(2)$ then it should show the same l -dependence. This decrease in the lightest glueball mass will thus set in at a much larger value of l than one would naively expect by using $\sigma = \sigma_f^{so4}$ and if observed provides a signature of the presence of pairs of such spinorial flux tubes in the $SO(4)$ spectrum.

In Fig. 30 we display the dependence on l of the lightest 0^+ and 2^+ glueball masses in $SO(4)$ and in $SU(2)$. The $SO(4)$ calculation is at a value of the lattice spacing $a\sqrt{\sigma_f^{so4}} \simeq 0.160$ and the $SU(2)$ one at $a\sqrt{\sigma_f^{su2}} \simeq 0.118$. Given that $\sqrt{\sigma_f^{SO4}} = 2\sqrt{\sigma_f^{SU2}}$, this means that the $SO(4)$ lattice spacing differs by only about 8% from the $SU(2)$ one, and so the calculations should be comparable once l and the glueball masses are expressed in physical units, as they are in Fig. 30. (For this we use the $l = \infty$ value of the mass gap.) We also plot the energy of twice the fundamental flux loop in both cases (as a rough estimate of the corresponding torelon masses). We observe that the l -dependence is very similar in $SU(2)$ and $SO(4)$. (The slight difference may be due to slightly different $O(a^2)$ corrections.) We also observe that the rapid decrease with decreasing l of the 2^+ glueball mass sets in, in the case of $SO(4)$, when the fundamental torelon is very much more massive, and presumably irrelevant, while the spinorial (i.e. fundamental $SU(2)$) torelon is comparable in mass. This provides quite compelling evidence that at small l the $SO(4)$ mass is dominated by a spinorial torelon.

Some comments. The dimension of the spinorial representation grows rapidly with N and the associated string tension presumably becomes larger than the fundamental string tension. So it can be ignored at larger N , as far as finite volume corrections are concerned. We have chosen not to perform the comparison for $SO(3)$ both for the reason already given and also because the $SO(3)$ fundamental flux tube is not stable (it corresponds to the adjoint of $SU(2)$) and so can, by itself, have a non-zero overlap onto glueball operators. Finally, using $SO(6)$ instead of $SO(4)$ would have been elegant, but since $\sigma_f^{SO6} = \sigma_{k=2}^{SU4} \simeq 1.35\sigma_{k=2}^{SU2}$ the effect would have been less striking than with $SO(4)$ unless one had significantly greater statistical accuracy.

7.3 strong coupling

We see from Table 1 that at low N the ‘bulk transition’ occurs at a small value of the lattice spacing when the latter is expressed in physical units such as the string tension or the mass gap. Given this fact and the fact that the physics, or most of it, appears to be continuous across the transition region, it is tempting to ask if any aspect of the continuum behaviour already appears on the strong coupling side of the transition. This question is peripheral to the main focus of this paper, so we address it only briefly.

We consider $SO(3)$ where the bulk transition is at the weakest coupling. We have calculated some glueball masses and the string tension for a range of couplings in the ‘strong coupling’ region, including the bulk cross-over region. As we go deeper into strong coupling, the value of a mass in lattice units, aM , will become larger, and so the correlators will fall more steeply and our estimate of the glueball mass becomes less reliable. We therefore focus here on the lightest $J^P = 0^+$ and $J^P = 2^-$ glueball masses and the string tension. We focus on glueballs with $J^P = 2^-$ rather than $J^P = 2^+$ because our volumes in the strong coupling region are not large enough to guarantee that the 2^+ is unaffected by finite volume torelon contributions.

We display in Fig 31 our calculated values in $SO(3)$ of

$$\frac{\beta_I}{2N^2}a\mu \equiv \frac{\beta\langle u_p \rangle}{2N^2}a\mu = \frac{\mu}{g_I^2 N} \quad ; \quad \mu = \sqrt{\sigma}, M_{0^+} \quad (59)$$

where $\langle u_p \rangle$ is the average plaquette, and the subscript I denotes the mean-field improvement of the (inverse) couplings. Note that in the cross-over region we do not use the anomalous, nearly massless and weakly coupled scalar glueball mass but rather the first excitation which is the one that is a clear continuation of the strong coupling mass gap. We show the best fits to the weak coupling values that are linear in $1/\beta_I$, and remark that attempting to include some of the strong coupling values with quadratic fits simply does not work. It is very clear from all this that the strong coupling dependence of μ/g^2 is qualitatively different from that on the weak coupling side, and does not provide useful information about the continuum limit of this ratio.

It is of course not surprising that the dependence on β of $\beta\mu$ should not be well captured by a low order expansion in powers of $1/\beta$ when we are on the strong coupling side of the bulk transition where the natural expansion is presumably in positive powers of β . A more relevant question to ask is whether any ratios of physical quantities are better behaved when plotted against a^2 . The point here is that perhaps a^2 is small enough on at least part of the strong coupling side for an operator product expansion in powers of a^2 to make sense even if an expansion in positive powers of ag^2 does not work. To address this question we plot in Fig 32 the ratios $m_{0+}/\sqrt{\sigma}$, $m_{2-}/\sqrt{\sigma}$ and m_{2-}/m_{0+} . We see that in this last case, where we have the ratio of two glueball masses, there is in fact no marked difference in the a^2 dependence between weak and strong coupling, and the weak-coupling linear extrapolation to the continuum limit appears to describe the physical mass ratios at strong coupling just as well, to a good approximation. In contrast to this, the continuum extrapolations of $m_{0+}/\sqrt{\sigma}$ and $m_{2-}/\sqrt{\sigma}$ clearly do not pass through the strong coupling values. However what is interesting is that it is possible to get good linear fits to (most of) the strong coupling values by themselves. These are shown as dashed lines in Fig 32. We recall a very similar observation in [8] for the deconfining temperature in units of the string tension. (In that case for $N \geq 4$ since no calculation for $SO(3)$ was attempted.) These strong coupling ‘continuum’ extrapolations differ from the weak-coupling ones, albeit by not very much. All this suggests that perhaps the expansion in a^2 makes sense on the strong coupling side, and perhaps it even makes sense to talk of a separate continuum limit to the strongly coupled gauge theory.

As an aside we remark that in $D = 3+1$ the bulk cross-over becomes a first-order transition, and the mass ratios appear to take very different values on either side of the transition. So here the strong-weak coupling transition appears to be much more conventional.

8 Conclusions

In this paper we set out to address several interesting questions about $SO(N)$ gauge theories. We have chosen to work in $D = 2 + 1$ rather than in $D = 3 + 1$, since the strong-to-weak coupling transition is awkwardly placed in the latter case, and because these questions apply equally well in $D = 2 + 1$. The quantities we focus upon are the low-lying mass (‘glueball’) spectrum, the confining string tension and the coupling. (Elsewhere [8] we have analysed the finite temperature deconfining transition.)

The main questions we address have to do with various relationships between $SO(N)$ and

$SU(N)$ gauge theories. At $N = \infty$ diagrammatic [1] and orbifold [2, 3] arguments lead us to expect that the theories have the same local physics in the $C = +$ sector, and we would like to confirm by explicit calculation that this is so for non-perturbative physics. At low N , we know that $SO(3)$, $SO(4)$ and $SO(6)$ have the same Lie algebras as $SU(2)$, $SU(2) \times SU(2)$ and $SU(4)$ respectively, so we would like to see if this means that the physics within each pair of theories is the same, or if the differing global properties of the groups leads, for example, to some glueball masses being different.

Another question we address is whether $SO(N)$ gauge theories are linearly confining. This question is particularly interesting when N is odd, because in that case the centre of the group is trivial, and one loses the standard connection between confinement and the unbroken centre symmetry.

To give convincing answers to these questions requires accuracy and precision, particularly because the $SU(N)$ spectra and string tensions with which one compares are now known with quite good accuracy [6, 12]. Unfortunately, as it turns out we are only able to achieve the intended accuracy in some of the lightest states. In the case of our $N = \infty$ extrapolations it is apparent from Tables 31,32 that the statistical errors on our $SO(\infty)$ mass ratios are typically some 3 to 5 times larger than the errors on the $SU(\infty)$ calculations despite the fact that nominally the ‘statistics’ of the two sets of calculations is comparable. While at small N one can point to the mediocre overlaps of our operators onto the glueballs as contributing to this, at larger N this ceases to be the case and it is our larger N results that should dominate the extrapolation to $N = \infty$. This suggests that our Monte Carlo algorithm for $SO(N)$ is less efficient than the one used for $SU(N)$ despite the superficial similarity of the heat bath. While this may be in part because we have not included some analogue of the $SU(N)$ over-relaxation in our $SO(N)$ update, this might not be the whole story. In any case, this is clearly something that needs to be addressed if one wishes to achieve real precision in $SO(N)$. Even more important for our comparisons is the mediocre overlap of our operator basis onto the states of interest, particularly at small N . This magnifies certain systematic errors and a significant part of our work in this paper has been devoting to deciding whether the observed mismatches between certain mass ratios in various $SO(N)$ and $SU(N')$ theories reflect a real difference or an underestimate of these systematic errors. To help guide the reader as to which states are most reliably calculated, we introduced a grading system. The masses of states labelled by α or β should be reliable, within the quoted errors, but this becomes less likely as we move to γ and beyond. The string tension calculations should be reliable, with some caution for $SO(3)$.

Despite the above caveats, we have been able to come to a number of useful conclusions. In the context of the N -dependence we found that when extrapolating to $N = \infty$ various ratios of string tensions, glueball masses and the 't Hooft coupling, a single fitting function encompasses both the odd N and even N values. That is to say the physics appears to be a single function of N , rather than there being separate functions for odd and for even N , which only converge at $N = \infty$. As for the $N = \infty$ limit, we found that our most accurately extrapolated ratios, those involving the mass gap, m_{0+} , the string tension, σ , and the coupling g^2 , agree well with the corresponding values for $SU(N \rightarrow \infty)$, with errors at the level of 1% or less. (In the case of g^2 the comparison includes, and so confirms, the factor of

2 that is predicted by the diagrammatic analysis.) Of the other states which we believe to be reliable (graded as β), the 2^+ and 2^- are consistent with the $SU(\infty)$ values, but the 0^{+*} is not. The discrepancy of the latter is around 4.7 standard deviations when using the more plausible higher order extrapolations to $N = \infty$. Whether this is a real mismatch between $SO(N \rightarrow \infty)$ and $SU(N \rightarrow \infty)$, or is due to unexpectedly large systematic errors remains an open question at this stage. As for the other, less well-determined mass ratios, these are in reasonable agreement with those in $SU(N \rightarrow \infty)$, except for the 2^{-*} . But given our grade of δ for the reliability of this state, this need not be a cause for concern.

Our comparison of the mass gap, string tension and coupling of $SU(2)$ with those of $SO(3)$ and $SO(4)$, and of $SU(4)$ with $SO(6)$, shows that the ratios agree once one translates the couplings and the string tension representations appropriately. (For example, the fundamental flux in $SO(6)$ corresponds to the $k = 2$ antisymmetric flux in $SU(4)$.) One should note, however, that when comparing the values of $\sqrt{\sigma/g^2}$ in $SO(3)$ and $SU(2)$ the errors are large due to the instability of the flux tube, which reduces the significance of the apparent agreement. For the continuum glueball mass ratios, M/m_{0^+} , listed in Table 33, the masses that are calculated reliably (i.e. α, β) do agree within 2σ . This is also the case for the other states in the comparison between $SO(3)$ and $SU(2)$ and in that between $SO(6)$ and $SU(4)$ except, in the latter case, for the 0^{+**} and 0^{+***} . There are more pronounced disagreements in the comparison between $SO(4)$ and $SU(2)$, which may be due to the unsuppressed presence of states that simultaneously contain glueballs from the two $SU(2)$ colour groups. In summary, it is striking that the physical quantities which we best control do in fact agree between the $SO(N)$ and $SU(N')$ theories that share the same Lie algebras. So in these cases at least, it appears that the difference in the global properties of the groups plays no role.

Our above discussion assumes a well defined string tension which presupposes that $SO(N)$ theories are linearly confining – if not exactly then at least for ‘all practical purposes’. This we have attempted to verify by calculating the ground state energy, $E_f(l)$, of a flux tube that winds once around a spatial torus, as a function of the length l of the torus and hence of the flux tube. For even N we found that $E_f(l)$ is well described by a fit that includes a linear term modified by the known universal corrections to the linear term, as in Fig. 9. This provides numerical evidence for linear confinement that is more-or-less as convincing as what one has in $SU(N)$ gauge theories. Odd N is more controversial because here the centre of the group is trivial. In the $N \rightarrow \infty$ planar limit we expect to recover linear confinement, so the question is what happens at smaller odd values of N . For $SO(3)$ the situation, as shown in Figs 14 and 15, is far from clear-cut, no doubt due to the significant instability of the flux tube, which is expected since it can be broken by gluon pairs from the vacuum. Nonetheless we can extract an effective string tension, albeit with large errors, similarly to the way one can extract an effective adjoint string tension in $SU(2)$ [6, 12]. For $SO(5)$ the evidence for linear confinement, as displayed in Figs 12 and 13, looks as convincing as what we find for even N . Of course, for neither odd nor even N does this demonstrate asymptotic linear confinement, something that a numerical calculation cannot do. However what it tells us is that even if the flux tube is not stable for odd N , its decay width is so small that we can safely extract a string tension within our errors – rather as if we were assigning a mass to a resonance with a decay width that while non-zero was so small as to be invisible in our calculations. What a

small but non-zero decay width of the flux tube might imply for absolute confinement is not obvious. Indeed that is what one has in QCD with light quarks (string-breaking by $q\bar{q}$ pairs) and that theory is believed to be absolutely confining. Moreover it appears that in QCD the vacuum expectation value of similarly blocked Polyakov loops is substantially larger than our bounds on that quantity in $SO(5)$. (See Figs 1,2 of [30].) The fact that we do observe a non-zero overlap of the vacuum onto our basis of winding operators in $SO(5)$, albeit not onto the ground state of the flux tube, motivates seeing what happens to this overlap as N grows. We therefore performed a more detailed study in Section 4.2 of the overlap of the vacuum onto the ground state of the flux tube for $N = 3, 5, 7, 9, 11$. This confirmed that apart, perhaps, from the case of $SO(3)$, any instability of the flux tube ground state is so small as to be consistent with zero within the small errors of our calculation, and, moreover, the overlap onto the whole basis of winding operators does decrease rapidly with increasing N . While this provides evidence that $SO(2N + 1)$ theories are linearly confining ‘for all practical purposes’ (at least for $2N + 1 \geq 5$) it does not answer the question of whether they are exactly confining. The lack of a non-trivial centre symmetry makes the question similar to the one for QCD with light quarks. Although QCD is believed to be exactly confining (i.e. the energy of an isolated coloured charge is infinite) our usual non-local order parameters (e.g. asymptotic exponential decay of Wilson loops) are not useful. Here we expect that the route to follow will be similar to that for $SO(3)$. The exact confinement of fundamental charges in $SO(3)$ is believed to follow from the exact confinement of adjoint charges in $SU(2)$, even though the adjoint Wilson loop in $SU(2)$ does not possess an asymptotic area decay. The natural generalisation of this argument is to note that $SO(N)$ and $Spin(N)$ share the same Lie algebra and that the latter has a non-trivial center and so it would be no surprise if it possesses exact linear confinement. To develop this argument in detail would be very interesting but would take us beyond the scope of the calculations in this paper.

We also briefly touched upon the interesting question of whether the spinorial flux tubes in $SO(4)$, which correspond to the fundamental flux tubes of $SU(2)$, affect the physics of the $SO(4)$ theory. By comparing the finite volume dependence of the tensor glueball mass in this pair of theories we obtained what we believe to be quite good evidence that the $SO(4)$ theory does indeed contain states composed of a spinorial flux tube and its conjugate, even if, somewhat paradoxically, it does not contain states composed of a single such spinorial flux tube. The issue being highlighted here is clearly much more general. For example, does $SO(6)$ contain states that correspond to a pair of $J^{PC} = 0^{--}$ $SU(4)$ glueballs (which together will form a $J^{PC} = 0^{++}$ state for even orbital angular momentum) even though it does not possess a state consisting of a single such glueball? After all, such states contribute to the decay width of a sufficiently excited 0^{++} glueball in $SU(4)$ and if the decay width is the same in $SO(6)$ then they are surely present in the latter theory? That is to say, a field theory may contain more states than is apparent from the ‘evident’ symmetries of the theory? We intend to address these interesting questions separately elsewhere.

Acknowledgements

Our interest in this project was originally motivated by Aleksey Cherman and Francis Bursa. We acknowledge, in particular, the key contributions made by Francis Bursa to this project in its early stages. The project originated in a number of discussions during the 2011 Workshop on ‘Large- N Gauge Theories’ at the Galileo Galilei Institute in Florence, and we are grateful to the Institute for providing such an ideal environment within which to begin collaborations. The numerical computations were carried out on the computing cluster in Oxford Theoretical Physics.

References

- [1] C. Lovelace, *Universality at large N* , Nuclear Physics B201 (1982) 333.
- [2] S. Kachru and E. Silverstein, *4D conformal field theories and strings on orbifolds*, Phys. Rev. Lett. 80 (1998) 4855 [arXiv:hep-th/9802183].
M. Bershadsky and A. Johansen, *Large N limit of orbifold field theories*, Nucl. Phys. B536 (1998) 141 [arXiv:hep-th/9803249].
Martin Schmaltz, *Duality of nonsupersymmetric large N gauge theories*, Phys. Rev. D59 (1999) 105018 [arXiv:hep-th/9805218].
M. Strassler, *On methods for extracting exact nonperturbative results in nonsupersymmetric gauge theories*, arXiv:hep-th/0104032.
A. Cherman, M. Hanada, and D. Robles-Llana, *Orbifold equivalence and the sign problem at finite baryon density*, Phys. Rev. Lett. 106 (2011) 091603 [arXiv:1009.1623].
A. Cherman and Brian C. Tiburzi, *Orbifold equivalence for finite density QCD and effective field theory*, JHEP 1106 (2011) 034 [arXiv:1103.1639].
M. Hanada and N. Yamamoto, *Universality of phases in QCD and QCD-like theories*, JHEP 1202 (2012) 138 [arXiv:1103.5480].
M. Blake and A. Cherman, *Large N_c Equivalence and Baryons*, Phys. Rev. D86 (2012) 065006 [arXiv:1204.5691].
- [3] P. Kovtun, M. Unsal and L. Yaffe, *Necessary and sufficient conditions for non-perturbative equivalences of large N orbifold gauge theories*, JHEP 0507 (2005) 008 [arXiv:hep-th/0411177].
M. Unsal and L. Yaffe, *(In)validity of large N orientifold equivalence*, Phys. Rev. D74 (2006) 105019 [arXiv:hep-th/0608180].
- [4] G.’t Hooft, *On the Phase Transition Towards Permanent Quark Confinement*, Nucl. Phys. B138 (1978) 1.
G.’t Hooft, *On the Phase Transition Towards Permanent Quark Confinement*, Nucl. Phys. B153 (1979) 141.
G.’t Hooft, *Confinement and Topology in Nonabelian Gauge Theories*, Acta Phys.Austriaca Suppl. 22 (1980) 531.

- [5] F. Bursa, R. Lau, and M. Teper, *SO(2N) and SU(N) gauge theories in 2 + 1 dimensions*, JHEP 1305 (2013) 025 [arXiv:1208.4547].
- [6] A. Athenodorou and M. Teper, *SU(N) gauge theories in 2+1 dimensions: glueball spectra and k-string tensions*, JHEP 1702 (2017) 015 [arXiv:1609.03873].
- [7] A. Athenodorou, R. Lau, and M. Teper, *On the weak N-dependence of SO(N) and SU(N) gauge theories in 2+1 dimensions*, Phys. Lett. B749 (2015) 448 [arXiv:1504.08126].
- [8] R. Lau and M. Teper, *The deconfining phase transition of SO(N) gauge theories in 2+1 dimensions*, JHEP 1603 (2016) 072 [arXiv:1510.07841].
- [9] R. Lau, *SO(N) gauge theories in 2+1 dimensions*, DPhil Thesis, University of Oxford, 2014.
- [10] G.'t Hooft, *A planar diagram theory for strong interactions*, Nucl. Phys. B72 (1974) 461.
- [11] M. Teper, *SU(N) gauge theories in 2+1 dimensions*, Phys.Rev. D59 (1999) 014512 [arXiv:hep-lat/9804008].
 B. Lucini, M. Teper and U. Wenger, *Glueballs and k-strings in SU(N) gauge theories : calculations with improved operators*, JHEP 0406:012 (2004) [arXiv:hep-lat/0404008].
 B. Lucini, M. Teper, *SU(N) gauge theories in four-dimensions: Exploring the approach to N = infinity*, JHEP 0106 (2001) 050 [arXiv:hep-lat/0103027].
- [12] A. Athenodorou and M. Teper, *Closed flux tubes in D=2+1 SU(N) gauge theories: dynamics and effective string description*, JHEP 1610 (2016) 093 [arXiv:1602.07634].
- [13] J. Ambjorn, P. Olesen and C. Peterson, *Stochastic Confinement and Dimensional Reduction. 2. Three-dimensional SU(2) Lattice Gauge Theory*, Nucl. Phys. B240 (1984) 533;
 J. Ambjorn, P. Olesen and C. Peterson, *Stochastic Confinement and Dimensional Reduction. 1. Four-Dimensional SU(2) Lattice Gauge Theory*, Nucl. Phys. B240 (1984) 189.
- [14] P.W. Stephenson, *Physical and unphysical effects in the mixed SU(2)/SO(3) gauge theory*, arXiv:hep-lat/9604008.
- [15] B. Bringoltz and M. Teper, *Closed k-strings in SU(N) gauge theories: 2+1 dimensions*, Phys. Lett. B663 (2008) 429 [arXiv:0802.1490].
- [16] H. B. Meyer, *Glueball Regge Trajectories*, D. Phil Thesis, University of Oxford, 2005 [arXiv: hep-lat/0508002].
- [17] O. Aharony and Z. Komargodski, *The Effective Theory of Long Strings*, JHEP 1305 (2013) 118 [arXiv:1302.6257].
 O. Aharony and M. Dodelson, *Effective String Theory and Nonlinear Lorentz Invariance*, JHEP 1202 (2012) 008 [arXiv:1111.5758].
 O. Aharony, M. Field and N. Klinghoffer, *The effective string spectrum in the orthogonal*

- gauge*, JHEP 1204 (2012) 048 [arXiv:1111.5757].
O. Aharony and N. Klinghoffer, *Corrections to Nambu-Goto energy levels from the effective string action*, JHEP 1012 (2010) 058 [arXiv:1008.2648].
O. Aharony and E. Karzbrun, *On the effective action of confining strings*, JHEP 0906 (2009) 012 [arXiv:0903.1927].
- [18] M. Lüscher and Peter Weisz, *String excitation energies in $SU(N)$ gauge theories beyond the free-string approximation*, JHEP 0407 (2004) 014 [arXiv:hep-th/0406205].
J. M. Drummond, *Universal Subleading Spectrum of Effective String Theory*, arXiv:hep-th/0411017.
- [19] S. Dubovsky and V. Gorbenko, *Towards a Theory of the QCD String*, JHEP 1602 (2016) 022 [arXiv:1511.01908].
P. Cooper, S. Dubovsky, V. Gorbenko, A. Mohsen and S. Storace, *Looking for Integrability on the Worldsheet of Confining Strings*, JHEP 1504 (2015) 127 [arXiv:1411.0703].
S. Dubovsky, R. Flauger and V. Gorbenko, *Flux Tube Spectra from Approximate Integrability at Low Energies*, J.Exp.Theor.Phys. 120 (2015) 399 [arXiv:1404.0037].
M. Caselle, D. Fioravanti, F. Gliozzi and R. Tateo, *Quantisation of the effective string with TBA*, JHEP 1307 (2013) 071 [arXiv:1305.1278].
S. Dubovsky, R. Flauger and V. Gorbenko, *Evidence for a new particle on the worldsheet of the QCD flux tube*, Phys. Rev. Lett. 111 (2013) 6, 062006 [1301.2325].
S. Dubovsky, R. Flauger and V. Gorbenko, *Solving the Simplest Theory of Quantum Gravity*, JHEP 1209 (2012) 133 [arXiv:1205.6805].
S. Dubovsky, R. Flauger and V. Gorbenko, *Effective String Theory Revisited*, JHEP 09 (2012) 044 [arXiv:1203.1054].
- [20] A. Athenodorou and M. Teper, *Closed flux tubes in higher representations and their string description in $D=2+1$ $SU(N)$ gauge theories*, JHEP 1306 (2013) 053 [arXiv:1303.5946].
A. Athenodorou, B. Bringoltz and M. Teper, *Closed flux tubes and their string description in $D=2+1$ $SU(N)$ gauge theories*, JHEP 1105 (2011) 042 [arXiv:1103.5854].
A. Athenodorou, B. Bringoltz and M. Teper, *On the spectrum of closed $k=2$ flux tubes in $D=2+1$ $SU(N)$ gauge theories*, JHEP 0905 (2009) 019 [arXiv:0812.0334].
A. Athenodorou, B. Bringoltz and M. Teper, *The closed string spectrum of $SU(N)$ gauge theories in $2+1$ dimensions*, Phys.Lett.B656 (2007) 132 [arXiv:0709.0693].
- [21] G.P. Lepage and P.B. Mackenzie, *Viability of lattice perturbation theory*, Phys. Rev. D48 (1993) 2250 [arXiv:hep-lat/9209022].
G. Parisi, *Recent Progresses in Gauge Theories*, AIP Conf Proc 68 (1980).
- [22] F. Bursa and M. Teper, *Strong to weak coupling transitions of $SU(N)$ gauge theories in $2+1$ dimensions*, Phys. Rev. D74 (2006) 125010 [arXiv:hep-th/0511081].
- [23] D. Gross and E. Witten, *Possible Third Order Phase Transition in the Large N Lattice Gauge Theory*, Phys. Rev. D21 (1980) 446.

- [24] Ph de Forcrand and O. Jahn, *Comparison of $SO(3)$ and $SU(2)$ lattice gauge theory*, Nucl. Phys. B651 (2003) 125 [arXiv:hep-lat/0211004].
- [25] H. Meyer and M. Teper, *Glueball Regge trajectories and the Pomeron – a lattice study*, Phys.Lett. B605 (2005) 344 [arXiv:hep-ph/0409183].
H. Meyer and M. Teper, *Glueball Regge trajectories in $(2+1)$ dimensional gauge theories*, Nucl.Phys. B668 (2003) 111 [arXiv:hep-lat/0306019].
H. Meyer and M. Teper, *High Spin Glueballs from the Lattice*, Nucl.Phys. B658 (2003) 113 [arXiv:hep-lat/0212026].
- [26] M. Luscher, *Volume Dependence of the Energy Spectrum in Massive Quantum Field Theories. 2. Scattering States*, Commun.Math.Phys. 105 (1986) 153.
M. Luscher, *Volume Dependence of the Energy Spectrum in Massive Quantum Field Theories. 1. Stable Particle States*, Commun.Math.Phys. 104 (1986) 177.
- [27] J. Liddle and M. Teper, *The deconfining phase transition in $D=2+1$ $SU(N)$ gauge theories*, arXiv:0803.2128, 2008.
J. Liddle, *The deconfining phase transition in $D=2+1$ $SU(N)$ gauge theories*, D.Phil thesis, University of Oxford, 2006.
K. Holland, M. Pepe, and U-J. Wiese, *Revisiting the deconfinement phase transition in $SU(4)$ Yang–Mills theory in $2+1$ dimensions*, JHEP 0802 (2008) 041 [arXiv:0712.1216].
K.Holland, *Another weak first order deconfinement transition: three-dimensional $SU(5)$ gauge theory*, JHEP 0601 (2006) 023 [arXiv:hep-lat/0509041].
- [28] M. Lüscher, *Symmetry Breaking Aspects of the Roughening Transition in Gauge Theories*, Nucl. Phys. B180 (1981) 317.
M. Lüscher, K. Symanzik and P. Weisz, *Anomalies of the Free Loop Wave Equation in the WKB Approximation*, Nucl. Phys. B173 (1980) 365.
- [29] K. Holland, M. Pepe and U.-J. Wiese, *The Deconfinement phase transition of $Sp(2)$ and $Sp(3)$ Yang-Mills theories in $(2+1)$ -dimensions and $(3+1)$ -dimensions*, Nucl. Phys. B694 (2004) 35 [arXiv:hep-lat/0312022].
- [30] A. Hart and M. Teper (UKQCD Collaboration), *On the glueball spectrum in $O(a)$ -improved lattice QCD*, Phys. Rev. D65 (2002) 034502 [arXiv:hep-lat/0108022].
- [31] G. 't Hooft, *Large N* , arXiv:hep-th/0204069.

group	$\beta_b \in$	$a\sqrt{\sigma} \sim$	$l^2 >$
SO(3)	[5.75,6.25]	0.15	50^2
SO(4)	[9.1,10.2]	0.22	30^2
SO(5)	[13.5,15.4]	0.27	22^2
SO(6)	[18.0,21.3]	0.31	16^2
SO(7)	[23.5,28.0]	0.35	12^2
SO(8)	[31,35]	0.39	10^2
SO(12)	[65,73]	0.46	9^2
SO(16)	[111,124]	0.54	8^2

Table 1: Location $\beta = \beta_b$ of bulk transition, with string tension on weak coupling side and smallest useful spatial volume on weak coupling side.

J^P	$SO(4), \beta = 15.1$		$SU(2), \beta = 16.0$
	Ops A on $50^2 56$	Ops B on $48^2 56$	Ops A on $68^2 48$
0^+	0.4807(13)	0.480(4)	0.4807(19)
0^{+*}	0.706(4)	0.712(6)	0.692(4)
0^{+**}	0.886(9)	0.925(11)	0.857(6)
0^{+***}	0.982(14)	1.020(19)	0.939(7)
0^{+****}	1.026(17)	1.028(19)	0.987(6)
2^+	0.8003(25)	0.820(6)	0.789(5)
2^-	0.8005(51)	0.816(4)	0.799(4)
2^{+*}	0.963(10)	1.029(42)	0.919(10)
2^{-*}	0.985(5)	0.992(19)	0.939(7)
0^-	1.005(17)	1.043(8)	1.005(8)
1^+	1.045(76)	1.180(26)	1.084(9)
1^-	1.137(28)	1.176(27)	1.068(9)
am_p	1.037(6)	0.993(4)	

Table 2: Spectrum at $\beta = 15.1$ in $SO(4)$ using two different operator bases. Also an $SU(2)$ calculation using basis A, with masses rescaled up by a factor 1.169 to a common mass gap. Also the flux loop mass, am_p .

$L_s^2 L_t$	12 ² 36	16 ² 36	20 ² 36	24 ² 36	28 ² 36	32 ² 36	36 ² 36
$l\sqrt{\sigma}$	1.61	2.15	2.68	3.22	3.76	4.30	4.83
am_P	0.1349(15)	0.2366(19)	0.3306(19)	0.4078(41)	0.4834(22)	0.5606(19)	0.6354(22)
$a\sqrt{\sigma}$	0.1243(5)	0.1303(5)	0.1338(4)	0.1339(6)	0.1340(4)	0.1343(3)	0.1344(3)
0 ⁺	0.247(10)	0.447(5)	0.494(9)	0.492(9)	0.506(2)	0.514(4)	0.511(3)
0 ⁺ *	0.252(11)	0.508(26)	0.675(17)	0.737(16)	0.769(4)	0.789(8)	0.773(7)
0 ⁺ **	0.489(29)	0.558(23)	0.836(38)	0.935(21)	0.968(30)	1.021(14)	0.994(11)
0 ⁺ ***	0.482(29)	0.854(29)	0.883(19)	0.996(33)	0.992(10)	1.021(6)	1.028(12)
0 ⁺ ****	0.523(25)	0.947(7)	1.005(20)	1.091(35)	1.098(11)	1.124(18)	1.088(17)
2 ⁺	0.228(6)	0.385(31)	0.874(11)	0.875(8)	0.859(7)	0.857(8)	0.850(8)
2 ⁺ *	0.668(34)	0.681(46)	0.899(18)	1.031(26)	1.058(10)	1.040(15)	1.054(13)
2 ⁻	0.471(10)	0.769(11)	0.854(12)	0.892(21)	0.852(5)	0.837(17)	0.869(4)
2 ⁻ *	0.783(19)	0.824(11)	1.035(24)	1.001(25)	1.052(8)	1.073(15)	1.071(15)
0 ⁻	1.124(7)	1.126(24)	1.117(22)	1.134(38)	1.095(11)	1.110(7)	1.118(19)
1 ⁺	1.308(33)	1.322(36)	1.277(36)	1.260(43)	1.252(14)	1.280(20)	1.265(23)
1 ⁻	1.286(26)	1.225(24)	1.274(33)	1.295(48)	1.270(12)	1.237(25)	1.246(20)

Table 3: Glueball masses, am_G , and the flux loop energy, am_P , with corresponding string tensions $a\sqrt{\sigma}$ extracted using the Nambu-Goto formula in eqn(24). On various volumes at $\beta = 84$ in $SO(8)$.

	$SO(3)$		$SO(4)$		$SO(6)$	
$L_s^2 L_t$	46 ² 46	62 ² 48	34 ² 44	44 ² 52	36 ² 44	54 ² 44
$a\sqrt{\sigma}$	0.1333(8)	0.1353(11)	0.1617(4)	0.1621(3)	0.12658(22)	0.12680(28)
$l\sqrt{\sigma}$	6.13	8.39	5.50	7.13	4.56	6.85
0 ⁺	0.3963(25)	0.3964(34)	0.5353(35)	0.5395(16)	0.457(3)	0.467(2)
0 ⁺ *	0.571(11)	0.5958(42)	0.770(14)	0.801(3)	0.695(7)	0.708(5)
0 ⁺ **	0.716(11)	0.716(12)	0.910(26)	1.030(5)	0.891(19)	0.910(17)
0 ⁺ ***	0.784(12)	0.801(16)	1.138(9)	1.099(26)	0.920(19)	0.929(15)
0 ⁺ ****	–	0.869(20)	1.046(14)	1.143(23)	1.014(7)	1.012(22)
2 ⁺	0.6783(21)	0.6660(51)	0.898(8)	0.908(9)	0.788(6)	0.768(9)
2 ⁺ *	0.796(15)	0.815(8)	1.088(6)	1.091(19)	0.966(7)	0.961(20)
2 ⁻	0.6750(37)	0.6756(45)	0.9145(36)	0.900(9)	0.777(4)	0.772(9)
2 ⁻ *	0.779(16)	0.785(12)	1.097(16)	1.090(22)	0.970(22)	0.974(8)
0 ⁻	0.882(10)	0.845(20)	1.183(24)	1.195(9)	1.003(9)	0.972(23)
1 ⁺	0.967(9)	0.977(12)	1.311(34)	1.404(15)	1.167(8)	1.165(10)
1 ⁻	0.938(28)	0.966(13)	1.322(31)	1.371(14)	1.158(10)	1.156(9)

Table 4: Finite volume test for glueball masses and the string tension in $SO(3)$, $SO(4)$ and $SO(6)$ at $\beta = 7.0, 13.7, 46.0$ respectively.

N	3	4	5	6	7	8	12	16
$l\sqrt{\sigma} \sim$	8.0(6.5)	7.0(4.5)	6.0	4.5	4.2	3.7	3.5	3.5

Table 5: Approximate values of $l\sqrt{\sigma}$ for $SO(N)$ mass spectrum calculations. In brackets the smaller volumes used at low N for the string tension.

$SO(6)$			$SO(8)$		
l_x	$l_y \times l_t$	$aE(l_x)$	l_x	$l_y \times l_t$	$aE(l_x)$
18	48×64	0.2582(11)	12	48×80	0.1504(35)
22	42×52	0.3280(13)	16	36×64	0.2360(39)
26	40×52	0.3972(16)	20	32×48	0.3149(47)
30	40×50	0.4596(28)	24	24×36	0.3844(29)
36	36×44	0.5586(23)	32	32×32	0.5317(35)
42	42×44	0.6606(30)	40	40×32	0.6727(40)

Table 6: Energy of the ground state flux tube versus its length, in $SO(6)$ at $\beta = 46$, and in $SO(8)$ at $\beta = 86$.

$SO(3)$				$SO(5)$		
l_x	$l_y \times l_t$	$aE(l_x)_{sub}$	$aE(l_x)_{nosub}$	l_x	$l_y \times l_t$	$aE(l_x)$
26	80×140	0.2133(36)	0.2292(84)	14	54×72	0.2245(17)
30	80×100	0.2501(55)	0.2508(71)	22	40×50	0.3980(17)
34	70×86	0.2724(82)	0.2724(75)	30	36×44	0.5572(22)
38	70×86	0.3462(49)	0.3462(45)	36	36×44	0.6780(18)
46	70×86	0.4354(72)	0.4335(71)	42	42×44	0.7859(84)
52	70×86	0.4964(62)	0.4963(62)			
62	62×60	0.5849(81)	0.5854(81)			
82	82×64	0.839(34)	0.824(33)			

Table 7: Energy of the ground state flux tube versus its length, in $SO(3)$ at $\beta = 9.0$, both vacuum subtracted and unsubtracted, and in $SO(5)$ at $\beta = 27.5$.

$SO(5)$					
l	$O_{gs}^2 \sim$	bl_{max}	$\langle \phi_{gs} \rangle$	$\sum_i \langle \phi_i \rangle ^2$	$aE_{eff}(t = a)$
14	0.994	4	0.0083(31)	0.00026(7)	0.2298(7)
		5	0.0122(31)	0.1438(5)	0.2290(7)
22	0.998	4	0.0026(22)	0.000038(15)	0.4049(8)
		5	0.0033(23)	0.0452(3)	0.4008(9)
30	0.993	4	-0.0017(15)	0.000024(8)	0.5711(9)
		5	-0.0018(15)	0.00395(8)	0.5642(8)
36	0.991	5	0.0006(9)	0.00016(2)	0.6873(7)
		6	0.0037(9)	0.2244(4)	0.6869(7)
42	0.970	5	-0.0016(10)	0.000023(6)	0.8063(9)
		6	-0.0015(10)	0.0431(4)	0.8061(9)

Table 8: Various overlaps versus length, as described in Section 4.2, in $SO(5)$ at $\beta = 27.5$.

$SO(3)$					
l	$O_{gs}^2 \sim$	bl_{max}	$\langle \phi_{gs} \rangle$	$\sum_i \langle \phi_i \rangle ^2$	$aE_{eff}(t = a)$
26	0.91	5	0.059(3)	0.3758(9)	0.2509(8)
		4	0.033(2)	0.0135(3)	0.2791(6)
30	0.83	5	0.023(3)	0.1306(5)	0.3027(9)
		4	0.011(3)	0.0014(1)	0.3360(8)
34	0.78	6	-0.019(3)	0.7579(4)	0.3427(12)
		5	0.010(3)	0.0421(3)	0.3499(11)
38	0.90	6	-0.019(3)	0.5733(3)	0.3952(10)
		5	0.000(3)	0.0118(2)	0.4015(9)
46	0.89	6	0.012(2)	0.2472(7)	0.4896(8)
		5	0.003(2)	0.00014(2)	0.4973(7)
52	0.86	6	-0.0011(13)	0.0645(4)	0.5615(8)
		5	-0.0006(13)	0.00004(1)	0.5674(7)
62	0.83	7	-0.006(1)	0.4975(5)	0.6689(11)
		6	-0.001(1)	0.0089(2)	0.6744(10)
		5	-0.000(8)	0.000007(2)	0.6850(8)
82	0.85	7	0.014(1)	0.1821(5)	0.9121(10)
		6	0.0014(7)	0.00009(1)	0.9130(11)
		5	0.0012(7)	0.00002(1)	0.9201(11)

Table 9: Various overlaps versus length, as described in Section 4.2, in $SO(3)$ at $\beta = 9.0$.

$SO(2N + 1); l = 36$						
group	β	bl_{max}	$O_{gs}^2 \sim$	$\langle \phi_{gs} \rangle$	$\sum_i \langle \phi_i \rangle ^2$	$aE_{eff}(t = a)$
SO(3)	7.0	5	0.869	-0.0014(8)	0.0030(2)	0.6958(14)
		6	0.886	-0.0028(8)	0.5338(15)	0.6890(18)
SO(5)	27.5	5	0.991	0.0006(9)	0.00016(2)	0.6873(7)
		6	0.991	0.0037(9)	0.2244(4)	0.6869(7)
SO(7)	64.0	5	0.995	0.0006(11)	0.000011(3)	0.5979(6)
		6	0.995	0.0004(11)	0.0606(2)	0.5979(6)
SO(9)	106.0	5	0.995	-0.0016(9)	0.000017(4)	0.6764(6)
		6	0.995	-0.0015(9)	0.00913(8)	0.6764(6)
SO(11)	164.0	5	0.995	0.0011(9)	0.000012(4)	0.6753(6)
		6	0.995	0.0011(9)	0.00121(3)	0.6753(6)

Table 10: Various overlaps versus N , as described in Section 4.2, at the couplings shown, on $36^2 \times 44$ lattices for $N \geq 5$ and on $36 \times 52 \times 64$ for $N = 3$.

$L_x L_y L_t$	β	$\frac{1}{N} \text{tr}(U_p)$	am_P	$a\sqrt{\sigma}$
30.46.60	6.5	0.8335266	0.5846(87)	0.1417(10)
34.52.64	7.0	0.8465520	0.5499(103)	0.1290(12)
42.62.80	8.5	0.8755635	0.4370(82)	0.1035(10)
46.70.86	9.0	0.8829150	0.4331(100)	0.0983(11)
50.76.90	10.0	0.8952681	0.3532(68)	0.0853(8)
54.80.100	11.0	0.9052486	0.3120(71)	0.0772(9)
62.90.110	12.0	0.9134837	0.2913(87)	0.0696(10)

Table 11: $SO(3)$ average plaquette values, masses of flux loops winding around the x -torus, and resulting string tensions on the lattices shown.

$L_s^2 L_t$	β	$\frac{1}{N}\text{tr}(U_p)$	am_P	$a\sqrt{\sigma}$
$20^2 28$	11.0	0.80135	0.8229(63)	0.2061(8)
$24^2 32$	12.2	0.82295	0.7810(46)	0.1829(5)
$28^2 36$	13.7	0.84402	0.6960(41)	0.1598(5)
$32^2 40$	15.1	0.85955	0.6336(51)	0.1425(6)
$36^2 44$	16.5	0.87223	0.5858(39)	0.1292(5)
$40^2 48$	18.7	0.88808	0.4946(27)	0.1127(4)

Table 12: $SO(4)$ average plaquette values, flux loop masses, and string tensions.

$L_s^2 L_t$	β	$\frac{1}{N}\text{tr}(U_p)$	am_P	$a\sqrt{\sigma}$
$26^2 30$	17.5	0.79176	1.4282(88)	0.23603(72)
$30^2 36$	20.0	0.82045	1.1955(55)	0.20109(46)
$36^2 40$	23.5	0.84929	0.9793(44)	0.16616(37)
$42^2 44$	27.5	0.87257	0.7857(85)	0.13786(73)
$52^2 56$	32.0	0.89138	0.6962(49)	0.11655(40)
$58^2 64$	36.0	0.90396	0.6017(70)	0.10262(59)

Table 13: $SO(5)$ average plaquette values, flux loop masses, and string tensions.

$L_s^2 L_t$	β	$\frac{1}{N}\text{tr}(U_p)$	am_P	$a\sqrt{\sigma}$
$20^2 28$	28.0	0.80677	0.9798(18)	0.22431(20)
$24^2 32$	33.0	0.83851	0.7938(27)	0.18438(30)
$32^2 40$	41.0	0.87194	0.6452(25)	0.14381(27)
$36^2 44$	46.0	0.88656	0.5620(19)	0.12657(21)
$42^2 48$	54.0	0.90406	0.4623(15)	0.10634(17)
$46^2 54$	60.0	0.91400	0.4004(17)	0.09463(19)

Table 14: $SO(6)$ average plaquette values, flux loop masses, and string tensions.

$L_s^2 L_t$	β	$\frac{1}{N}\text{tr}(U_p)$	am_P	$a\sqrt{\sigma}$
$16^2 24$	35.0	0.78116	1.0714(9)	0.26275(11)
$20^2 28$	42.0	0.82117	0.8584(10)	0.21035(12)
$24^2 32$	49.0	0.84862	0.7143(23)	0.17517(27)
$28^2 36$	57.0	0.87112	0.5925(14)	0.14778(17)
$32^2 40$	64.0	0.88592	0.5245(11)	0.13004(13)
$36^2 44$	70.0	0.89613	0.4832(17)	0.11761(20)

Table 15: $SO(7)$ average plaquette values, flux loop masses, and string tensions.

$L_s^2 L_t$	β	$\frac{1}{N}\text{tr}(U_p)$	am_P	$a\sqrt{\sigma}$
16 ² 24	51.0	0.80206	0.8721(24)	0.23789(31)
20 ² 28	62.0	0.84000	0.6888(11)	0.18914(15)
24 ² 32	73.0	0.86561	0.5672(9)	0.15672(12)
28 ² 36	84.0	0.88409	0.4841(15)	0.13405(20)
32 ² 40	94.0	0.89696	0.4323(11)	0.11845(14)
36 ² 44	105.0	0.90815	0.3831(10)	0.10513(13)

Table 16: $SO(8)$ average plaquette values, flux loop masses, and string tensions.

$L_s^2 L_t$	β	$\frac{1}{N}\text{tr}(U_p)$	am_P	$a\sqrt{\sigma}$
16 ² 24	132.0	0.82178	0.7263(13)	0.21791(19)
20 ² 28	155.0	0.85007	0.6290(13)	0.18107(18)
24 ² 32	175.0	0.86820	0.5760(14)	0.15788(18)
28 ² 36	200.0	0.88546	0.4999(16)	0.13614(21)
32 ² 40	225.0	0.89871	0.4409(19)	0.11958(25)
36 ² 48	250.0	0.90920	0.3954(15)	0.10675(19)

Table 17: $SO(12)$ average plaquette values, flux loop masses, and string tensions.

$L_s^2 L_t$	β	$\frac{1}{N}\text{tr}(U_p)$	am_P	$a\sqrt{\sigma}$
16 ² 24	247.0	0.82758	0.6960(18)	0.21353(26)
20 ² 28	302.0	0.86092	0.5450(15)	0.16909(22)
24 ² 32	353.0	0.88192	0.4627(20)	0.14216(29)
28 ² 36	408.0	0.89848	0.3940(18)	0.12147(26)
32 ² 40	456.0	0.90954	0.3524(13)	0.10740(19)
36 ² 48	512.0	0.91974	0.3113(14)	0.09519(20)

Table 18: $SO(16)$ average plaquette values, flux loop masses, and string tensions.

$SO(N)$			$SU(N)$	
N	$\sqrt{\sigma}/(g^2N)$	$\bar{\chi}_{\text{dof}}^2$	N	$\sqrt{\sigma}/(2g^2N)$
3	0.04273(68)	0.66	2	0.08373(6)
4	0.06019(54)	0.38	3	0.09195(8)
5	0.06763(36)	0.72	4	0.09479(8)
6	0.07339(15)	0.45	6	0.09665(6)
7	0.07686(10)	1.09	8	0.09743(8)
8	0.07991(14)	0.70	12	0.09779(12)
12	0.08625(19)	0.06	16	0.09775(14)
16	0.08898(22)	0.98		
∞	0.09897(25) ^a	1.76	∞	0.09818(6)
	0.09821(57) ^b	1.67		
	0.09749(43) ^c	2.32		

Table 19: $SO(N)$ continuum string tensions, $\sqrt{\sigma}$, in units of the 't Hooft coupling, g^2N , and the χ^2 per degree of freedom of each continuum extrapolation. (Labels a,b,c denote different extrapolations: $O(1/N)$ extrapolation for $N \geq 4$, $O(1/N^2)$ extrapolation for $N \geq 4$, $O(1/N)$ extrapolation for $N \geq 3$ respectively.) Also shown are $SU(N)$ values from [6], in units of $2g^2N$.

$L_s^2 L_t$		54 ² 40	62 ² 48	74 ² 60	82 ² 64	90 ² 70	100 ² 80	88 ² 90
β		6.5	7.0	8.5	9.0	10.0	11.0	12.0
$l\sqrt{\sigma}$		8.0	8.4	7.9	8.3	8.0	8.1	6.5
0 ⁺	α	0.434(3)	0.397(4)	0.3185(25)	0.2996(22)	0.2650(21)	0.2421(15)	0.218(2)
0 ⁺⁺	α	0.652(11)	0.595(8)	0.4652(65)	0.4364(42)	0.4003(45)	0.3540(49)	0.318(6)
0 ⁺⁺⁺	β	0.768(33)	0.706(23)	0.587(12)	0.5595(57)	0.484(10)	0.4366(73)	–
0 ⁺⁺⁺⁺	γ	0.882(20)	0.782(32)	0.663(15)	0.631(11)	0.553(16)	0.492(12)	–
0 ^{*****}	δ	0.962(12)	0.869(20)	0.7081(84)	0.636(14)	0.591(11)	0.5143(96)	–
2 ⁺	α	0.734(11)	0.666(5)	0.5362(45)	0.472(8)	0.4504(47)	0.3918(91)	–
2 ⁺⁺	γ	0.839(22)	0.809(14)	0.606(28)	0.584(16)	0.542(10)	0.478(11)	–
2 ⁻	α	0.728(11)	0.673(9)	0.5282(66)	0.4898(53)	0.4438(44)	0.3986(30)	0.364(4)
2 ^{-*}	γ	0.857(22)	0.785(12)	0.6284(59)	0.581(20)	0.5464(81)	0.485(11)	0.440(8)
0 ⁻	δ	0.966(32)	0.845(19)	0.715(23)	0.661(27)	0.581(17)	0.5172(77)	0.472(7)
1 ⁺	ϕ	1.012(58)	0.979(31)	0.793(15)	0.741(24)	0.650(14)	0.517(27)	0.514(20)
1 ⁻	ϕ	1.020(52)	0.838(57)	0.818(13)	0.670(46)	0.669(29)	0.527(25)	0.508(18)

Table 20: $SO(3)$ glueball masses am_G . Grades, e.g. α , explained in Section 3.6.6.

$L_s^2 L_t$		34 ² 42	38 ² 46	44 ² 52	48 ² 56	54 ² 62	62 ² 70
β		11.0	12.2	13.7	15.1	16.5	18.7
$l\sqrt{\sigma}$		7.2	7.0	7.1	6.9	7.0	7.0
0 ⁺	α	0.6963(18)	0.6170(25)	0.5394(23)	0.4801(35)	0.4308(26)	0.3787(23)
0 ⁺⁺	α	1.045(10)	0.9137(76)	0.7970(68)	0.7116(55)	0.6354(92)	0.5733(75)
0 ⁺⁺⁺	γ	1.286(26)	1.123(16)	1.028(16)	0.952(28)	0.806(20)	0.716(11)
0 ⁺⁺⁺⁺	δ	1.462(46)	1.258(39)	1.143(23)	1.020(20)	0.943(17)	0.8249(88)
0 ^{*****}	ϕ	1.547(72)	1.288(42)	1.105(25)	1.028(20)	0.955(14)	0.841(12)
2 ⁺	β	1.188(15)	1.018(13)	0.9099(87)	0.8200(63)	0.734(13)	0.6390(86)
2 ⁺⁺	δ	1.426(50)	1.268(32)	1.091(20)	0.987(17)	0.897(31)	0.794(18)
2 ⁻	β	1.186(13)	1.035(14)	0.8997(89)	0.8132(88)	0.724(14)	0.6371(71)
2 ^{-*}	δ	1.355(45)	1.187(31)	1.090(22)	0.988(21)	0.923(36)	0.773(21)
0 ⁻	γ	1.522(70)	1.297(38)	1.188(27)	1.015(21)	0.908(15)	0.8374(95)
1 ⁺	ϕ	1.60(9)	1.41(8)	1.412(47)	1.175(26)	1.067(19)	0.968(11)
1 ⁻	ϕ	1.56(13)	1.43(7)	1.336(54)	1.176(27)	1.106(20)	0.945(10)

Table 21: $SO(4)$ glueball masses am_G . Grades, e.g. α , explained in Section 3.6.6.

$L_s^2 L_t$		26 ² 30	30 ² 36	36 ² 40	42 ² 44	52 ² 56	58 ² 64
β		17.5	20.0	23.5	27.5	32.0	36.0
$l\sqrt{\sigma}$		6.1	6.0	6.0	5.8	6.1	6.0
0 ⁺	α	0.8354(29)	0.7087(20)	0.5878(22)	0.4889(22)	0.4146(22)	0.3624(13)
0 ⁺ *	β	1.242(14)	1.065(11)	0.861(22)	0.7133(83)	0.6145(51)	0.5412(46)
0 ⁺ **	γ	1.590(60)	1.340(22)	1.037(36)	0.927(21)	0.787(11)	0.6917(77)
0 ⁺ ***	γ	1.623(70)	1.430(37)	1.191(16)	1.005(12)	0.850(14)	0.732(10)
0 ⁺ ****	ϕ	1.78(12)	1.489(43)	1.257(22)	1.031(14)	0.8998(79)	0.7970(59)
2 ⁺	β	1.384(24)	1.182(16)	0.9804(94)	0.8184(59)	0.6944(44)	0.6153(32)
2 ⁺ *	δ	1.644(89)	1.414(30)	1.209(18)	0.991(26)	0.808(15)	0.7275(90)
2 ⁻	β	1.394(28)	1.200(18)	0.933(33)	0.802(12)	0.693(10)	0.6110(65)
2 ⁻ *	δ	1.710(14)	1.439(7)	1.174(23)	1.012(12)	0.8447(46)	0.7518(42)
0 ⁻	δ	1.80(11)	1.524(40)	1.284(31)	0.998(35)	0.893(18)	0.8033(92)
1 ⁺	ϕ	1.95(15)	1.653(72)	1.475(50)	1.193(18)	0.988(11)	0.8979(81)
1 ⁻	ϕ	1.85(15)	1.739(71)	1.22(17)	1.118(45)	0.971(30)	0.877(12)

Table 22: $SO(5)$ glueball masses am_G . Grades, e.g. α , explained in Section 3.6.6.

$L_s^2 L_t$		26 ² 28	30 ² 32	42 ² 44	46 ² 48	56 ² 60	62 ² 70
β		28.0	33.0	41.0	46.0	54.0	60.0
$l\sqrt{\sigma}$		5.8	5.5	6.0	5.8	6.0	5.9
0 ⁺	α	0.8212(20)	0.6756(22)	0.5258(19)	0.4633(24)	0.3893(18)	0.3454(17)
0 ⁺ *	β	1.232(13)	1.021(11)	0.7938(67)	0.7030(53)	0.5959(31)	0.5255(33)
0 ⁺ **	γ	1.583(37)	1.291(20)	1.026(12)	0.8965(91)	0.7553(45)	0.6823(48)
0 ⁺ ***	δ	1.631(43)	1.346(21)	1.041(13)	0.948(10)	0.7931(59)	0.7023(36)
0 ⁺ ****	ϕ	1.651(54)	1.415(32)	1.092(52)	0.933(27)	0.844(15)	0.727(19)
2 ⁺	β	1.352(19)	1.124(14)	0.8767(78)	0.7718(51)	0.6546(44)	0.5852(36)
2 ⁺ *	γ	1.667(51)	1.372(31)	1.082(15)	0.907(27)	0.800(16)	0.708(9)
2 ⁻	β	1.370(24)	1.137(12)	0.8805(93)	0.7729(63)	0.6534(32)	0.5813(36)
2 ⁻ *	γ	1.653(50)	1.364(26)	1.064(10)	0.930(25)	0.791(14)	0.706(8)
0 ⁻	δ	1.717(67)	1.506(40)	1.134(22)	1.025(11)	0.827(14)	0.770(9)
1 ⁺	ϕ	1.835(83)	1.646(66)	1.259(27)	1.113(16)	0.905(26)	0.835(15)
1 ⁻	ϕ	1.84(11)	1.635(60)	1.250(29)	1.115(14)	0.914(19)	0.826(14)

Table 23: $SO(6)$ glueball masses am_G . Grades, e.g. α , explained in Section 3.6.6.

$L_s^2 L_t$		16 ² 24	20 ² 28	24 ² 32	28 ² 36	32 ² 40	36 ² 44
β		35.0	42.0	49.0	57.0	64.0	70.0
$l\sqrt{\sigma}$		4.2	4.2	4.2	4.1	4.2	4.2
0 ⁺	α	0.9823(14)	0.7865(10)	0.6578(16)	0.5518(22)	0.4842(16)	0.4394(20)
0 ⁺ *	β	1.487(14)	1.198(8)	1.001(9)	0.8329(57)	0.7332(21)	0.6759(40)
0 ⁺ **	β	1.907(44)	1.512(27)	1.262(14)	1.080(7)	0.9522(47)	0.8731(60)
0 ⁺ ***	γ	1.958(66)	1.546(24)	1.301(15)	1.1230(76)	0.9776(48)	0.8876(49)
0 ⁺ ****	ϕ	2.039(80)	1.646(28)	1.381(24)	1.187(9)	1.052(7)	0.956(9)
2 ⁺	β	1.623(19)	1.310(13)	1.064(24)	0.915(15)	0.8212(70)	0.7352(71)
2 ⁺ *	γ	1.977(70)	1.594(24)	1.287(54)	1.154(34)	0.991(11)	0.901(12)
2 ⁻	β	1.628(29)	1.240(39)	1.097(22)	0.928(8)	0.824(7)	0.737(9)
2 ⁻ *	δ	2.004(74)	1.573(24)	1.330(16)	1.122(29)	0.996(13)	0.918(14)
0 ⁻	δ	1.95(9)	1.655(27)	1.350(53)	1.202(52)	1.024(12)	0.934(21)
1 ⁺	ϕ	2.31(19)	1.951(59)	1.649(31)	1.375(44)	1.167(24)	1.081(20)
1 ⁻	ϕ	2.15(15)	1.904(60)	1.604(32)	1.383(62)	1.135(21)	1.050(28)

Table 24: $SO(7)$ glueball masses am_G . Grades, e.g. α , explained in Section 3.6.6.

$L_s^2 L_t$		16 ² 24	20 ² 28	24 ² 32	28 ² 36	32 ² 40	36 ² 44
β		51.0	62.0	73.0	84.0	94.0	105.0
$l\sqrt{\sigma}$		3.8	3.8	3.8	3.7	3.8	3.8
0 ⁺	α	0.901(4)	0.7160(19)	0.5959(14)	0.5057(19)	0.4493(21)	0.3973(18)
0 ⁺ *	α	1.370(3)	1.0833(74)	0.9140(26)	0.7708(38)	0.6890(30)	0.6108(30)
0 ⁺ **	γ	1.681(39)	1.381(17)	1.072(28)	0.9916(24)	0.8704(59)	0.7576(96)
0 ⁺ ***	γ	1.791(50)	1.433(22)	1.175(12)	1.003(10)	0.898(8)	0.8009(52)
0 ⁺ ****	ϕ	1.836(66)	1.562(30)	1.281(17)	1.098(11)	0.9750(60)	0.861(13)
2 ⁺	γ	1.502(20)	1.209(11)	1.007(9)	0.8593(72)	0.7555(49)	0.6831(30)
2 ⁺ *	γ	1.748(58)	1.434(27)	1.139(33)	1.0573(91)	0.9371(60)	0.8343(55)
2 ⁻	β	1.494(19)	1.202(12)	0.994(7)	0.8520(54)	0.7464(73)	0.6645(59)
2 ⁻ *	δ	1.877(55)	1.433(27)	1.210(16)	1.053(8)	0.9466(59)	0.8466(55)
0 ⁻	δ	1.797(65)	1.537(36)	1.206(53)	1.095(12)	0.978(9)	0.8725(53)
1 ⁺	ϕ	2.17(13)	1.790(50)	1.39(8)	1.204(49)	1.090(27)	0.971(18)
1 ⁻	ϕ	2.21(16)	1.760(61)	1.467(20)	1.270(13)	1.114(10)	0.993(8)

Table 25: $SO(8)$ glueball masses am_G . Grades, e.g. α , explained in Section 3.6.6.

$L_s^2 L_t$		16 ² 24	20 ² 28	24 ² 32	28 ² 36	32 ² 40	36 ² 44
β		132.0	155.0	175.0	200.0	225.0	250.0
$l\sqrt{\sigma}$		3.5	3.6	3.8	3.8	3.8	3.8
0 ⁺	α	0.8537(29)	0.7057(23)	0.6170(40)	0.5288(41)	0.4711(42)	0.4128(30)
0 ⁺ *	β	1.270(18)	1.081(12)	0.951(7)	0.813(8)	0.7209(31)	0.6455(28)
0 ⁺ **	γ	1.641(14)	1.362(10)	1.207(5)	1.053(6)	0.9246(37)	0.8127(59)
0 ⁺ ***	ϕ	1.683(13)	1.424(9)	1.236(6)	1.051(13)	0.9204(93)	0.801(16)
0 ⁺ ****	ϕ	1.67(10)	1.556(9)	1.317(31)	1.182(6)	0.997(14)	0.916(10)
2 ⁺	β	1.392(28)	1.187(17)	1.036(11)	0.871(10)	0.7833(61)	0.7084(53)
2 ⁺ *	δ	1.753(16)	1.4602(66)	1.2789(53)	1.110(7)	0.965(12)	0.8655(81)
2 ⁻	β	1.432(8)	1.2013(52)	1.0450(39)	0.886(10)	0.7871(77)	0.7067(65)
2 ⁻ *	δ	1.772(13)	1.414(35)	1.2686(56)	1.1145(73)	0.974(11)	0.8691(72)
0 ⁻	δ	1.73(10)	1.460(40)	1.345(27)	1.157(21)	0.936(26)	0.873(24)
1 ⁺	ϕ	2.112(25)	1.762(14)	1.481(37)	1.300(26)	1.143(13)	0.997(22)
1 ⁻	ϕ	2.105(22)	1.749(13)	1.475(37)	1.295(23)	1.139(17)	1.001(23)

Table 26: $SO(12)$ glueball masses am_G . Grades, e.g. α , explained in Section 3.6.6.

$L_s^2 L_t$		16 ² 24	20 ² 28	24 ² 32	28 ² 36	32 ² 40	36 ² 44
β		247.0	302.0	353.0	408.0	456.0	512.0
$l\sqrt{\sigma}$		3.4	3.4	3.4	3.4	3.4	3.4
0 ⁺	α	0.8480(26)	0.6622(44)	0.5671(29)	0.4827(21)	0.4268(21)	0.3779(17)
0 ⁺ *	β	1.262(23)	1.006(13)	0.852(11)	0.7398(32)	0.6565(22)	0.5794(35)
0 ⁺ **	γ	1.560(61)	1.079(69)	1.068(19)	0.959(11)	0.8130(63)	0.7246(50)
0 ⁺ ***	δ	1.693(74)	1.233(26)	1.087(16)	0.956(11)	0.8549(91)	0.745(13)
0 ⁺ ****	δ	1.59(11)	1.416(33)	1.233(27)	1.066(16)	0.902(25)	0.814(18)
2 ⁺	β	1.421(8)	1.1310(54)	0.935(15)	0.812(6)	0.7176(57)	0.6402(41)
2 ⁺ *	γ	1.720(14)	1.390(9)	1.151(27)	0.987(12)	0.869(9)	0.7833(55)
2 ⁻	β	1.412(9)	1.134(6)	0.9529(53)	0.8065(65)	0.7123(47)	0.6411(49)
2 ⁻ *	δ	1.601(90)	1.387(37)	1.149(20)	1.003(12)	0.872(8)	0.7945(71)
0 ⁻	δ	1.569(90)	1.453(11)	1.236(8)	1.044(5)	0.924(13)	0.8187(60)
1 ⁺	ϕ	1.88(18)	1.594(60)	1.356(32)	1.169(17)	0.996(29)	0.911(21)
1 ⁻	ϕ	2.09(20)	1.659(74)	1.208(85)	1.160(44)	1.030(33)	0.905(21)

Table 27: $SO(16)$ glueball masses am_G . Grades, e.g. α , explained in Section 3.6.6.

$M_G/\sqrt{\sigma}$								
J^P	$SO(3)$	$\bar{\chi}_{\text{dof}}^2$	$SO(4)$	$\bar{\chi}_{\text{dof}}^2$	$SO(5)$	$\bar{\chi}_{\text{dof}}^2$	$SO(6)$	$\bar{\chi}_{\text{dof}}^2$
0^+	3.132(34)	0.43	3.343(23)	0.36	3.545(17)	0.42	3.656(13)	0.08
0^{+*}	4.558(70)	1.75	4.966(64)	1.06	5.249(46)	0.63	5.597(31)	0.51
0^{+**}	5.81(15)	0.19	6.49(13)	1.75	6.760(92)	1.14	7.187(54)	0.71
0^{+***}	6.56(18)	0.26	7.47(14)	0.36	7.30(11)	0.64	7.487(54)	1.02
0^{+****}	6.73(14)	1.44	7.63(17)	1.68	7.86(10)	0.71	7.864(49)	1.24
2^+	5.13(9)	4.15	5.711(81)	1.36	6.008(46)	0.13	6.190(38)	0.36
2^{+*}	6.30(16)	1.81	7.02(20)	0.23	7.07(12)	1.15	7.49(11)	0.61
2^-	5.16(7)	1.41	5.598(81)	0.44	5.919(71)	1.04	6.140(38)	0.19
2^{-*}	6.40(12)	1.02	7.22(22)	0.60	7.301(48)	1.56	7.46(10)	0.06
0^-	6.79(14)	0.43	7.39(15)	2.43	7.82(13)	1.07	8.10(11)	1.93
1^+	7.45(24)	1.49	8.85(21)	1.73	8.75(14)	1.34	8.89(17)	0.72
1^-	7.61(28)	4.21	8.71(21)	0.70	8.55(18)	0.95	8.78(17)	0.58

Table 28: Continuum glueball masses in string tension units, $M_G/\sqrt{\sigma}$, for $SO(3)$, $SO(4)$, $SO(5)$, $SO(6)$, with the χ^2 per degree of freedom of the linear extrapolation. Reliability as graded in Tables 20-23.

$M_G/\sqrt{\sigma}$								
J^P	$SO(7)$	$\bar{\chi}_{\text{dof}}^2$	$SO(8)$	$\bar{\chi}_{\text{dof}}^2$	$SO(12)$	$\bar{\chi}_{\text{dof}}^2$	$SO(16)$	$\bar{\chi}_{\text{dof}}^2$
0^+	3.737(10)	0.94	3.788(14)	0.92	3.878(24)	0.73	3.973(15)	1.22
0^{+*}	5.655(25)	2.42	5.773(43)	1.23	6.096(38)	0.45	6.178(38)	0.45
0^{+**}	7.419(57)	0.93	7.389(70)	2.60	7.791(45)	1.89	7.725(88)	3.14
0^{+***}	7.610(60)	0.96	7.614(68)	0.61	7.53(11)	0.57	8.30(15)	0.80
0^{+****}	8.237(83)	0.15	8.298(94)	0.48	8.43(12)	1.01	8.90(20)	1.42
2^+	6.297(54)	0.72	6.498(36)	1.21	6.636(64)	1.60	6.714(40)	0.41
2^{+*}	7.68(11)	0.35	8.112(72)	1.43	8.165(65)	0.27	8.218(63)	1.10
2^-	6.348(60)	0.99	6.346(48)	0.28	6.622(48)	0.88	6.706(39)	1.26
2^{-*}	7.79(12)	0.45	8.144(70)	1.98	8.33(11)	0.98	8.40(11)	1.28
0^-	7.98(14)	0.45	8.450(81)	0.65	8.28(24)	2.49	8.60(8)	0.69
1^+	9.09(21)	0.77	9.16(20)	0.42	9.43(13)	0.72	9.45(30)	0.81
1^-	8.90(23)	1.50	9.49(13)	0.13	9.41(14)	0.44	9.67(30)	0.47

Table 29: Continuum glueball masses in string tension units, $M_G/\sqrt{\sigma}$, for $SO(7)$, $SO(8)$, $SO(12)$, $SO(16)$, with the χ^2 per degree of freedom of the linear extrapolation. Reliability as graded in Tables 24-27.

$SO(N)$		
N	$M_{0^+}/(g^2N)$	$\bar{\chi}_{\text{dof}}^2$
3	0.1357(14)	0.59
4	0.2008(18)	0.92
5	0.2397(13)	0.32
6	0.2679(14)	0.21
7	0.2869(11)	0.34
8	0.3024(18)	0.77
12	0.3330(32)	0.71
16	0.3542(20)	1.61
∞	0.4017(14)	0.81

Table 30: Lightest $SO(N)$ glueball, M_{0^+} , in units of the 't Hooft coupling, g^2N , and the χ^2 per degree of freedom of each continuum extrapolation. Also shown is the large- N extrapolation.

J^P		$M_G/\sqrt{\sigma}$						
		$O(1/N^2)$			$O(1/N)$			$SU(\infty)$
		$SO(\infty)$	$\bar{\chi}_{\text{dof}}^2$	$N \geq$	$SO(\infty)$	$\bar{\chi}_{\text{dof}}^2$	$N \geq$	
0^+	α	4.150(33)	1.34	3	4.179(16)	1.30	3	4.116(6)
0^{+*}	β	6.628(68)	2.07	3	6.578(35)	2.07	3	6.308(10)
0^{+**}	γ	7.93(16)	1.44	3	8.276(81)	2.40	3	7.844(14)
0^{+***}	ϕ	8.12(15)	3.05	3	8.171(70)	2.56	3	8.147(19)
0^{+****}	ϕ	9.12(22)	1.45	3	9.11(11)	2.01	3	8.950(25)
2^+	β	6.987(88)	0.87	3	7.129(43)	1.47	3	6.914(13)
2^-	β	7.044(84)	0.55	3	7.090(40)	0.51	3	6.930(13)
2^{+*}	γ	8.61(14)	3.63	3	8.77(7)	3.25	3	8.423(15)
2^{-*}	δ	9.14(19)	2.53	3	8.98(9)	2.35	3	8.488(21)
0^-	δ	8.84(18)	1.46	3	9.11(10)	1.76	3	8.998(28)
1^+	ϕ	9.53(34)	1.11	3	9.98(16)	1.35	3	9.912(26)
1^-	ϕ	9.90(36)	2.02	3	10.10(16)	1.70	3	9.886(27)

Table 31: Continuum glueball masses in units of the string tension extrapolated to $N = \infty$, with the χ^2 per degree of freedom and range in N : for the best linear and quadratic fits in $1/N$. Also the values for $SU(\infty)$ from [6]. Grades, e.g. α , explained in Section 3.6.6.

M_G/M_{0+}					
J^P	$SO(\infty)$	$c_1/c_0 \sim$	$\bar{\chi}_{\text{dof}}^2$	$N \geq$	$SU(\infty)$
0^{+*}	1.585(12)	-0.27	1.62	3	1.533(4)
0^{+**}	1.966(24)	+0.27	1.60	3	1.906(5)
0^{+***}	1.983(24)	-0.10	2.80	3	1.979(6)
0^{+****}	2.189(31)	-0.02	1.91	3	2.174(7)
2^+	1.708(14)	-0.05	1.04	3	1.680(4)
2^-	1.704(13)	-0.09	0.49	3	1.684(4)
2^{+*}	2.114(21)	-0.13	2.84	3	2.046(6)
2^{-*}	2.166(26)	-0.21	2.11	3	2.062(7)
0^-	2.175(26)	+0.06	1.36	3	2.186(8)
1^+	2.389(45)	+0.16	1.72	3	2.408(8)
1^-	2.421(46)	+0.09	1.72	3	2.402(8)

Table 32: Continuum glueball masses in units of the scalar glueball mass extrapolated to $N = \infty$, with the χ^2 per degree of freedom and range of the best linear fit $c_0 + c_1/N$ shown. The values for $SU(N)$ are from [6]. Grades as in Table 31.

M_G/M_{0+}								
J^P	$SO(3)$		$SO(4)$		$SU(2)$	$SO(6)$		$SU(4)$
0^{+*}	1.455(27)	α	1.485(22)	α	1.449(4)	1.531(10)	β	1.518(5)
0^{+**}	1.855(52)	β	1.941(41)	γ	1.770(4)	1.966(17)	γ	1.869(7)
0^{+***}	2.095(62)	γ	2.235(45)	δ	1.959(4)	2.048(17)	δ	1.961(9)
0^{+****}	2.149(51)	δ	2.282(53)	ϕ	2.050(5)	2.151(16)	ϕ	2.131(13)
2^+	1.638(34)	α	1.708(27)	β	1.639(3)	1.693(12)	β	1.672(6)
2^-	1.647(28)	α	1.675(27)	β	1.646(3)	1.679(12)	β	1.673(6)
2^{+*}	2.011(56)	γ	2.100(62)	δ	1.923(5)	2.048(30)	γ	2.027(8)
2^{-*}	2.043(44)	γ	2.160(68)	δ	1.926(6)	2.040(27)	γ	2.011(9)
0^-	2.168(51)	δ	2.211(48)	γ	2.087(6)	2.216(31)	δ	2.170(9)
1^+	2.379(81)	ϕ	2.647(65)	ϕ	2.228(7)	2.432(47)	ϕ	2.346(16)
1^-	2.430(93)	ϕ	2.605(65)	ϕ	2.225(7)	2.402(47)	ϕ	2.357(13)

Table 33: Continuum glueball masses in units of the mass gap: comparing the spectra of $SO(N)$ gauge theories with those of $SU(N')$ with the same Lie algebra. Grades, e.g. α , explained in Section 3.6.6.

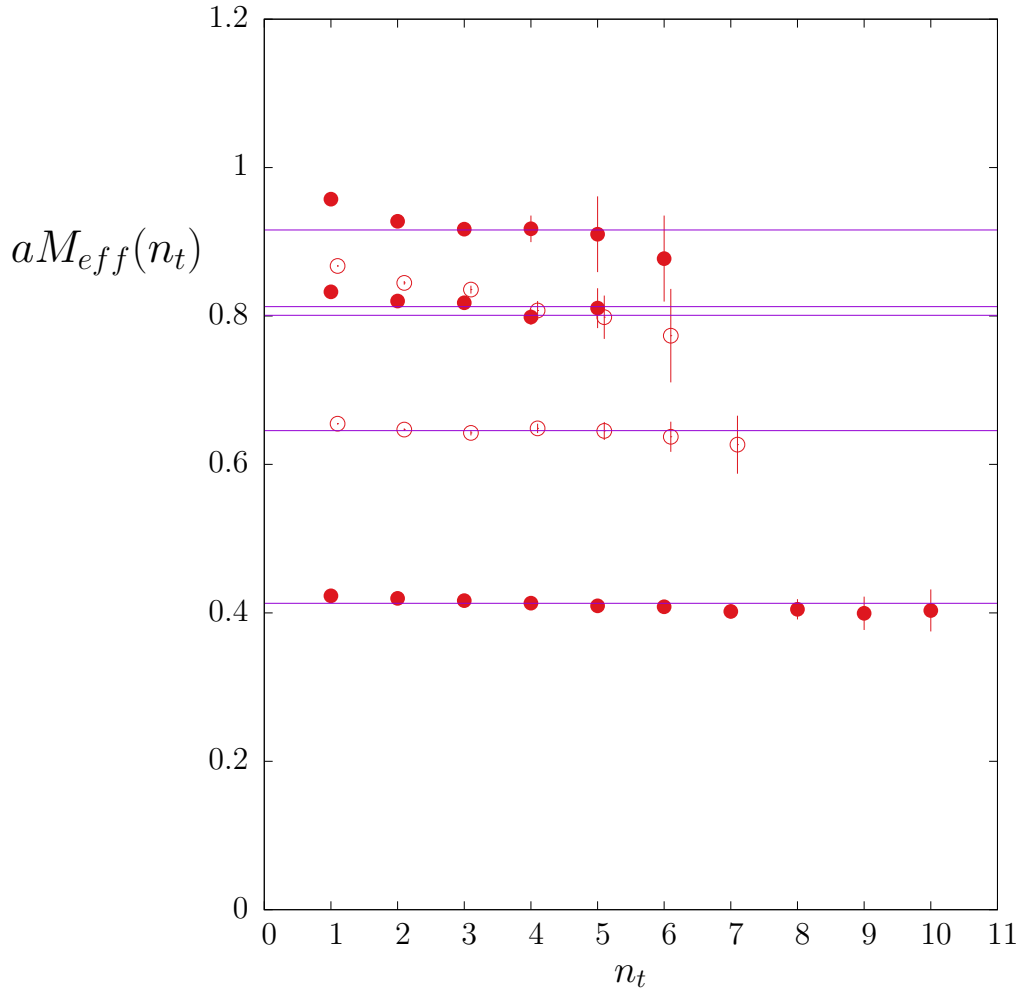


Figure 2: Effective masses of the lightest five $J^P = 0^+$ glueballs in $SO(12)$ at $\beta = 250$. Lines are mass estimates.

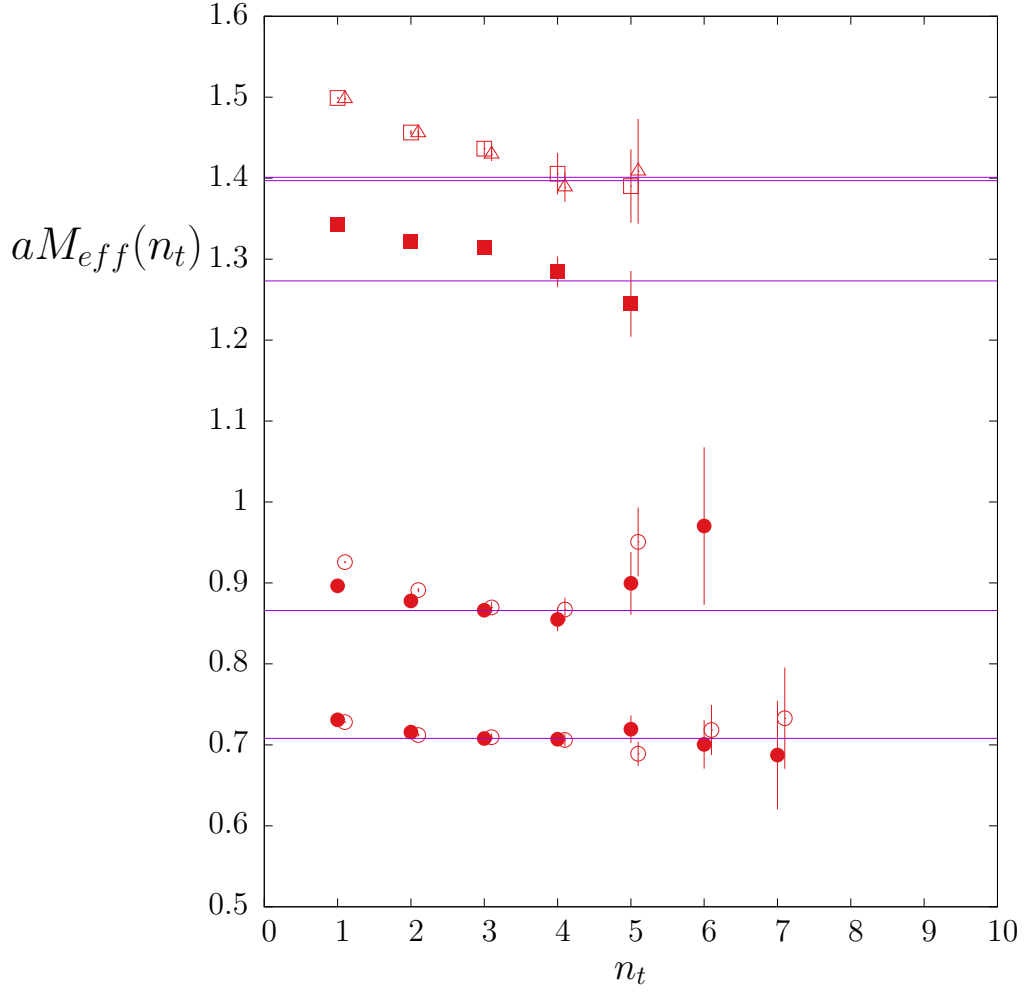


Figure 3: Effective masses of the lightest and first excited $J^P = 2^+$ (●) and $J^P = 2^-$ (○) glueballs and the ground state $J^P = 0^-$ (■), $J^P = 1^-$ (□) and $J^P = 1^+$ (△) glueballs, all in $SO(12)$ at $\beta = 250$. The 0^- and 1^\pm values have been shifted by $+0.4$ for clarity. Lines are mass estimates

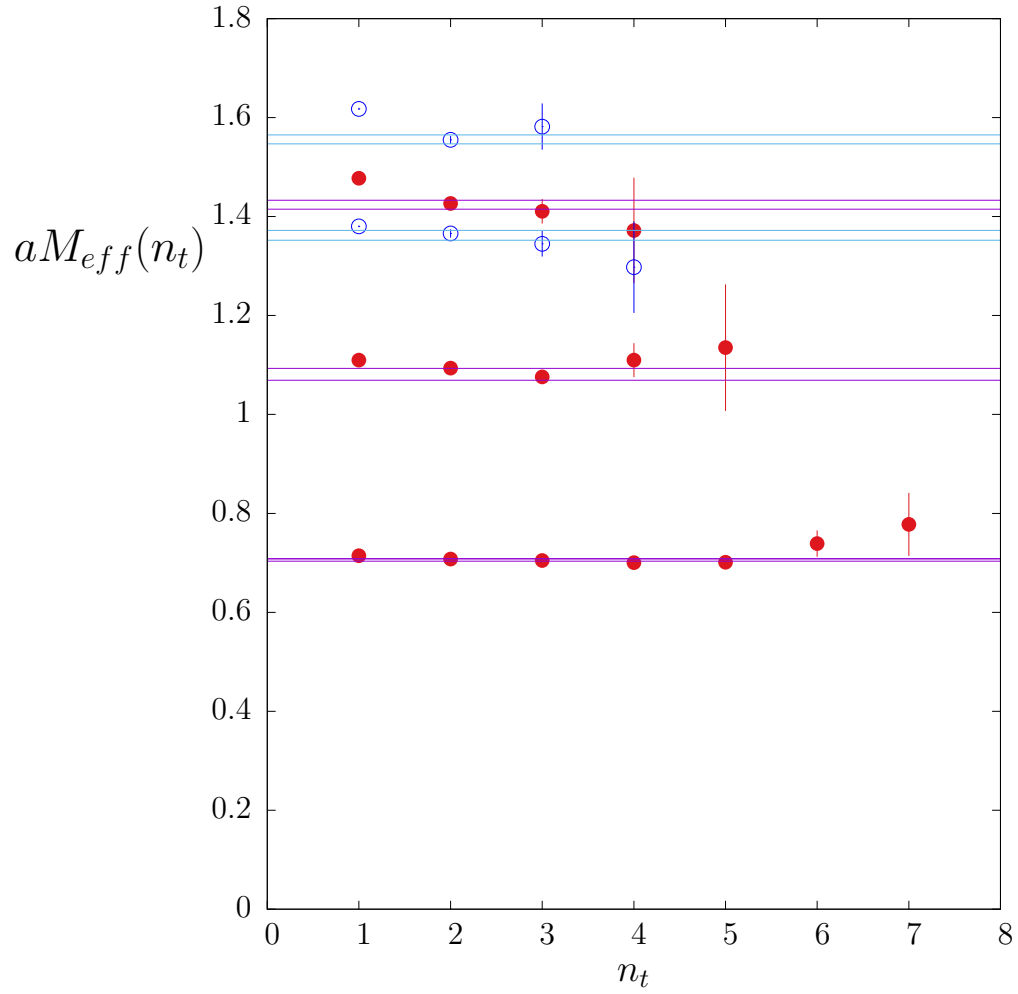


Figure 4: Effective masses of the lightest five $J^P = 0^+$ glueballs in $SO(12)$ at $\beta = 155$. Lines are $\pm 1\sigma$ mass estimates.

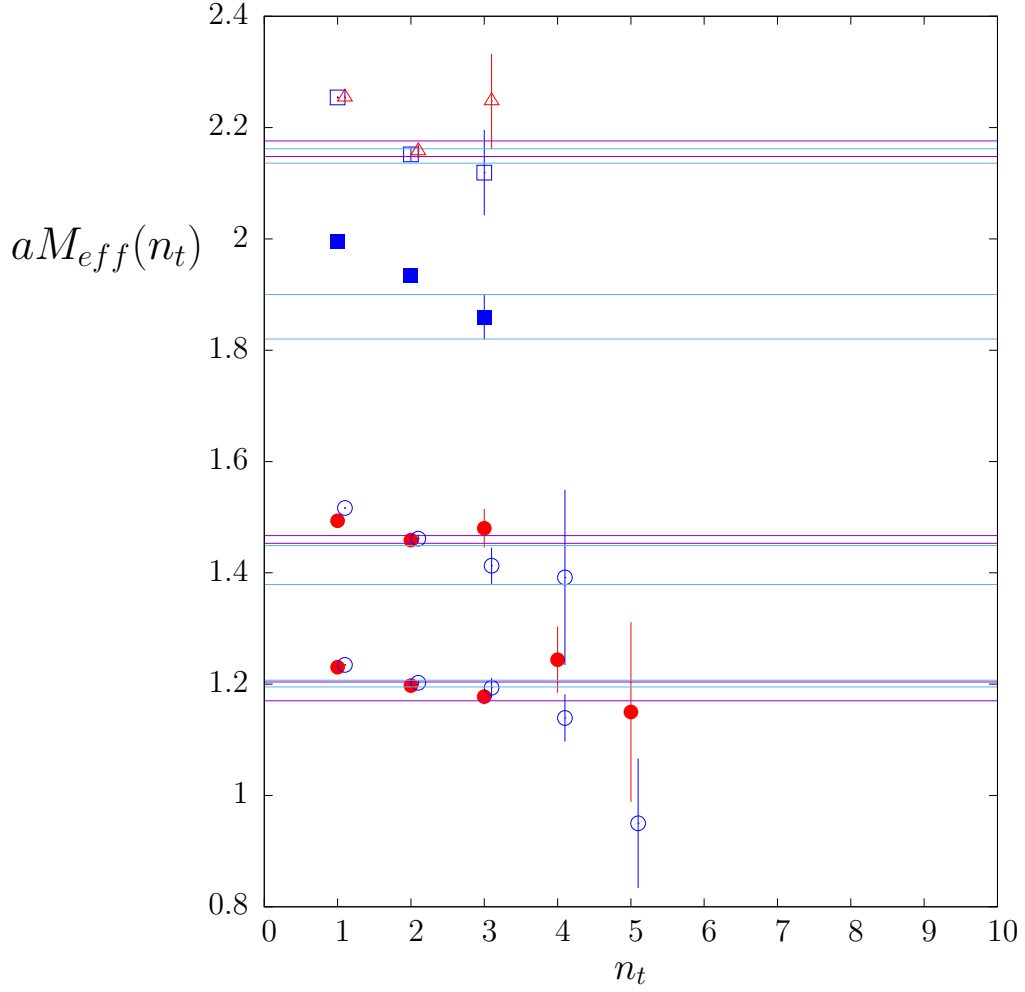


Figure 5: Effective masses of the lightest and first excited $J^P = 2^+$ (●) and $J^P = 2^-$ (○) glueballs and the ground state $J^P = 0^-$ (■), $J^P = 1^-$ (□) and $J^P = 1^+$ (△) glueballs, all in $SO(12)$ at $\beta = 155$. The 0^- and 1^\pm values have been shifted by $+0.4$ for clarity. Lines are $\pm 1\sigma$ mass estimates

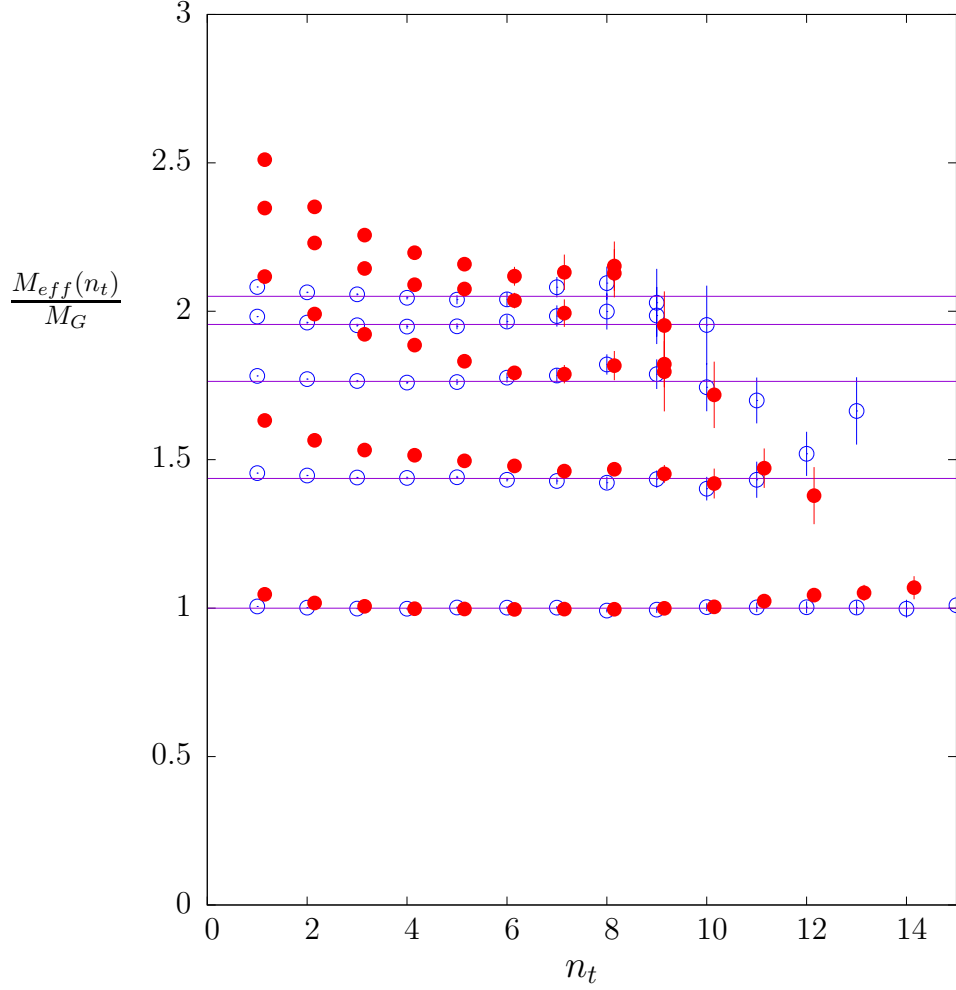


Figure 6: Effective masses of the lightest five scalar glueballs in $SO(3)$ (\bullet) at $\beta = 11$ on a $100^2 80$ lattice and in $SU(2)$ (\circ) at $\beta = 26.5$ on a $104^2 80$ lattice, in units of their respective mass gaps. Lines are $SU(2)$ mass estimates.

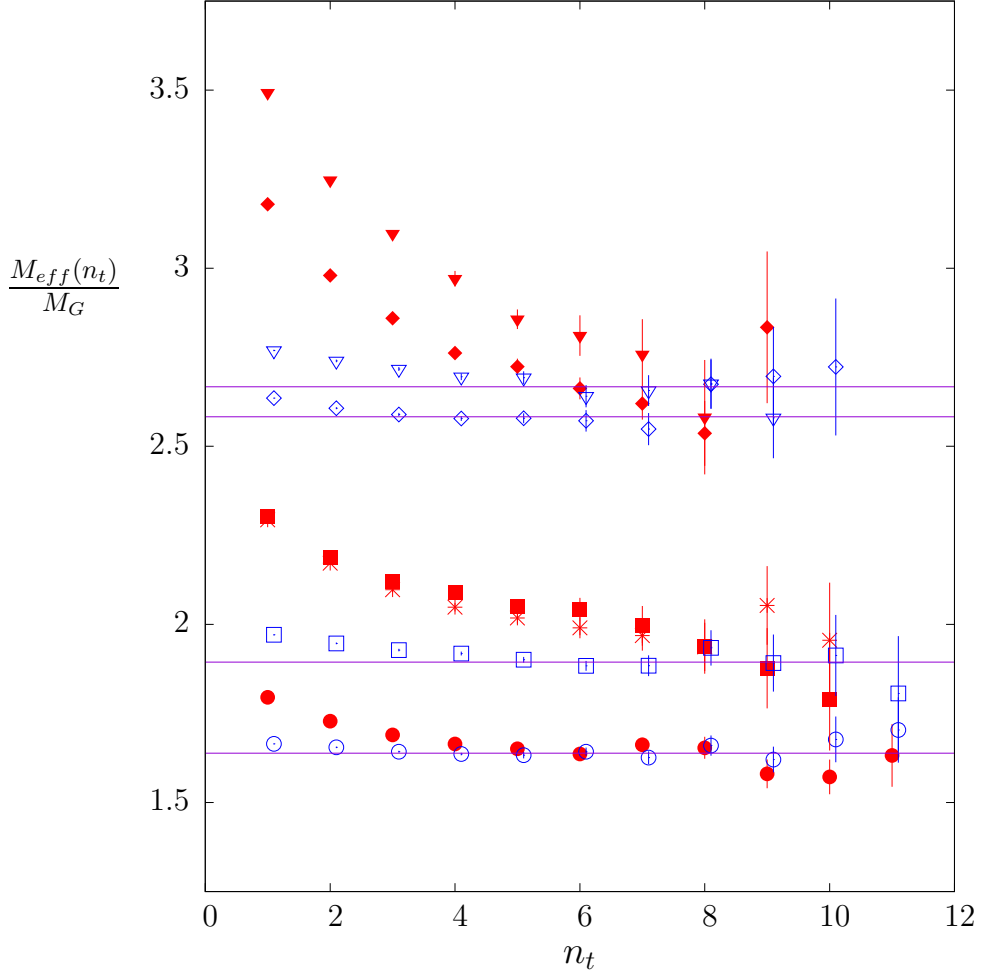


Figure 7: Effective $SO(3)$ masses of the lightest two 2^- glueballs (\bullet , \blacksquare), the lightest 0^- glueball (\blacklozenge) and the lightest 1^- glueball (\blacktriangledown), with open points being the corresponding $SU(2)$ effective masses. Also the $SO(3)$ mass of the first excited 2^+ (\star). All in units of their respective mass gaps and on the same lattices as in Fig 6. Lines are $SU(2)$ mass estimates. The 0^- and 1^- values have been shifted upwards by 0.5 for clarity.

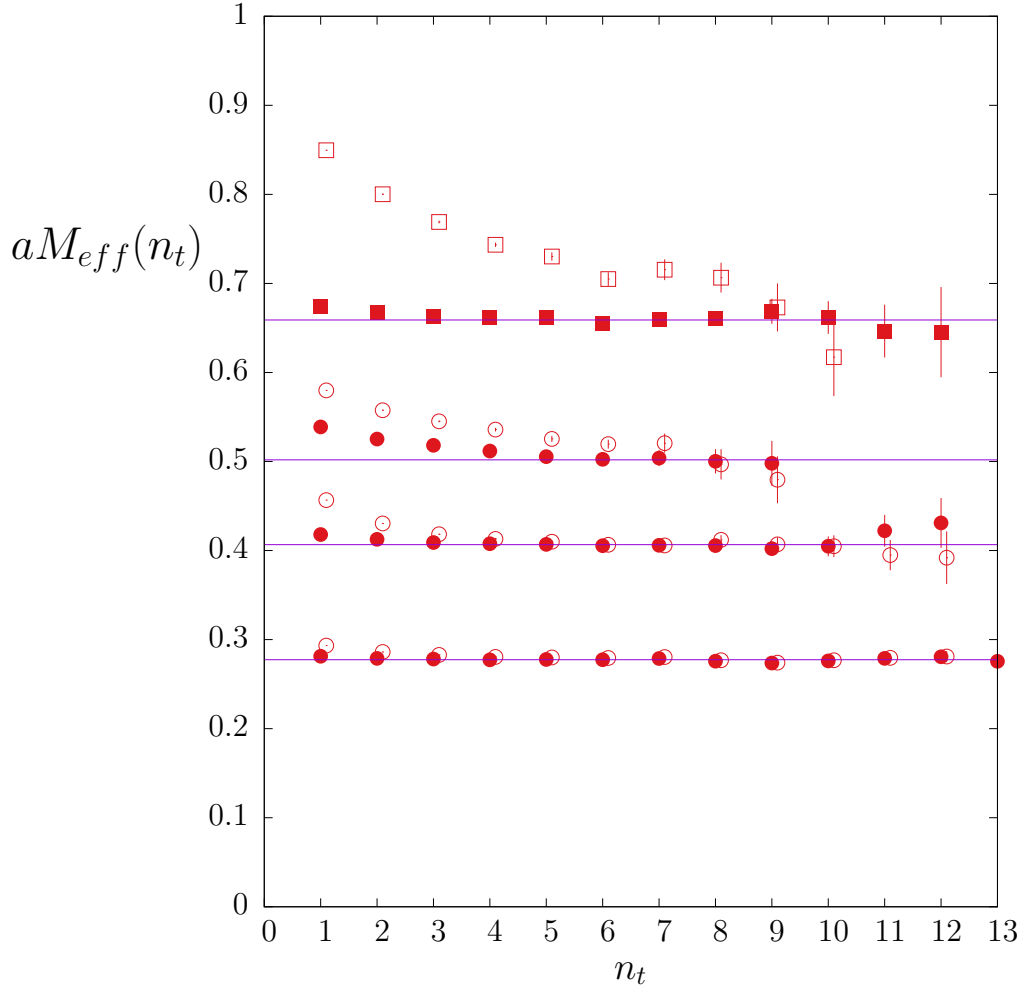


Figure 8: Effective masses of the lightest three 0^+ glueballs (\bullet, \circ) and the lightest 2^+ glueball (\blacksquare, \square) in SU(2) on a $96^2 64$ lattice at $\beta = 23.5$. The 2^+ values have been shifted by $+0.2$ for clarity. Filled points use operators in the fundamental and open points in the adjoint representations. Lines are mass estimates.

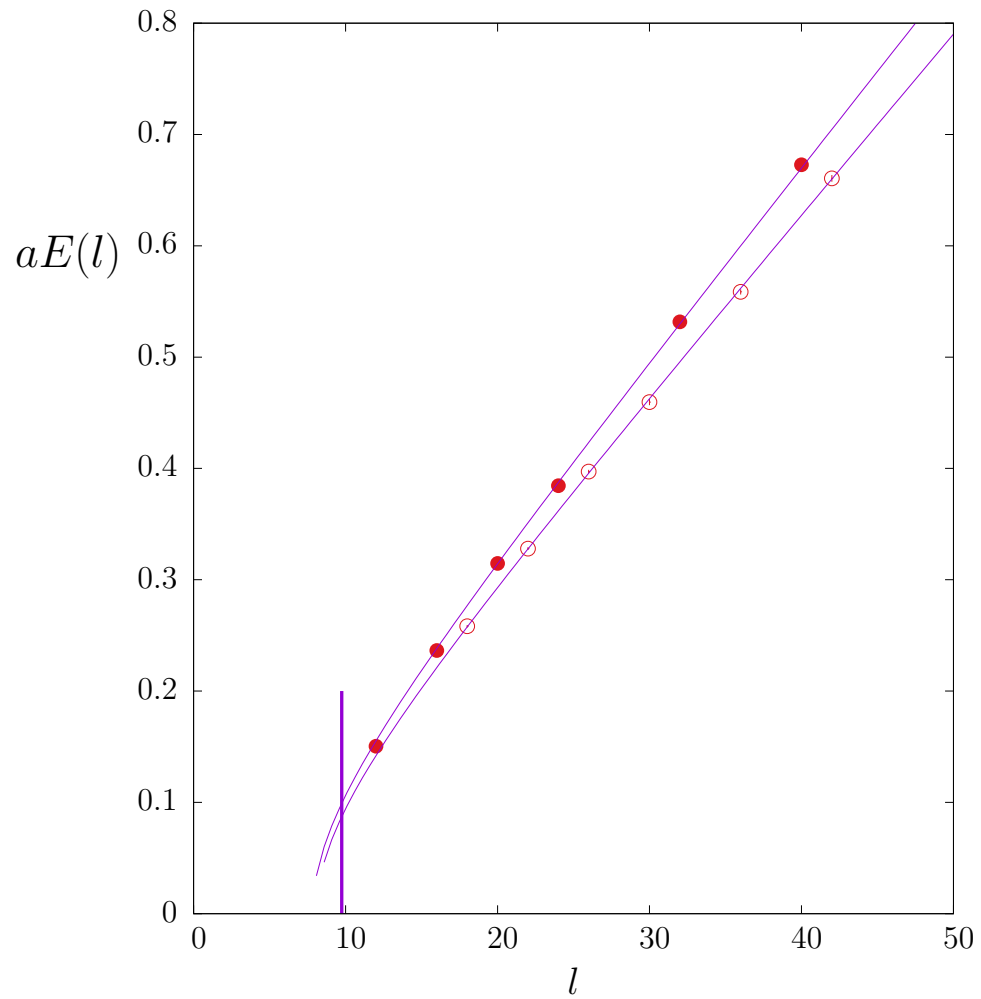


Figure 9: Ground state energy of a flux tube of length l in $SO(8)$ at $\beta = 86$, \bullet , and in $SO(6)$ at $\beta = 46$, \circ . Nambu-Goto fits shown. Vertical line is location of $SO(6)$ deconfining transition.

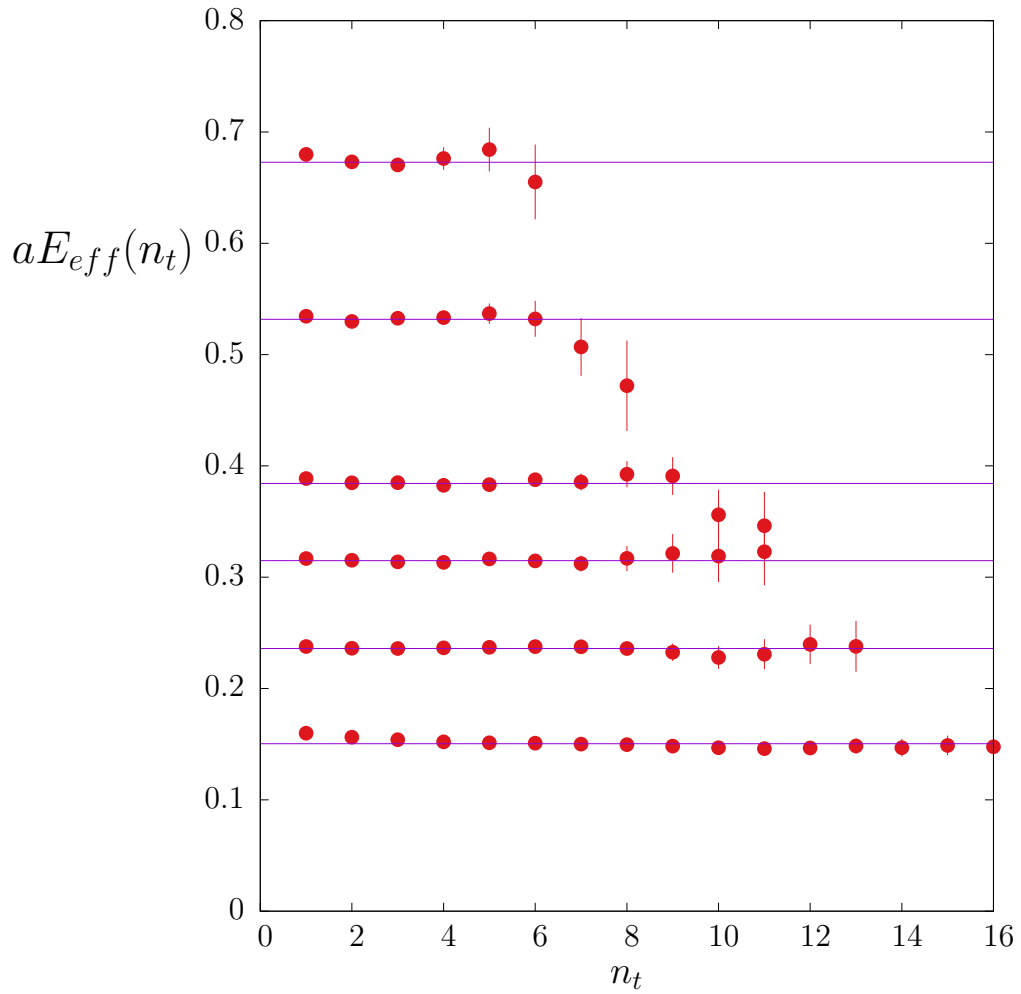


Figure 10: Effective energy of a flux tube of length l in $SO(8)$ at $\beta = 86$, as a function of $n_t = t/a$ for $l = 12, 16, 20, 24, 32, 40$. Lines are our energy estimates.

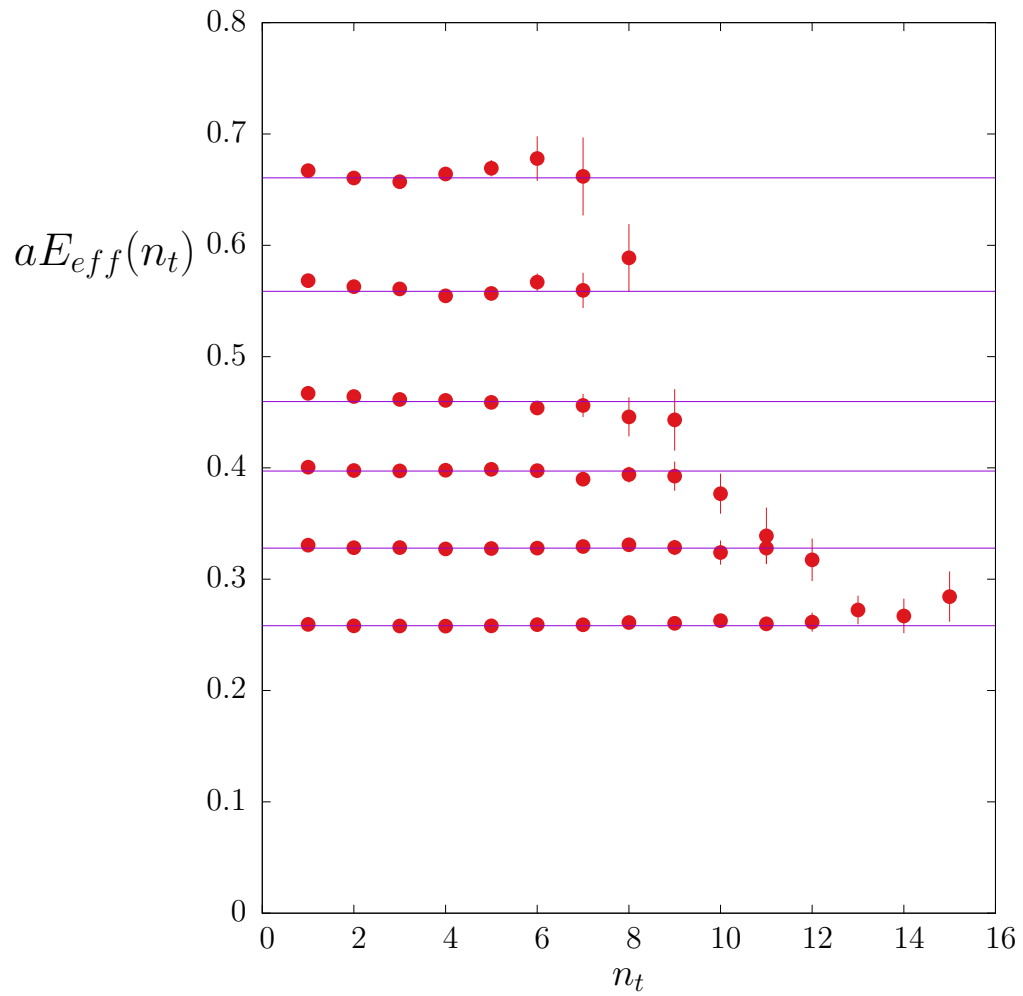


Figure 11: Effective energy of a flux tube of length l in $SO(6)$ at $\beta = 46$, as a function of $n_t = t/a$ for $l = 18, 22, 26, 30, 36, 42$. Lines are our energy estimates.

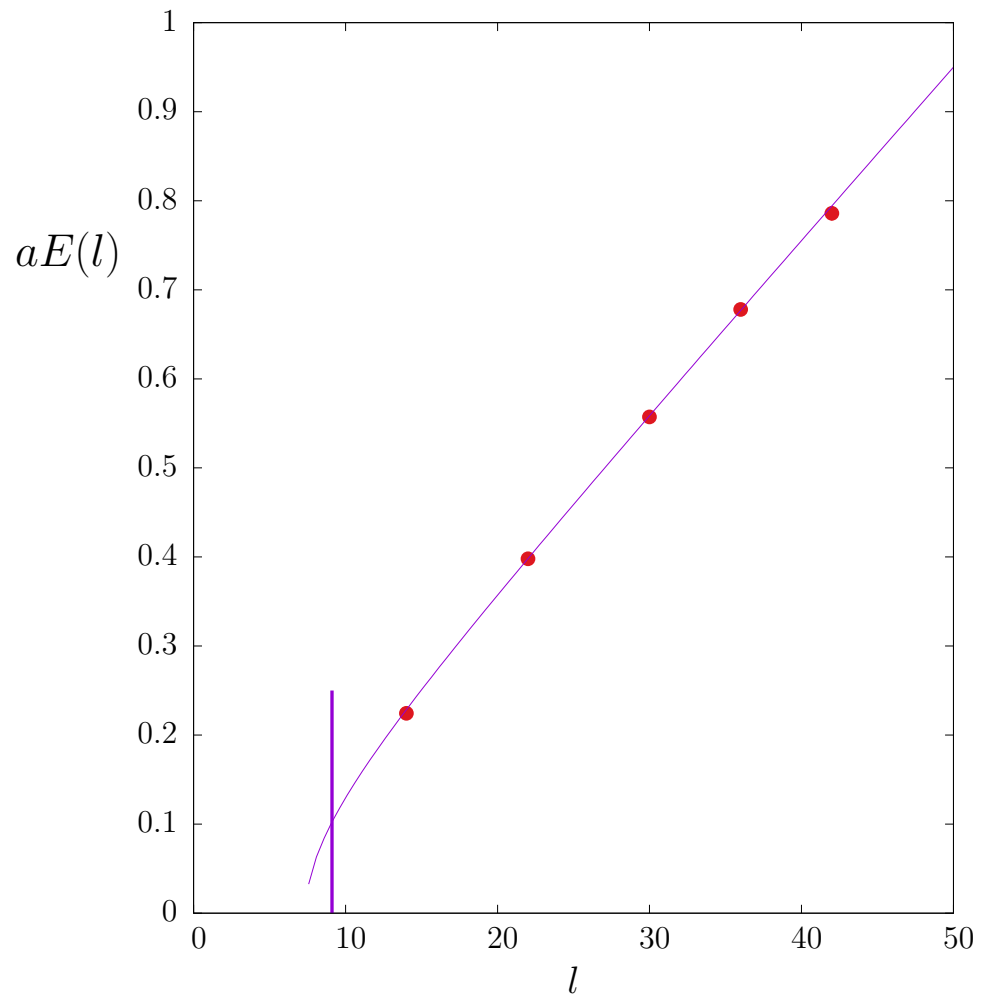


Figure 12: Ground state energy of a flux tube of length l in $SO(5)$ at $\beta = 27.5$. Nambu-Goto fit shown. Vertical line gives location of the deconfining transition.

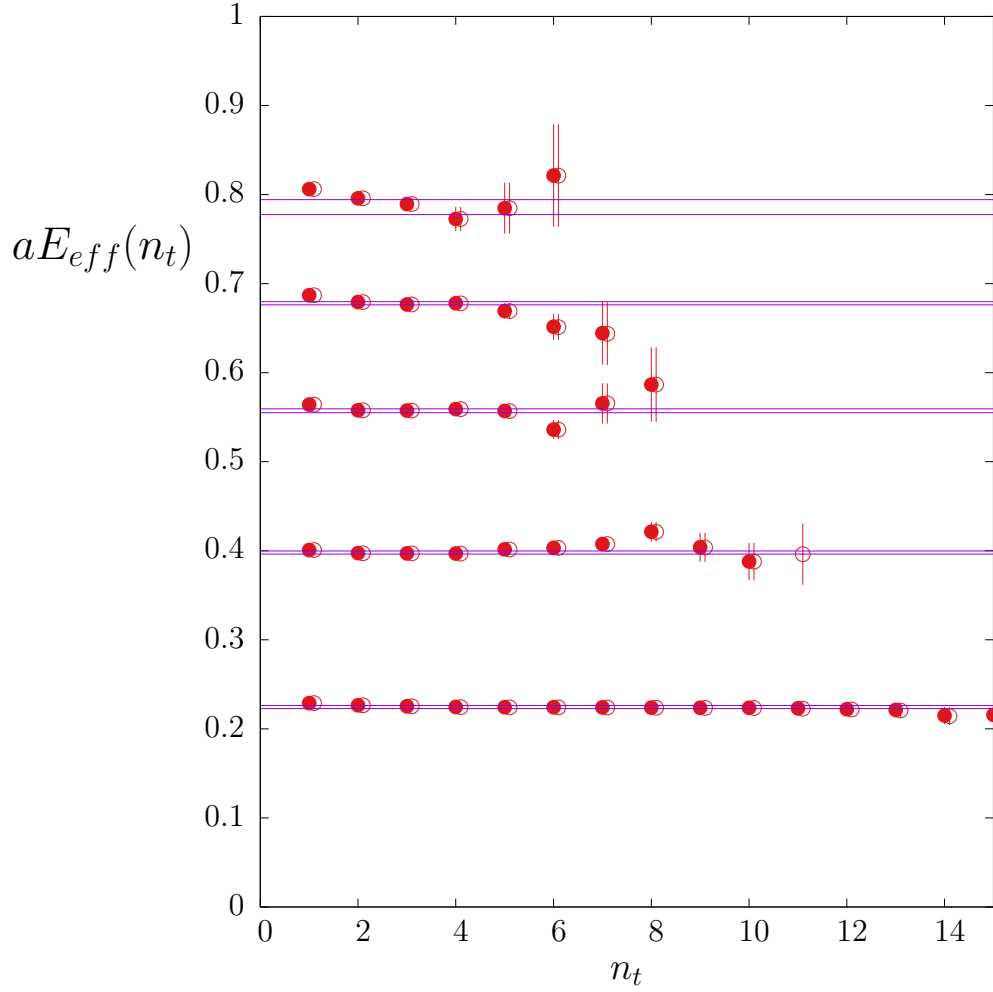


Figure 13: Effective energy of a flux tube of length l in $SO(5)$ at $\beta = 27.5$, as a function of $n_t = t/a$ for $l = 14, 22, 30, 36, 42$. Bands show our energy estimates with errors. Closed (open) points are with (without) vacuum subtraction. (Points shifted for clarity.)

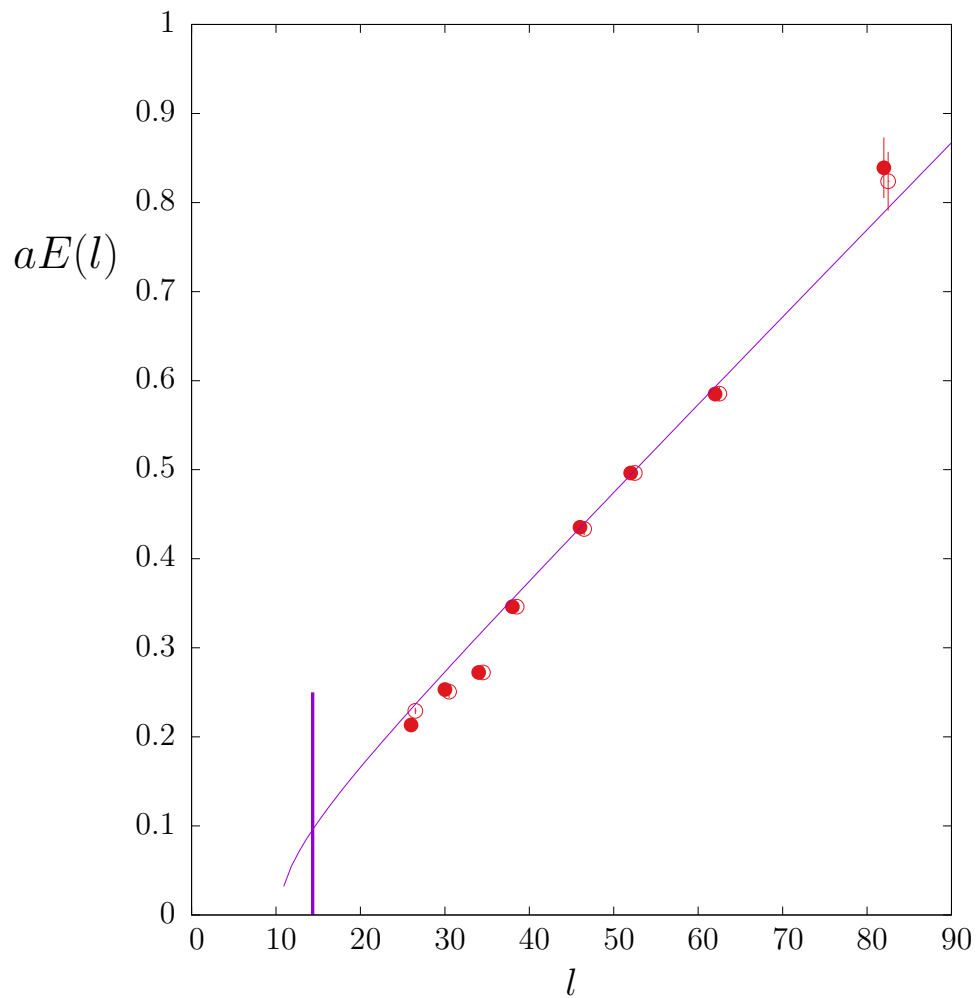


Figure 14: Ground state energy of a flux tube of length l in $SO(3)$ at $\beta = 9.0$ with (●) and without (○) vacuum subtraction. Nambu-Goto fit shown. Vertical line gives location of deconfining transition.

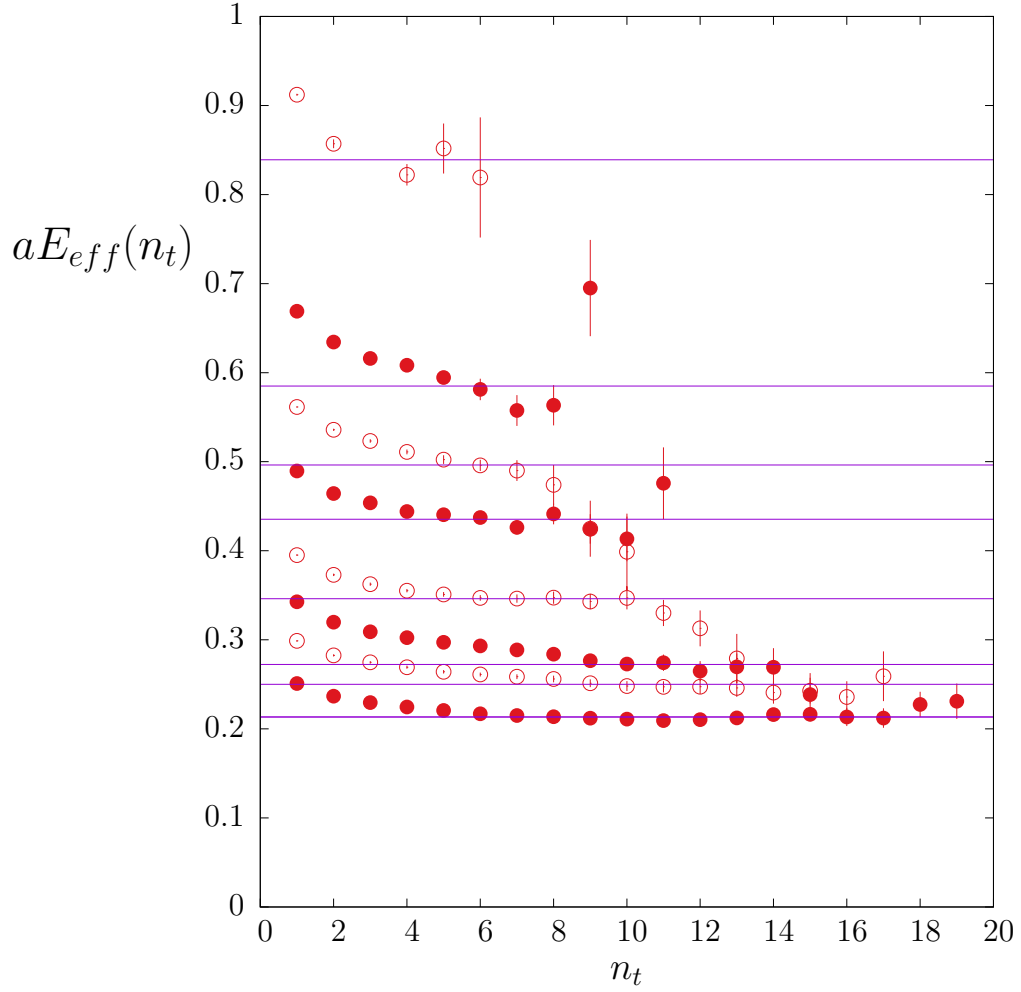


Figure 15: Effective energy of a flux tube of length l in $SO(3)$ at $\beta = 9.0$, as a function of $n_t = t/a$ for $l = 26, 30, 34, 38, 46, 52, 62, 82$. Correlators not vacuum subtracted. Lines represent our energy estimates.

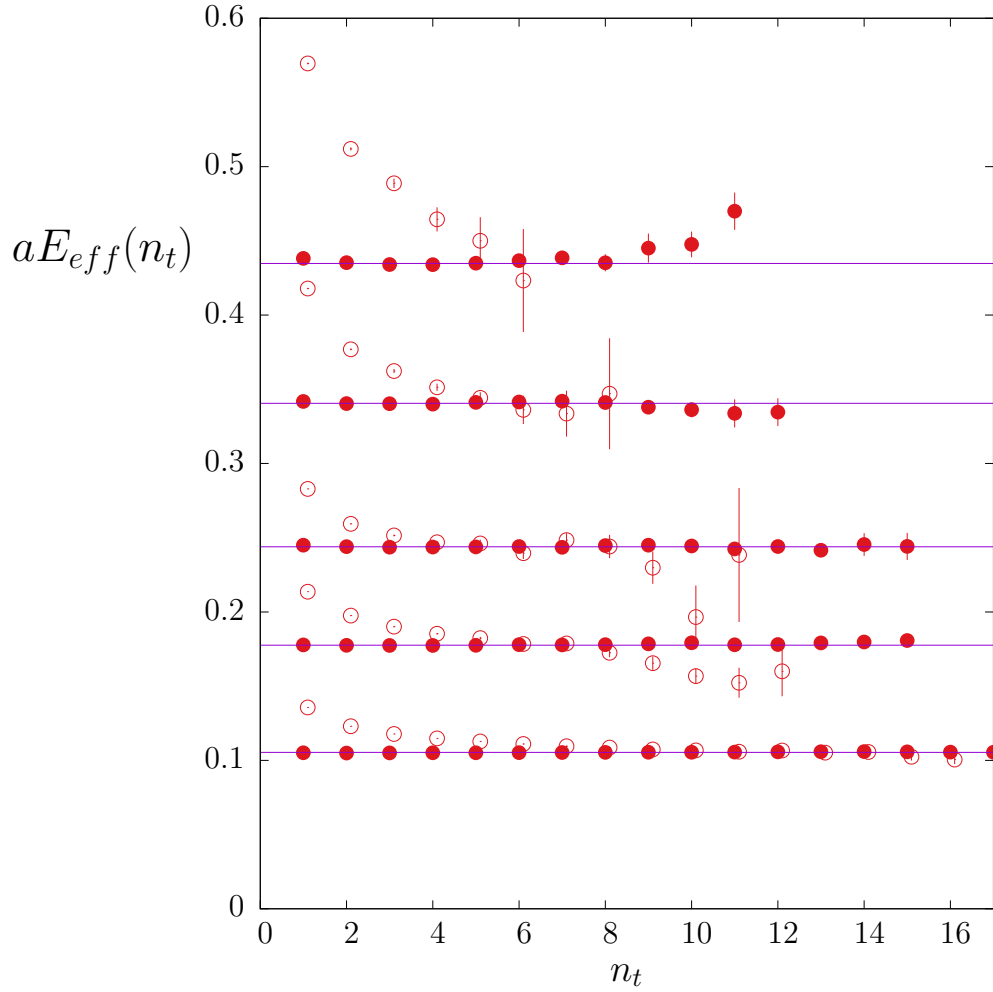


Figure 16: Effective energies of flux tubes of length $l = 18, 26, 34, 46, 58$ in $SU(2)$ at $\beta = 16.0$, as a function of $n_t = t/a$ for flux in the fundamental, \bullet , and in the adjoint, \circ . Adjoint values have been rescaled to asymptote to the fundamental energies. Lines shown are (fundamental) energy estimates.

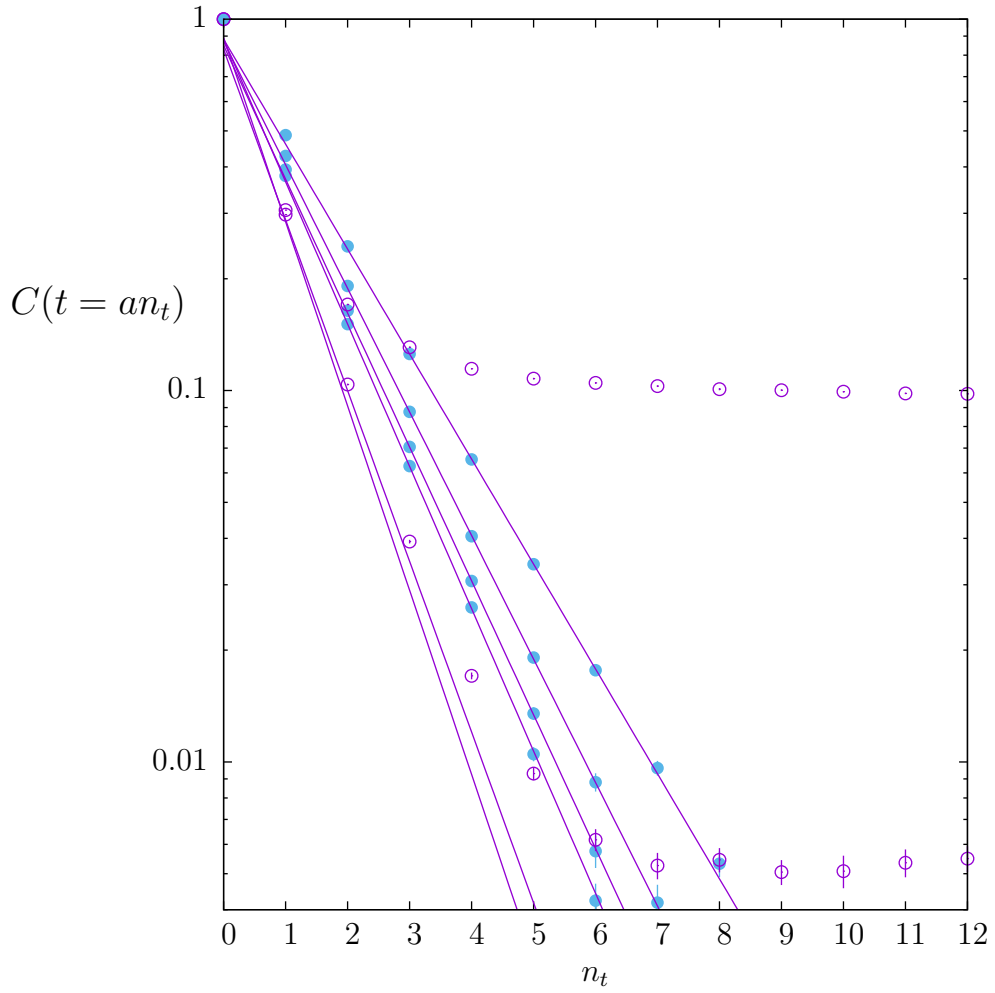


Figure 17: Correlation functions of the ground and first 3 excited flux tube states (●) and also the 8'th and 10'th excited states (○). Exponential fits also shown, as described in text. In $SO(3)$ at $\beta = 11$.

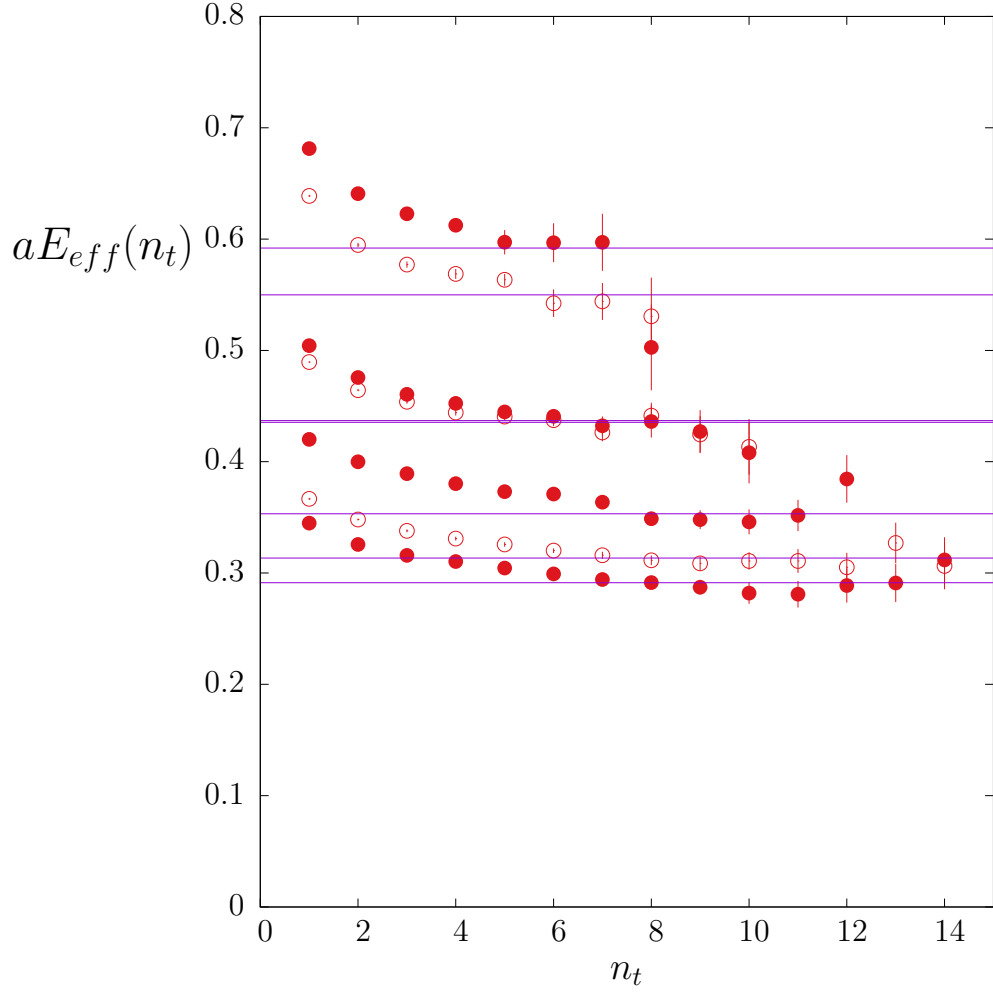


Figure 18: Effective energies of flux tubes of approximately the same physical length, $l\sqrt{\sigma} \sim 4.2$, in $SO(3)$ at $\beta = 6.5, 7.0, 8.5, 9.0, 10.0, 11.0, 12.0$, as a function of $n_t = t/a$. Correlators vacuum subtracted. Lines represent our energy estimates.

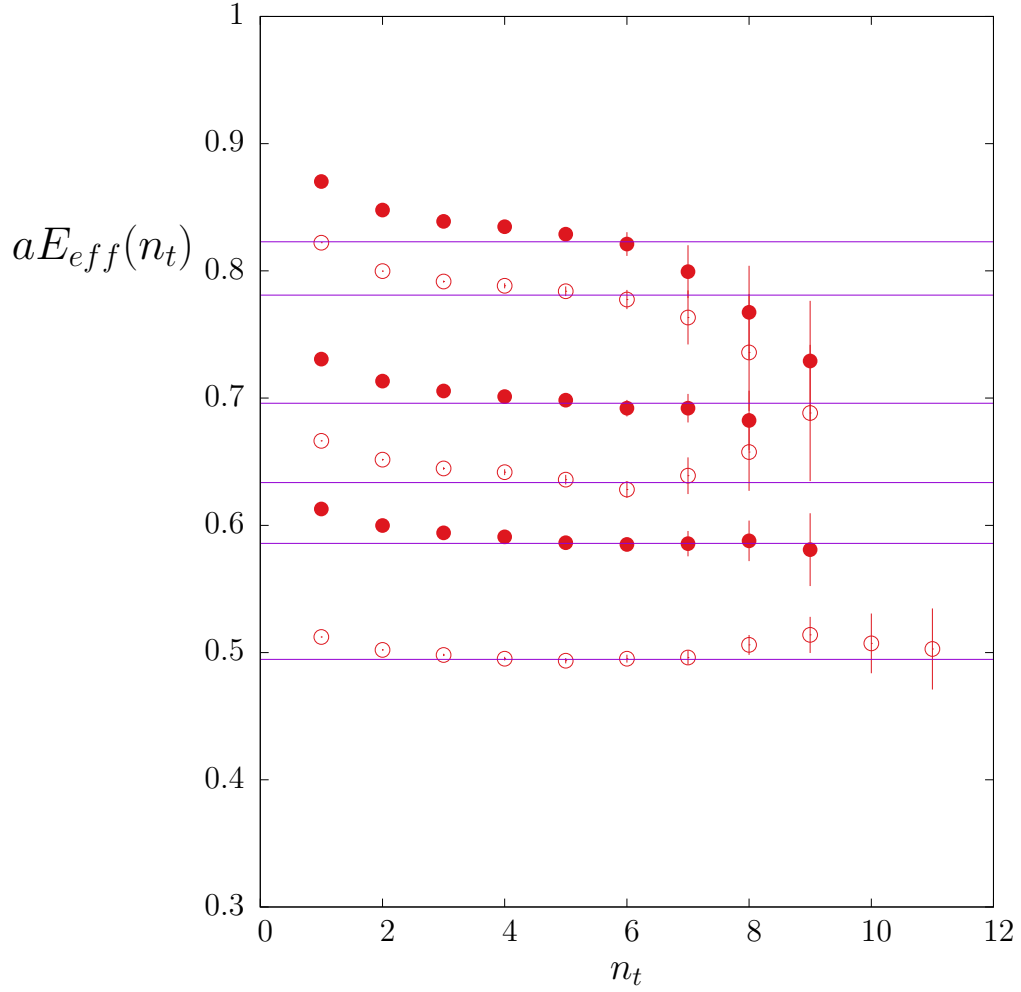


Figure 19: Effective energies of flux tubes of approximately the same physical length, $l\sqrt{\sigma} \sim 4.4$, in $SO(4)$ at $\beta = 11.0, 12.2, 13.7, 15.1, 16.5, 18.7$ as a function of $n_t = t/a$. Lines represent our energy estimates.

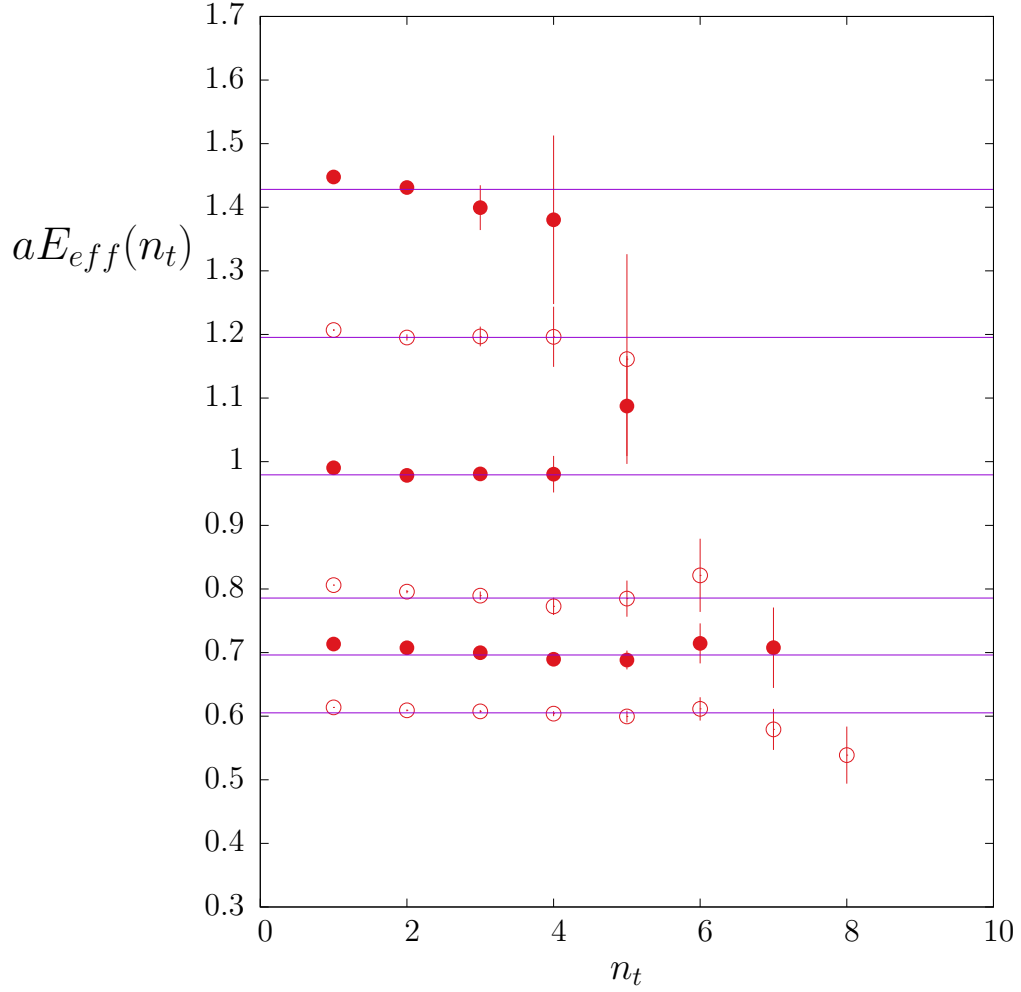


Figure 20: Effective energies of flux tubes of approximately the same physical length, $l\sqrt{\sigma} \sim 6.0$, in $SO(5)$ at $\beta = 17.5, 20.0, 23.5, 27.5, 32.0, 36.0$ as a function of $n_t = t/a$. Lines represent our energy estimates.

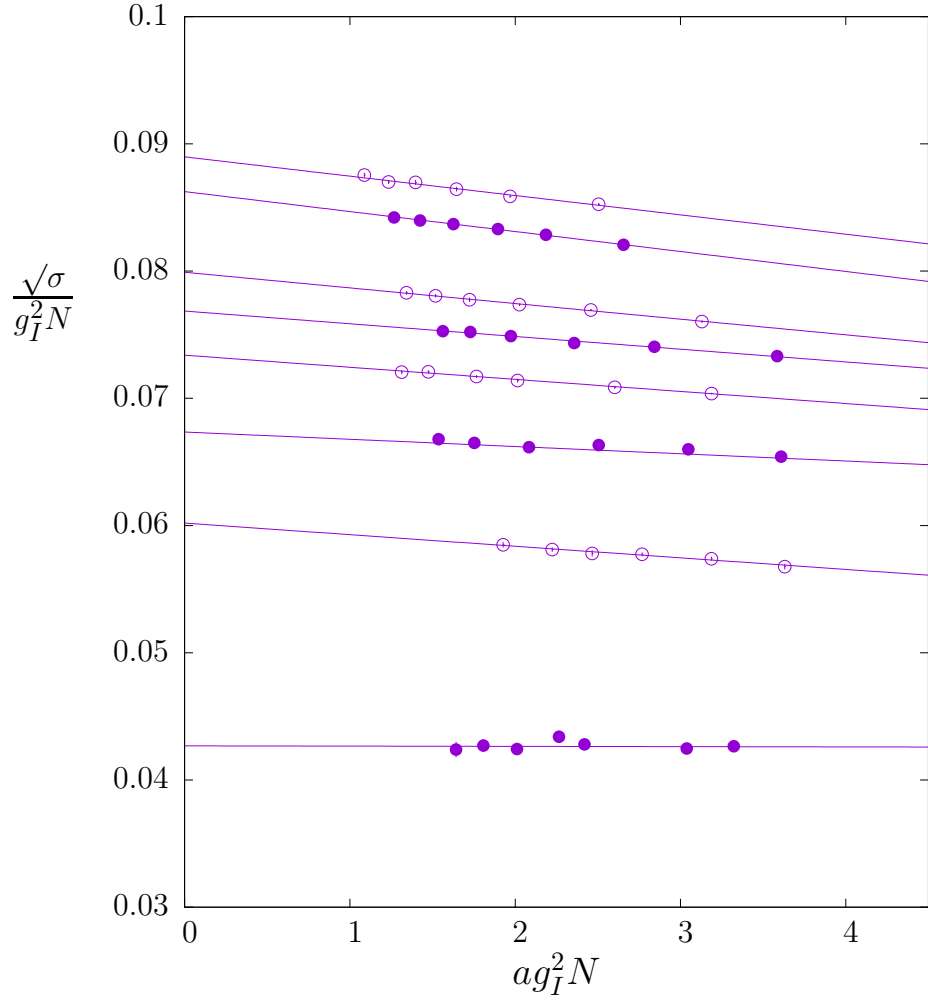


Figure 21: Lattice values of $\sqrt{\sigma}/g_I^2 N$ for SO(3), SO(4), SO(5), SO(6), SO(7), SO(8), SO(12), SO(16) in ascending order, with continuum extrapolations.

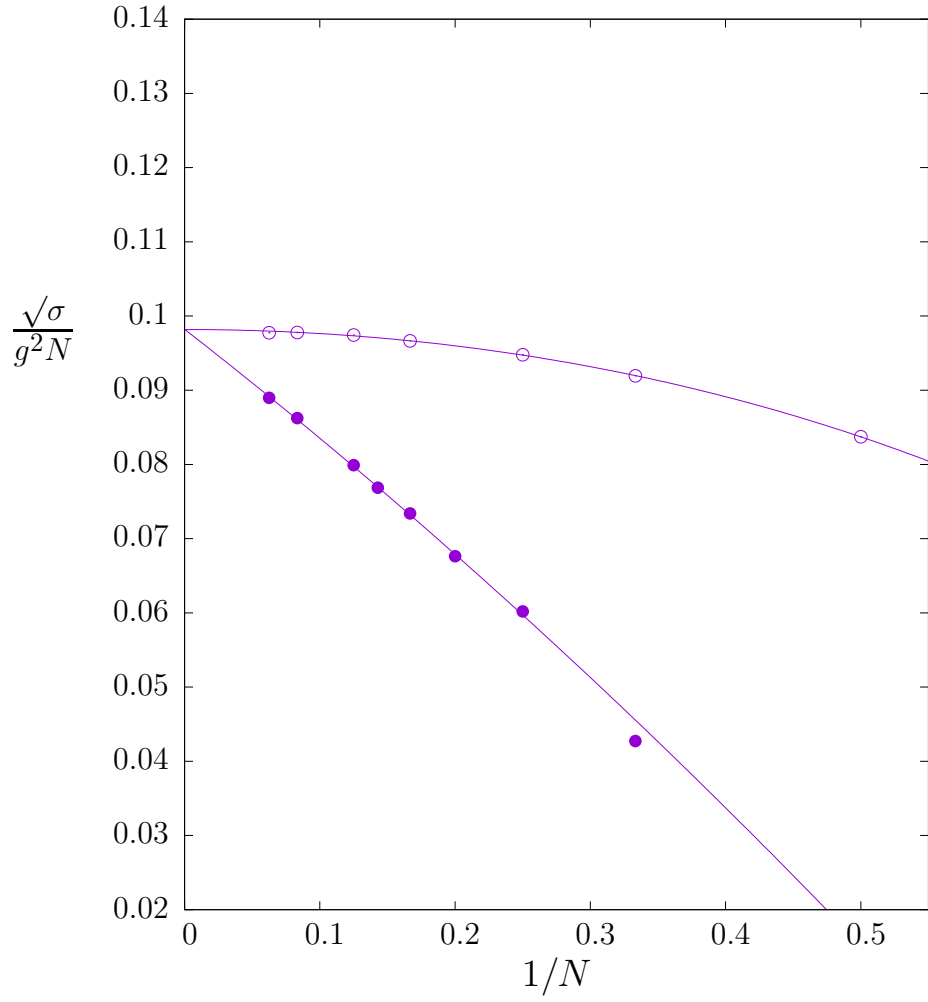


Figure 22: Continuum values of $\sqrt{\sigma}/g^2N$ in $SO(N)$, \bullet , with extrapolation to $N = \infty$ as in eqn(41). Also shown are $SU(N)$ values of $\sqrt{\sigma}/2g^2N$, \circ , with the large N fit given in eqn(42).

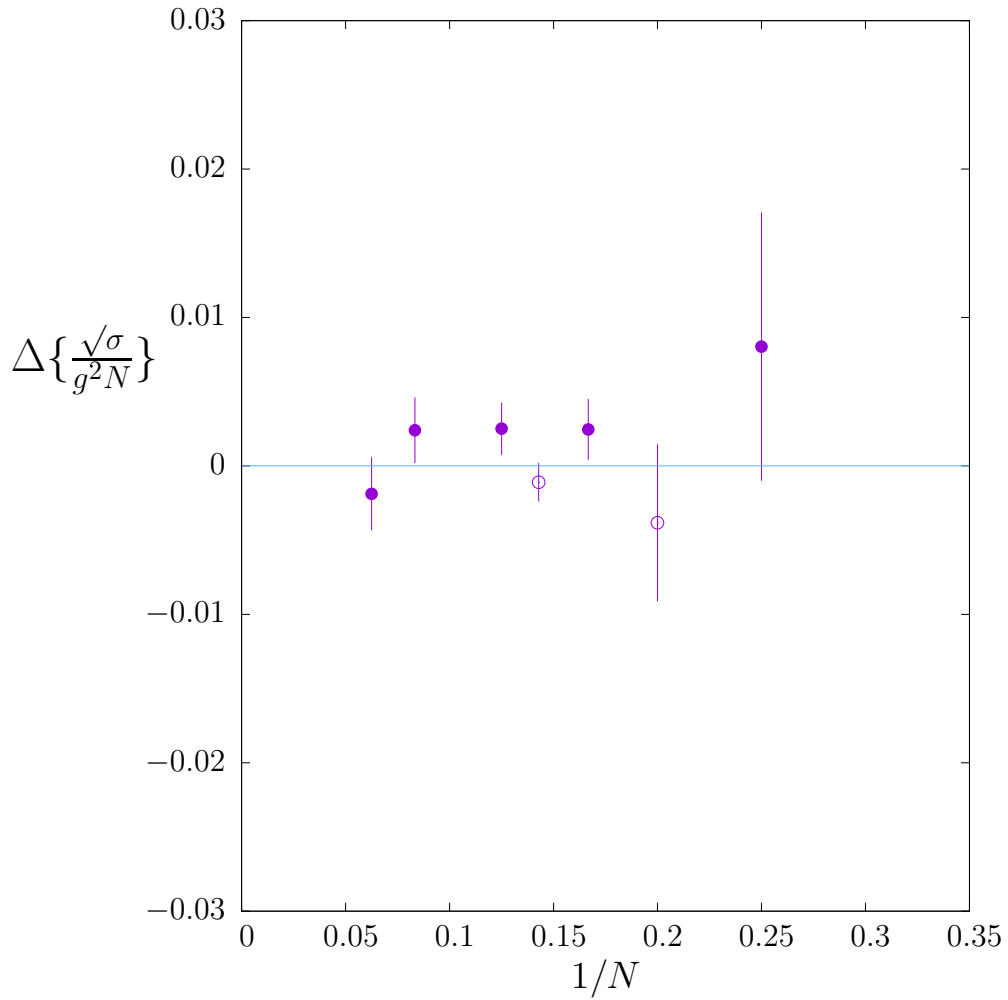


Figure 23: Difference between value of $\sqrt{\sigma}/g^2N$ and the best fit in eqn(41), normalised by its value. Open points are N odd, full points are N even. ($SO(3)$ is off the plot.)

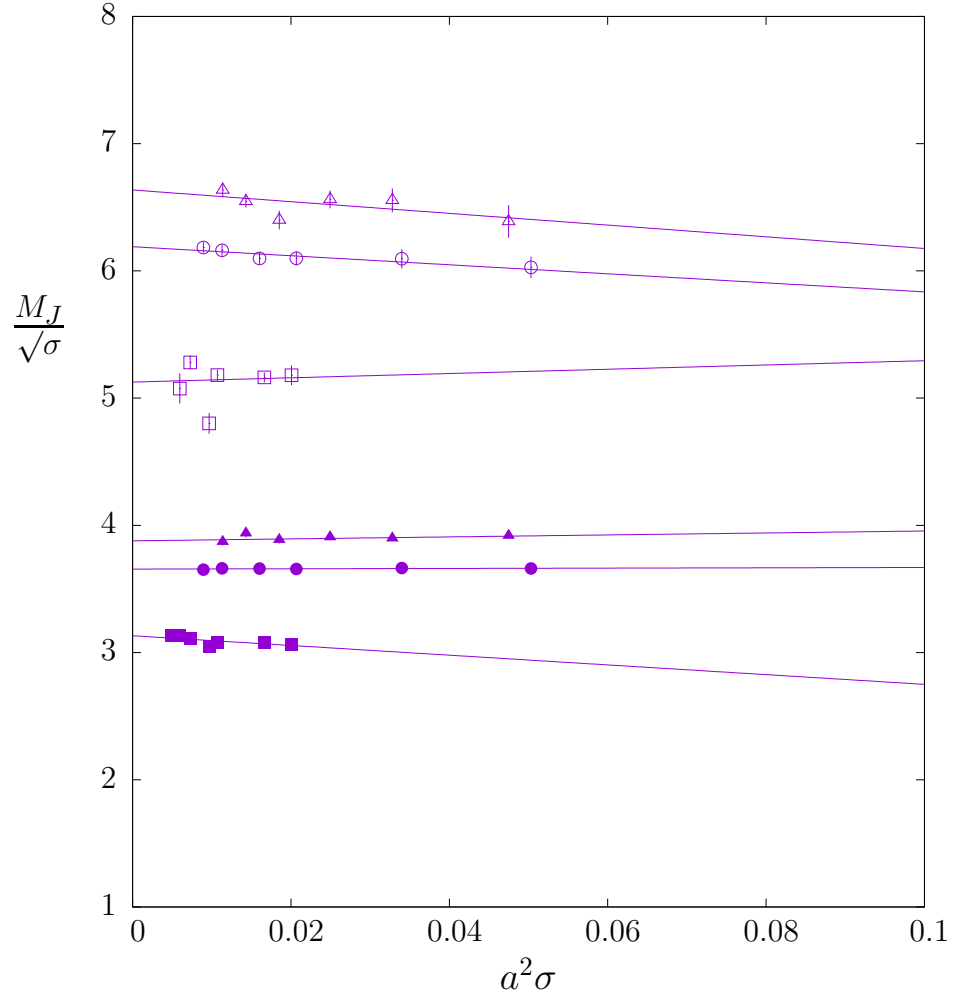


Figure 24: Lightest 0^+ glueball in $SO(3)$ (■), $SO(6)$ (●), $SO(12)$ (▲), and lightest 2^+ glueball in $SO(3)$ (□), $SO(6)$ (○), $SO(12)$ (△), all in units of the string tension and plotted versus the string tension, with linear extrapolations to the continuum limit.

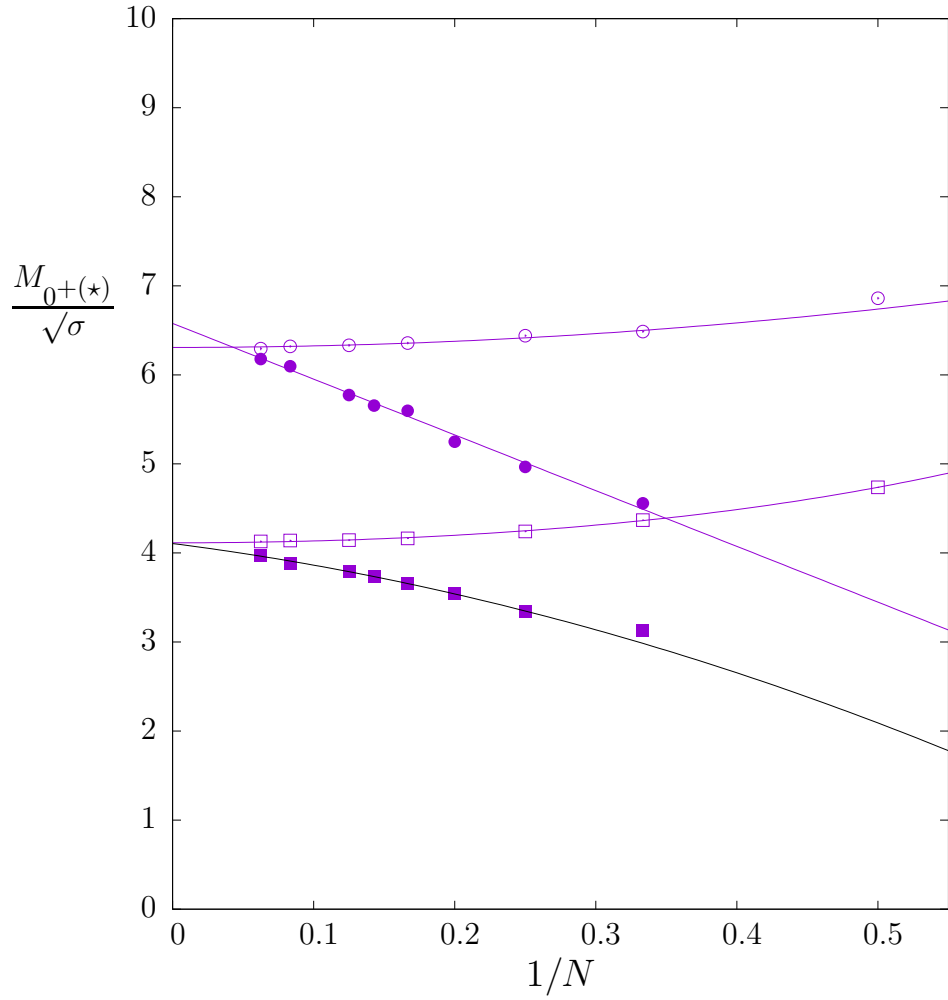


Figure 25: Lightest two 0^+ glueballs in units of the string tension in $SO(N)$ (\blacksquare, \bullet) and in $SU(N)$ (\square, \circ) with typical extrapolations to $N = \infty$.

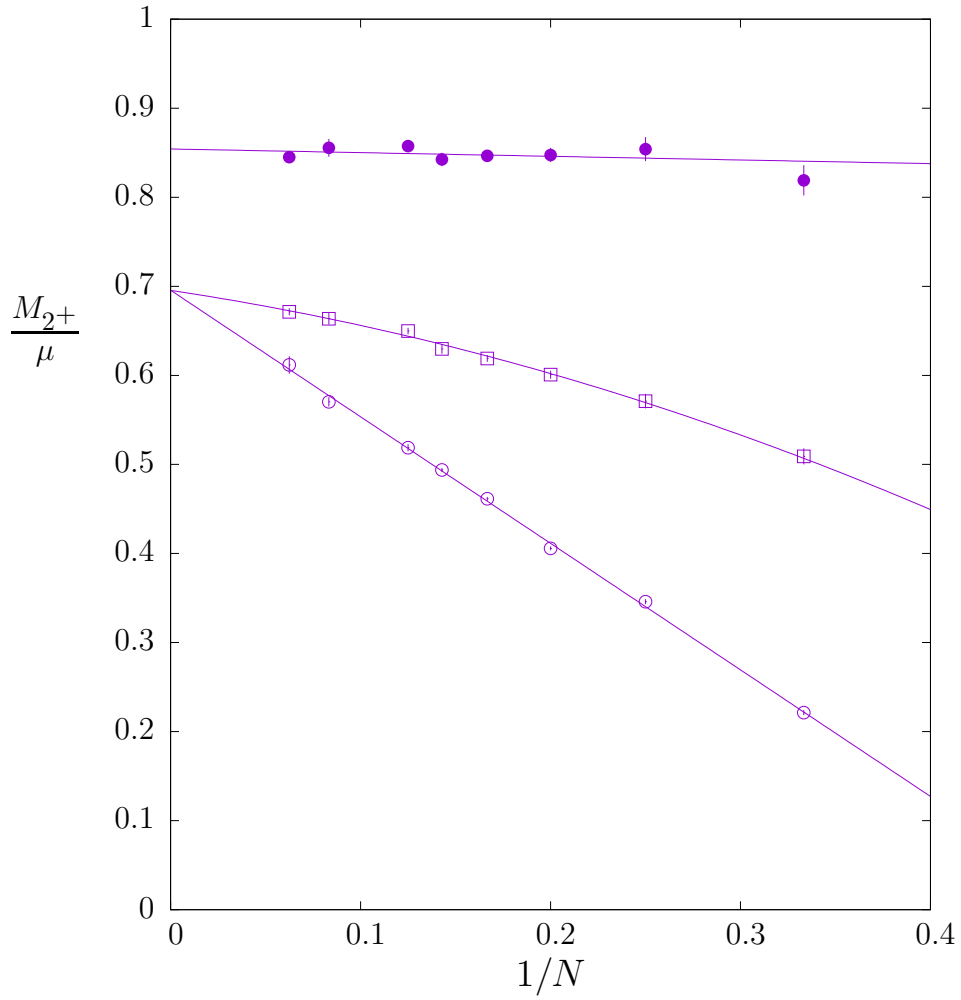


Figure 26: Mass ratios M_{2+}/μ versus $1/N$ for $\mu = 2M_{0+}$ (\bullet), $\mu = g^2N$ (\circ) and $\mu = 10\sqrt{\sigma}$ (\square). Fits shown to guide the eye.

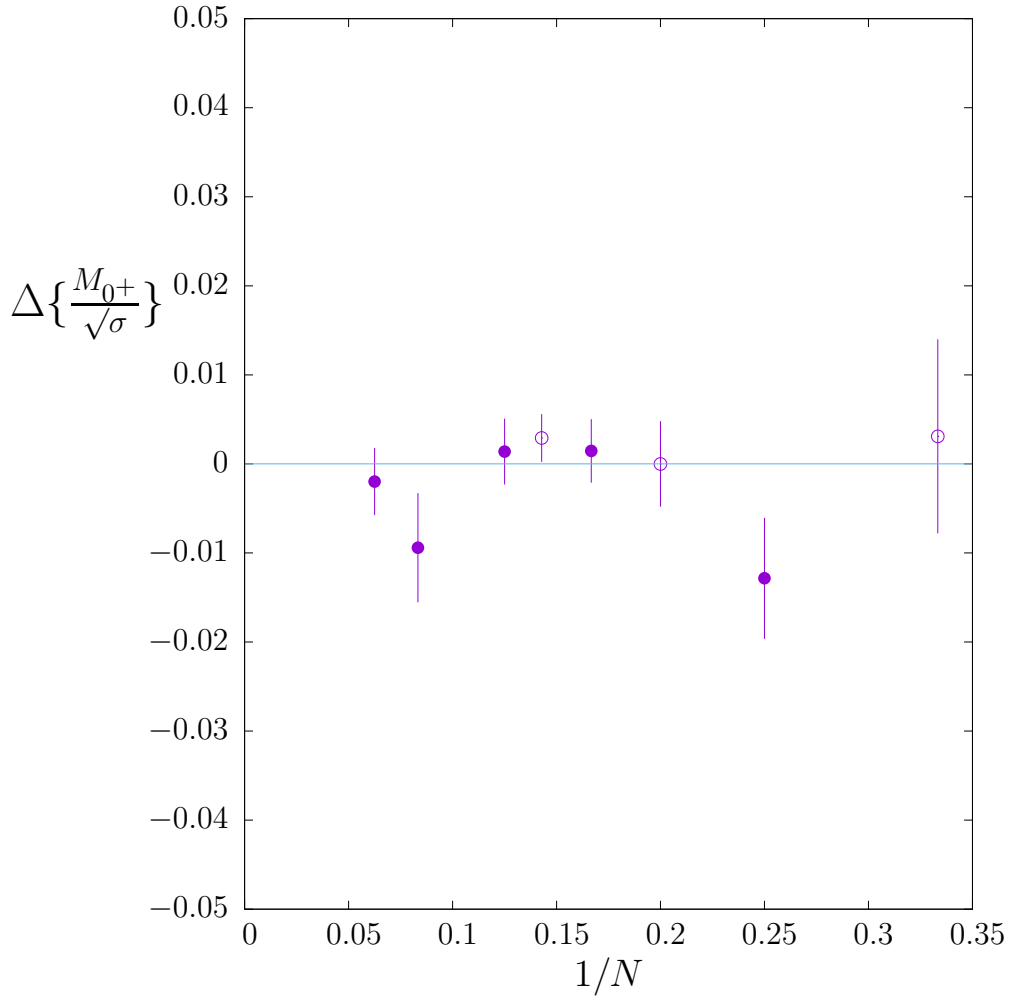


Figure 27: Difference between value of $M_{0+}/\sqrt{\sigma}$ and the best fit eqn(50), normalised by value of ratio. Open points are N odd, filled points are N even.

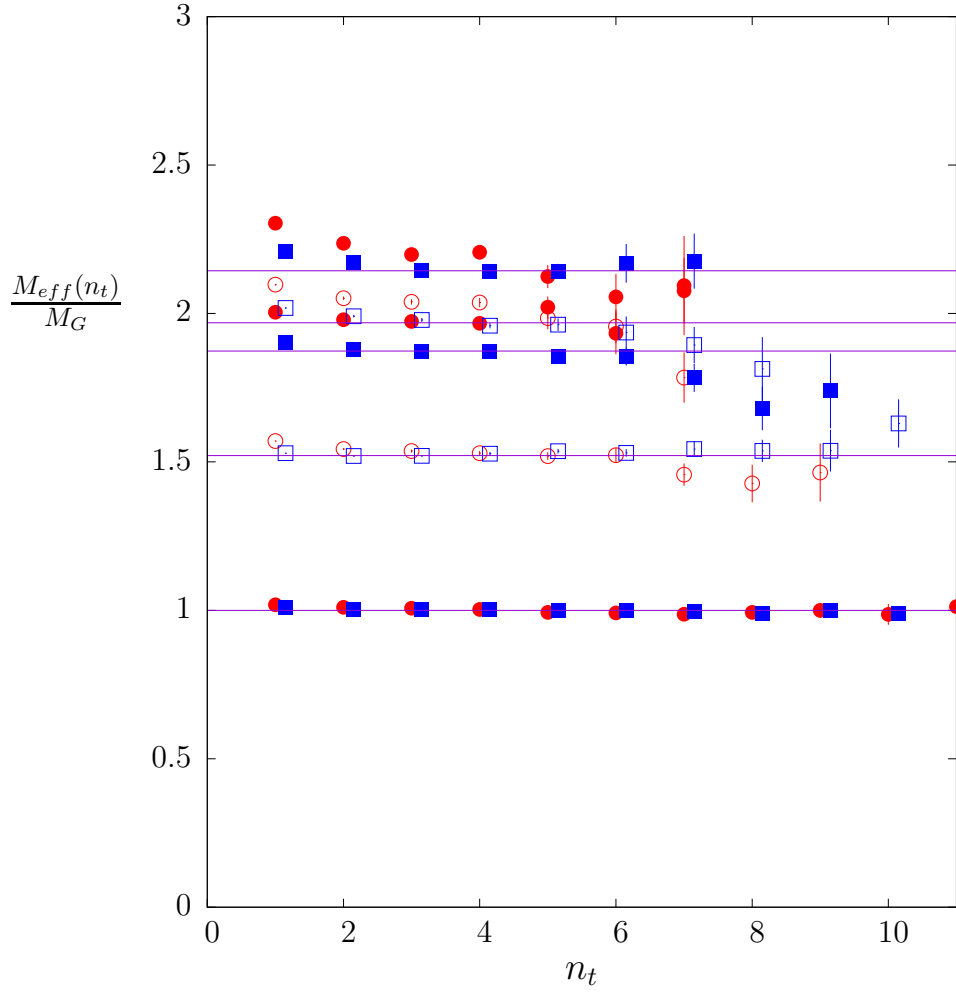


Figure 28: Lightest five 0^+ glueball effective masses in $SU(4)$ (\square, \blacksquare) and $SO(6)$ (\circ, \bullet), in units of their respective mass gaps, and at the smallest values of a in each case.

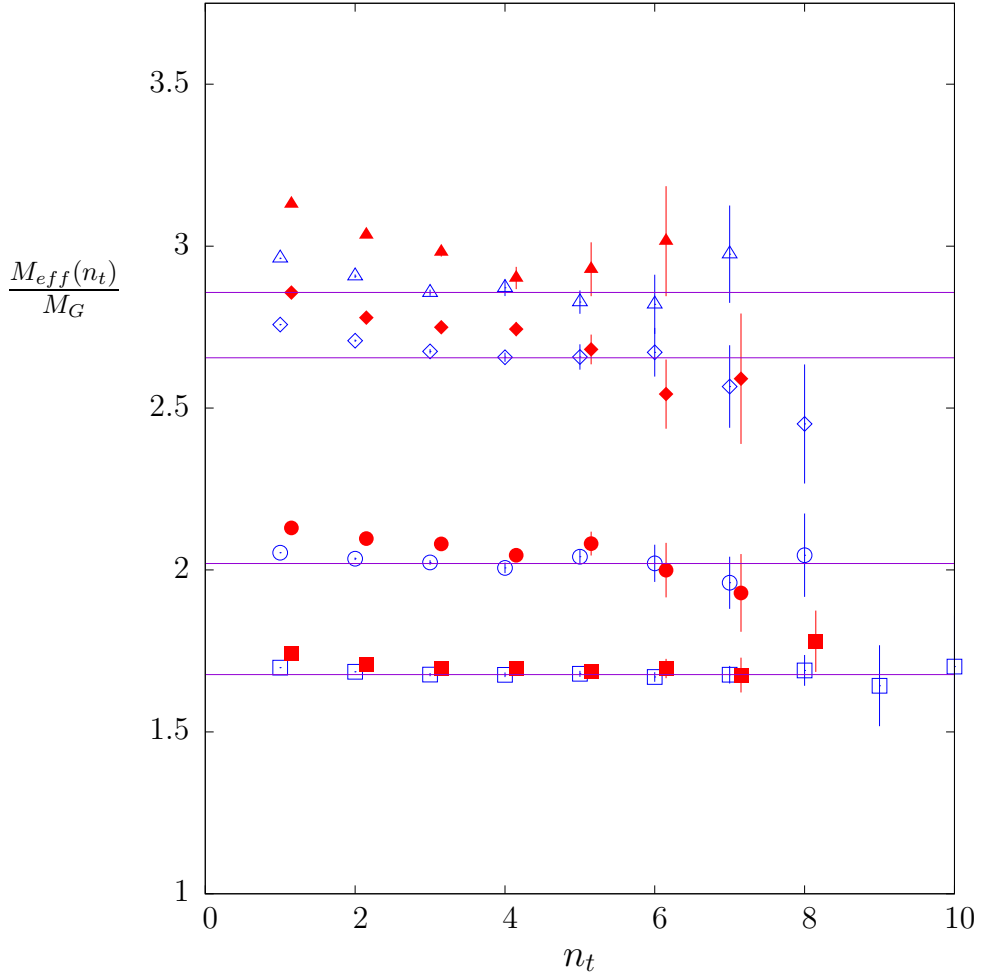


Figure 29: Some glueball effective masses in $SU(4)$ (open points) and $SO(6)$ (filled points), in units of their respective mass gaps, and at our smallest value of a : lightest 2^+ , \square , first excited 2^+ , \circ , lightest 0^- , \diamond , and lightest 1^+ , \triangle . The 1^+ and 0^- have been shifted up by $+0.5$ for clarity.

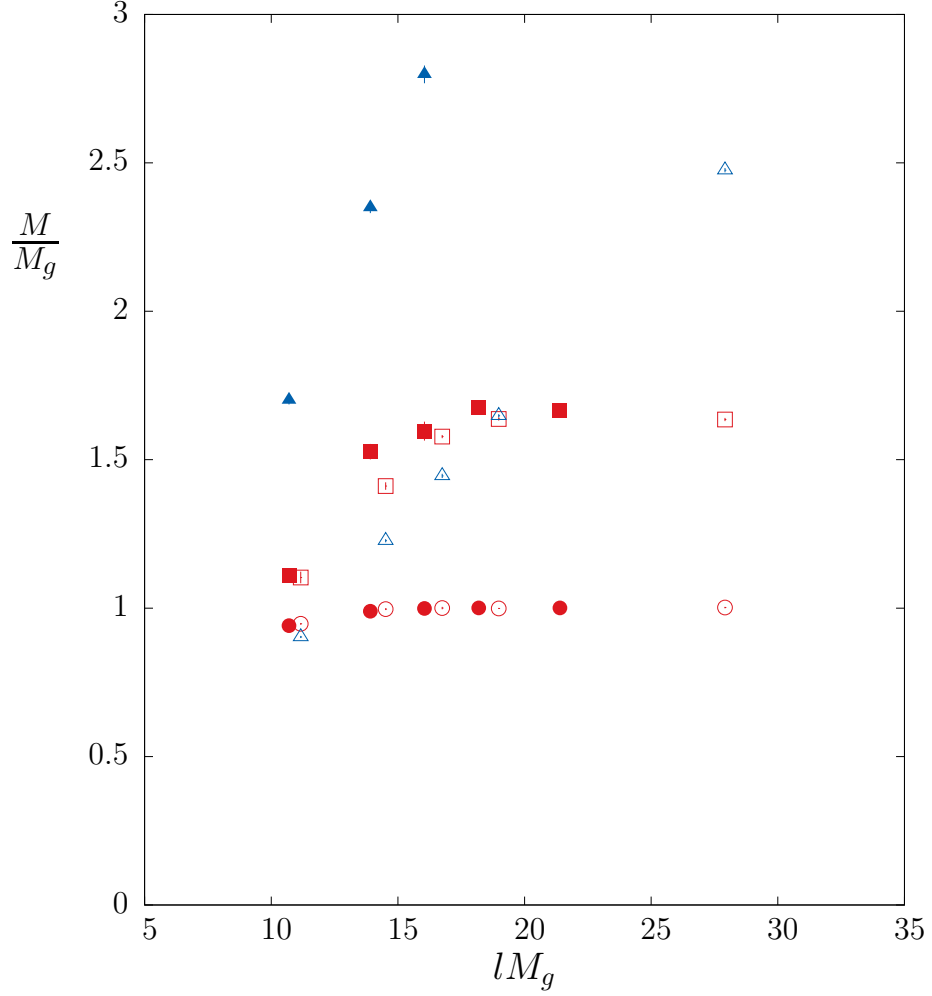


Figure 30: Lightest scalar (\circ) and tensor (\square) glueballs in SU(2) on various spatial volumes, l^2 , all in units of the infinite volume mass gap M_g . And same for SO(4) (\bullet , \blacksquare respectively). Also shown is twice the fundamental flux loop mass in SU(2) (\triangle) and SO(4) (\blacktriangle).

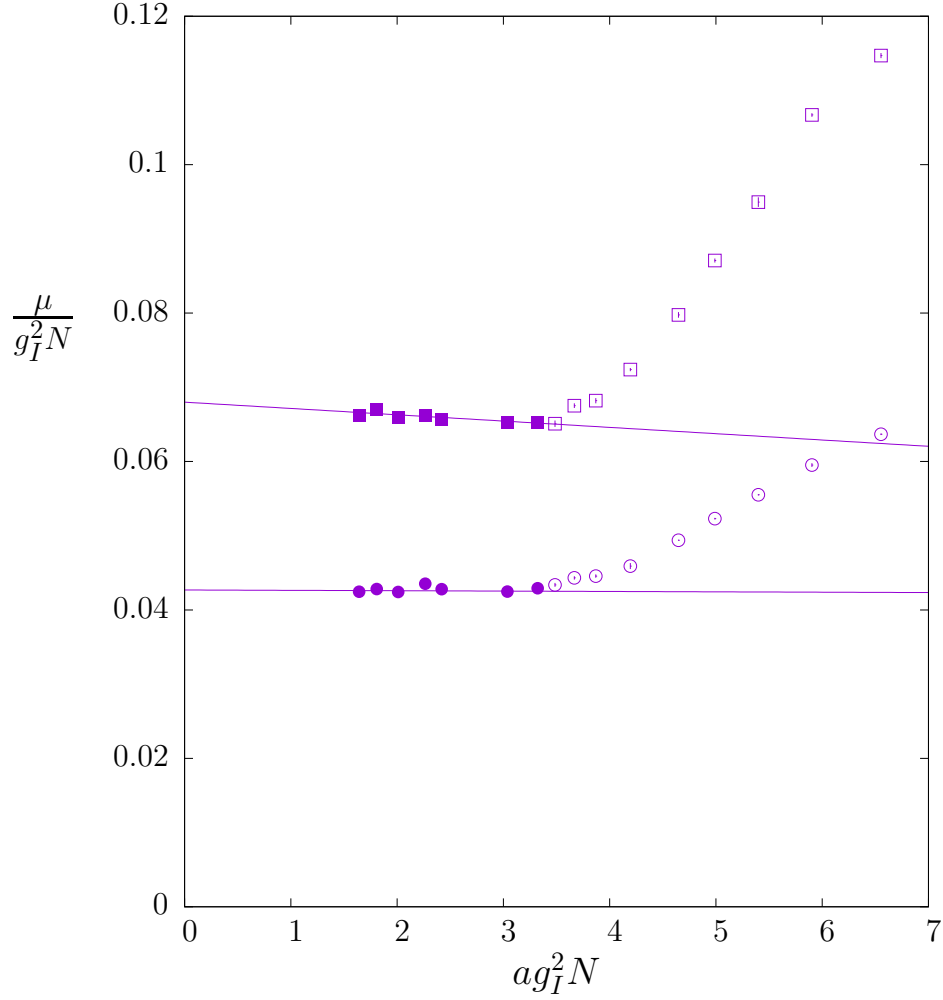


Figure 31: String tension, $\sqrt{\sigma}/g_I^2 N$ (\circ, \bullet), and lightest scalar glueball, $0.5 \times M_{0+}/g_I^2 N$ (\square, \blacksquare), both in units of the (improved) 't Hooft coupling and plotted against $ag_I^2 N$; all in $SO(3)$. Open points are in the strong coupling and cross-over region, and filled points are on the weak coupling side.

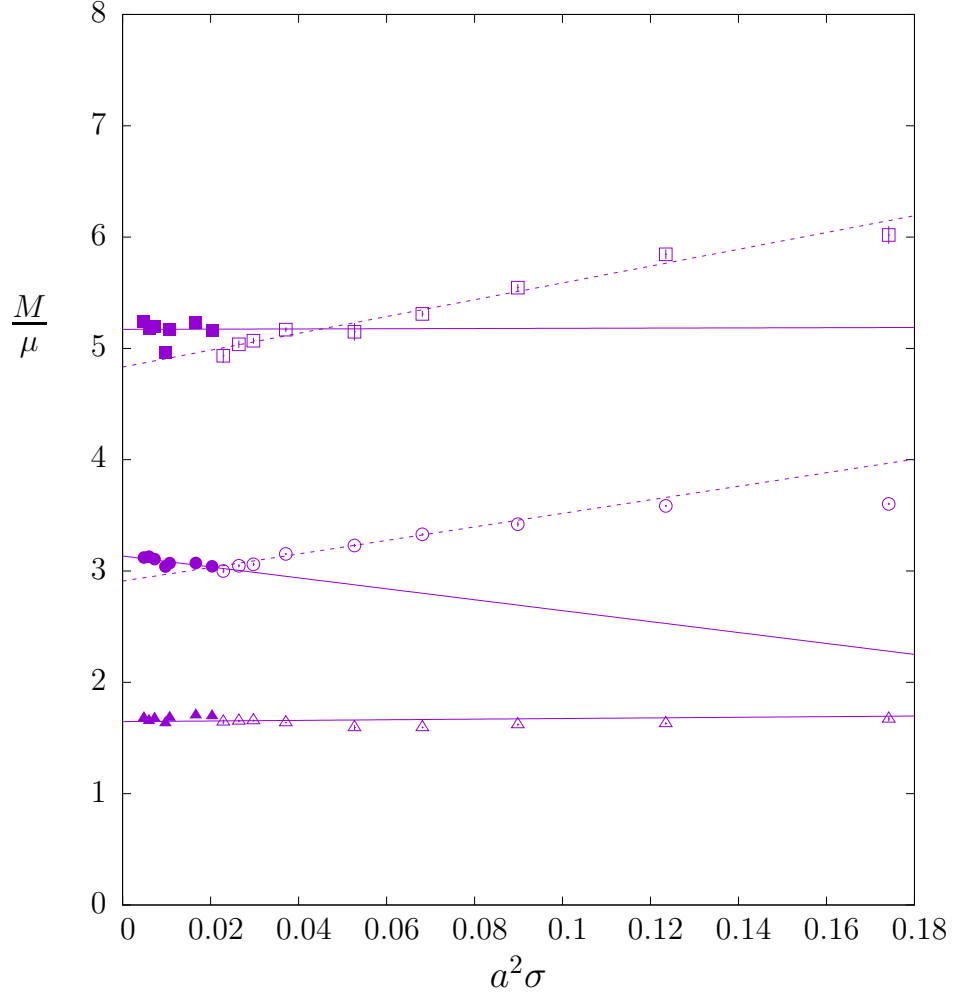


Figure 32: Mass ratios $M_{0+}/\sqrt{\sigma}$ (\circ, \bullet), $M_{2-}/\sqrt{\sigma}$ (\square, \blacksquare), and M_{2-}/M_{0+} ($\triangle, \blacktriangle$) plotted against $a^2\sigma$, with open and filled at strong and weak coupling respectively; all in $SO(3)$. Linear fits to strong and weak coupling values shown as dashed and solid lines respectively.